Modelling the Subdiffusive Motion of Bacteriophages within Mucus

A Thesis
submitted in partial fulfillment of
the degree of

Doctor of Philosophy

of the
Indian Institute of Technology Bombay, India
and
Monash University, Australia
by

Silpa Mariya

Supervisors:

Prof. P. Sunthar (IITB)

Prof. J. Ravi Prakash (Monash University)

and

Prof. Jeremy Barr (Monash University)

The course of study for this award was developed jointly by
Monash University, Australia and the Indian Institute of Technology Bombay, India
and was given academic recognition by each of them.
The programme was administrated by The IITB-Monash Research Academy.

2025

Declaration

I hereby declare that the work presented in this thesis is the result of my own original research, except where otherwise indicated and acknowledged. Where ideas or words of others have been incorporated, proper citation and referencing have been provided to acknowledge the original sources accurately. I affirm that I have adhered to all principles of academic honesty and integrity throughout this work, and I have not misrepresented, fabricated, or falsified any data, ideas, facts, or sources in this submission. I am aware that any violation of these standards may result in disciplinary actions by the Institute and could also have legal implications if appropriate permissions were not obtained when required. Additionally, I declare that this thesis includes material directly from my first-author publication Mariya *et al.* (2024).

Silpa Mariya

Date: 12 May 2025

Abstract

Mucosal surfaces are the entry points of pathogens into the animal body and act as the primary sites of defence against infections. It is a network made of the mucin glycoprotein molecules. Experiments show that viruses called bacteriophages, that reside in the mucus layer, undergo subdiffusive motion within mucus. According to the Bacteriophage Adherence to Mucus (BAM) model, this subdiffusion is due to the adherence between the Hoc proteins on the phage capsid and the glycans on the mucin network. Confirming this hypothesis are experimental results obtained using a non-adherent phage, which are found to be diffusive within mucus. However, the details of the interaction between the phage and glycans are unknown. The aim of our research is to explain the motion of phages within mucus and their interaction with mucus networks using Brownian dynamics simulations of associative polymers.

We model the polymers as coarse-grained bead-spring chains that have associative groups (stickers) on them. The phages are modelled as dendrimers, and the mucus layer is a network of linear polymers. Three types of stickers are implemented in the system, which permit only network formation and dendrimer-linear chain interactions to occur. The stickers on these polymers are modelled using the Soddemann-Duenweg-Kremer (SDK) potential, the well depth of which can be varied to change the interaction strength between stickers. The Brownian Dynamics code developed in this research is capable of simulating any number of polymers of arbitrary architecture in solutions of semidilute concentration with hydrodynamic interactions.

In the first part of the research, semidilute solutions of linear chain polymers were studied with dendrimers diffusing through them. Though their architectures are different, dendrimers and linear chains followed the same scaling laws for the radius of gyration and diffusivity as functions of concentration. Dynamics of dendrimers larger than the correlation length of the solution exhibited some qualitative similarities with that of nanoparticles in semidilute polymer solutions. However, they do not follow the scaling law for the diffusivity of nanoparticles as a function of their size relative to the solution correlation length. Therefore, a new scaling law for dendrimer diffusivity in semidilute polymer solutions has been proposed.

Next, the static and dynamics of sticky and non-sticky dendrimers in associative polymer networks were analysed. The properties of non-sticky dendrimers in the network did not differ from

those in a semidilute solution of linear polymers with no network forming stickers. However, sticky dendrimers showed some characteristic features due to their adherence to the network. Analysis of the radius of gyration and internal dendrimer bead densities reveals that the size of sticky dendrimers increases initially as the concentration of linear chains increases due to binding to the network, while decreasing with further increase in concentration due to screening of excluded volume interactions. It was also observed that the mesh size distribution of the background network is influenced by the presence of dendrimers.

From the mean squared displacement plots, it is clear that sticky dendrimers become subdiffusive even when their size is smaller than the mesh size, with a non-Gaussian probability distribution of displacements. The terminal diffusivity of dendrimers follows theories developed for nanoparticles in similar environments. The diffusion exponents of dendrimers are also compared with those of bacteriophages diffusing in mucosal layers (Barr *et al.*, 2015). Our simulations, in which sticky dendrimers mimic the behaviour of the phages, show quantitative agreement with the experimentally observed diffusion exponents for the phages with an appropriate choice of simulation parameters.

Table of Contents

List of Figures

List of Tables

List of Symbols

Roman Symbols

$E_{a,b}$	Mittag-Leffler function	64
f	Functionality of dendrimer	21
g	Generation number of dendrimer	21
H	Spring constant	25
h^*	Hydrodynamic interaction parameter	27
k_B	Boltzmann constant	16
L	Length of the simulation box	25
l_H	Non-dimensionalization factor for length	25
m	Order of dendra	21
N_b	Number of beads on a polymer molecule	25
N_c	Number of polymer molecules in a simulation box	25
N_x	Number of monomers between two adjacent crosslinks	12
$n_\mathrm{b}(x)$	Number of beads of a molecule within a distance x along the major axis	30
$N_{s,f}$	Number of springs on each dendrimer arm	35
Q_0	Maximum stretchable length of a single spring	26
R	Universal gas constant	11
r_c	Cutoff distance of the SDK potential	27
R_e	End-to-end distance of linear chains	49
R_CM	Centre of mass of the molecule	29
R_g	Radius of Gyration	29
R_H	Hydrodynamic radius	11
R_{NP}	Radius of the nanoparticle	11
s	Spacer length of dendrimer	21
U_SDK	SDK potential	26

U_{RD}	Ratio between radius of gyration and hydrodynamic radius 30
U_{FENE}	FENE spring potential 26
V	Volume of the simulation box 25
x_{CM}	x-components of the centre of mass of the molecule 32
K	Effective diffusion coefficient 8
MSD	Mean squared displacement 8
T	Temperature 11

Greek Symbols

α	Diffusion exponent 8
χ	Size ratio between dendrimer and linear chain 29
Δ_h	Mean jump length 12
$\delta_{\mu\nu}$	Kronecker delta 25
ϵ	Well depth of the potential 27
ϵ_{bb}	Interaction strength between homopolymer beads 28
ϵ_D	B-C sticker interaction strength 28
ϵ_N	A-A sticker interaction strength 28
η_s	Solvent viscosity 25
κ^2	Relative shape anisotropy 30
$\lambda_1^2, \lambda_2^2, \lambda_3^2$	Eigen values of gyration tensor 30
λ_H	Non-dimensionalization factor for time 25
ν	Flory exponent 29
$\boldsymbol{\delta}$	Unit tensor 25
$\boldsymbol{\Omega}_{\mu\nu}$	Hydrodynamic interaction tensor 25
σ	Non-dimensional distance 27

τ	Time 8
τ_h	Mean hopping time 12
τ_x	Rouse relaxation time of a network strand a_x 12
τ_{d}	Relaxation time of a chain segment with a size equal to the size of the dendrimer 32
τ_ξ	Relaxation time of a correlation blob 32
ξ	Correlation length 11
ζ	Stokes friction coefficient 25

Chapter 1

Introduction

The animal body harbours diverse species of microbes, whose population outnumbers the total number of cells per individual by an order of magnitude (Savage, 1977). The entry points of these microbes are the respiratory, gastrointestinal and reproductive tracts. The first line of defence of the body against harmful pathogens is the mucus, which acts as a selective barrier to large particles (Bustos *et al.*, 2023). Structurally, mucus is a hydrogel made of mucin glycoprotein molecules and has viscoelastic properties (shown in Figure 1.1(a)). It is permeable to small molecules and microbes and hosts a diverse population of microbes, including viruses. The most abundant are bacteriophages or phages, which are viruses that infect bacteria. The phage virus is, in fact, a defence mechanism of the body against the invasion of pathogenic bacteria. They are a so-called "good virus"! A schematic representation of the mucin network and a bacteriophage is shown in Figure 1.1(b).

The phages are highly specific to certain strains of bacteria and are capable of infecting almost all organisms. One of the well-studied strains is the T4 bacteriophage that infects the *E.coli* bacteria. The T4 phage infects the *E.coli* bacteria in the mucosal layer. The longer the phage stays in the mucus layer, the higher the chances of it encountering the bacteria and infecting it. A recent study by Barr *et al.* (2013a) observed the effect of T4 phages in mucus on *E.coli* population reduction. They found that the the main reason for the reduction is the adherence of phages to glycans present on the mucus network. A special class of proteins called the highly antigenic outer capsid (Hoc) protein present on the phage capsid is responsible for the adherence of the phage to the glycans of the mucus network. A mutated strain of T4 phage, called T4Δ*hoc*, which lacked the Hoc protein, resulted in a reduced adherence of the phage to the mucus network and led to an increased population of *E.coli*. This study suggests the increased residence time of phages in the mucus layer due to the adhesion is desirable as a good defence mechanism against pathogenic bacteria.

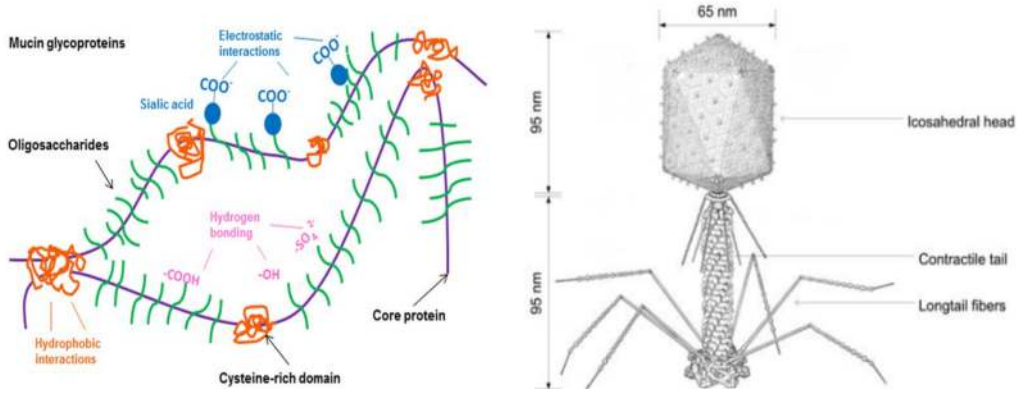

(a) (b)

Figure 1.1: (a) Schematic representation of mucin network made of mucin glycoprotein molecules. Image reproduced from Yang *et al.* (2012), for illustration purposes only, under fair use for research. (b) Structure of bacteriophage. Image reproduced from Jabrane *et al.* (2010), for illustration purposes only, under fair use for research.

Barr *et al.* (2015) further quantified the motion of T4 and T4Δ*hoc* phages in mucus using particle tracking experiments. They found that the T4 phage exhibited a subdiffusive motion in mucus, while the T4Δ*hoc* phage showed a diffusive motion. The Bacteriophage Adherence to Mucus (BAM) model of immunity proposed by Barr *et al.* (2015) suggests that phages enter the outer mucus layers, encounter larger mesh sizes due to the initial low mucin concentration, and as they move towards the epithelial layer, the mesh size decreases due to increasing concentration, slowing them down. The adherent phages bind to the glycans present on mucin glycoprotein using Hoc proteins on its capsid. This adherence causes them to be subdiffusive at critical mucin concentrations.

A model system that is close to the phage-mucus system is the diffusion of nanoparticles in polymer solutions and networks, which have been studied extensively in the literature. Diffusion of nanoparticles in unentangled (Poling-Skutvik *et al.*, 2015) and concentrated (Guo *et al.*, 2012) polymer solutions show a scaling behaviour of the diffusion coefficient with the particle diameter and polymer concentration (through the polymer chain correlation length). These observations have been explained by the theoretical frameworks for nanoparticle diffusion in complex media (Holyst *et al.*, 2009; Cai *et al.*, 2011; Dell and Schweizer, 2014; Cai *et al.*, 2015). Recent simulations using a range of model systems have validated these theories as well (Zhou and Chen, 2009; Chen *et al.*, 2017; Kumar *et al.*, 2019; Cho *et al.*, 2020; Sorichetti *et al.*, 2021).

1.1 Research objective

While the BAM model suggests that the subdiffusion of bacteriophages in mucus is due to its adherence to glycans present on the mucus network, there is no mathematical model of the underlying physics that explains the subdiffusive behaviour. While there are scaling theories for the diffusion coefficient of nanoparticles in polymer solutions and networks, there is no detailed study of the sub-diffusivity aspects, particularly the lowering of intermediate diffusion exponents and the role of adhesion and mesh size of the network.
A proper understanding of these mechanisms will enable researchers to effectively employ phages in various applications. Hence, there is a need for a comprehensive study of this system, which incorporates the interaction between phages and mucus network as well as the viscoelastic nature of the mucus layer.

1.2 Model hypothesis and methodology

We propose to model the phage as a dendrimer and the mucus network as a network of associative polymers. A dendrimer is a branched polymer with a well-defined architecture. By tuning the architecture of the dendrimer, we hope to throw light on a gamut of diffusive behaviours from a flexible polymer to rigid spherical nanoparticles. The dendrimer and associative polymer network are both modelled as a collection of beads connected by springs. The addition of stickers to the outermost beads on the arms of the dendrimers lets us study the influence of nanoparticle adhesion to the polymer network.
We intend to use a coarse-grained Brownian Dynamics Simulation (BDS) technique to study the diffusive motion of dendrimers in semidilute solutions and networks of associative polymers. BDS is a technique that simulates the motion of particles in a fluid by solving the Langevin equation in which the inertia of the particles is neglected, and the collective motion of the solvent molecules is captured by a stochastic term determined by the fluctuation-dissipation theorem.

1.3 Thesis outline

The chapter-wise breakup of this thesis is as follows: Chapter 2 gives an overview of the experimental results and theories developed for analysing the dynamics of mesoscopic bodies in a viscoelastic medium, details of the proposed model and the various systems investigated in this thesis. Chapter 3 gives the details of the simulation technique and the various interactions included in the model. In Chapter 4, the different stages of code development and validation studies conducted at each stage is explained. Chapter 5 contains the results of the study on the

universal behaviour of a non-sticky dendrimer in a semidilute solution of linear polymers. The static and dynamic properties of dendrimers in a polymer network are provided in Chapters 6 and 7 respectively. This includes simulations of both sticky and non-sticky dendrimers. We have also compared our simulations with experimental results of bacteriophages in mucus in Chapter 7. Chapter 8 contains some concluding remarks and future works.

Chapter 2

Subdiffusion of mesoscopic bodies in viscoelastic medium

2.1 Bacteriophages in mucus

2.1.1 The mucus

The animal body provides a habitat for a diverse and abundant microbiome, with the mucus layer being the major entry point of these microbes to host bodies. It is basically a biological hydrogel that is present in the inner lining of soft organs and tracts, such as the reproductive, respiratory, and gastrointestinal tracts. The building blocks of the mucus network are the mucin glycoprotein molecules. A schematic diagram of the mucin network is shown in Figure 1.1(a). These are macromolecules with each weighing about 10^6—10^9 Da and are responsible for the viscoelastic properties of the mucus layer. It has a proteinaceous backbone (also called the apomucin core) which consists of repeated sequences of proline, threonine, and serine (PTS) domains of variable lengths interspersed by the cysteine-rich regions at the amino and carboxy terminals (Wagner *et al.*, 2018). The bottle brush-like structure of mucin is due to the O-glycosylation of the hydroxyl groups on threonine and serine (Barr *et al.*, 2013b; Bustos *et al.*, 2023; McShane *et al.*, 2021). Several of these variable, branched glycans extend outward (up to 5 nm) from the backbone to the surrounding environment of the mucin molecule. Mucin glycans are rich in sialic acid and sulfate which gives it a negative charge. The cysteine-rich zones on mucin molecules join via disulfide bonds to form the mucin network as shown in Figure 1.1(a). Therefore, it is an extensive three-dimensional network of mucin strands (Barr, 2017). There is a constant outward movement of the mucus network from the underlying goblet cells, where it is produced, towards the lumen. This results in a gradient of mesh sizes within the network.

2.1.2 Microbes in the mucus

The mucus layer hosts an extensive and genetically diverse species of microbes, including transient species, host-specific commensals, potential pathogens, and symbiotic organisms (Schwiertz, 2016; Altveş *et al.*, 2020; Bik, 2009; Barr *et al.*, 2013b). The transport of these microbes and other molecules through mucus is through size and interaction filtration, thus making it a selectively permeable barrier (Bustos *et al.*, 2023). Viruses are the most abundant among them (Edwards and Rohwer, 2005) and are capable of infecting almost all organisms. The most prevalent type of virus are the bacterial viruses, also called bacteriophages or phages. As the name suggests, they infect and replicate within bacteria. Its high specificity to certain strains of bacteria along with its abundance within mucus suggests that phages are effective antimicrobials within mucus. The basic structural forms of bacteriophages include the polyhedral head (usually icosahedral) and the filamentous phage (Sanz-Gaitero *et al.*, 2021). The T4 bacteriophage infects the *Escherichia coli* bacteria by the lytic life cycle (Leiman *et al.*, 2003). Its head or capsid is decorated with the Hoc protein, along with other proteins (Rao and Black, 2010) as shown in Figure 1.1(b). Each of the Hoc proteins has three immunoglobulin-like (Ig-like) domains and one non-Ig domain in it (Sathaliyawala *et al.*, 2010).

The presence and abundance of T4 phage in a range of mucosal surfaces were investigated by Barr *et al.* (2013a). Using epifluorescence microscopy, the phage-to-bacteria (PBR) ratio within mucus was found to be 4.4-fold higher than in its surroundings. In vitro studies also showed that upon treatment of the mucus-producing cells with T4 phage and *E. coli*, the number of bacterial cells and the death of underlying cells due to bacterial infection reduced compared to that in the non-mucus producing cells. Further, this was shown to be due to the adherence of the T4 phage to the mucin glycoprotein molecules which in turn provides immunity against bacterial infections. It was also confirmed through their experiments that the Ig-like domains found in the Hoc proteins on phage capsid mediated the adherence mechanism between the phage and mucus. Ig-like domains are known to play a significant role in recognition and adhesion processes (Fraser *et al.*, 2007). The homologs of these domains found in the T4 Hoc protein were found to be structurally similar to a sugar-binding domain in plants which has specific carbohydrate-binding properties. The T4 phage with Hoc also showed preferential binding to O-linked glycan residues which are present on mucin glycoproteins.

2.1.3 T4 - mucus interaction

In order to better understand the dynamics of the T4 phage in vivo, Barr *et al.* (2015) developed a microfluidic device using poly-dimethylsiloxane. The chip has a microfluidic channel with a glass microscope slide. The channel and its in and out ports help maintain a constant fluid flow.

Thus, the chip imitates in vivo conditions with a constant flow across its surface. The human lung epithelial cells (mucus-producing) were allowed to grow in the channel for seven days. The interaction between bacteria, phage and mucus was studied using *E. coli* bacteria, T4 phage (mucus adherent) and T4Δ*hoc*. T4Δ*hoc* is a normal infective phage devoid of the Hoc protein on its capsid. It, therefore, cannot adhere to the mucus. The phage media with T4, T4Δ*hoc* and no phage was supplied to the chips with epithelial cells for 24 hours. It was then perfused with no-phage media to remove free phages from the mucosal layer. *E. coli* bacteria were then introduced into the chip through the input port. Both bacteria and phages were allowed to grow and replicate. It was observed that T4 and T4Δ*hoc* infected bacteria; however, there was a significant decrease in the bacterial population in the chip with T4 phage compared to that in the T4Δ*hoc* and no phage chips. This suggests that the adherence interaction between the T4 phage and mucus, along with the turnover dynamics of mucus layer is responsible for the increased antibacterial activity and phage abundance within mucus.

2.1.4 Diffusion of phages in mucus

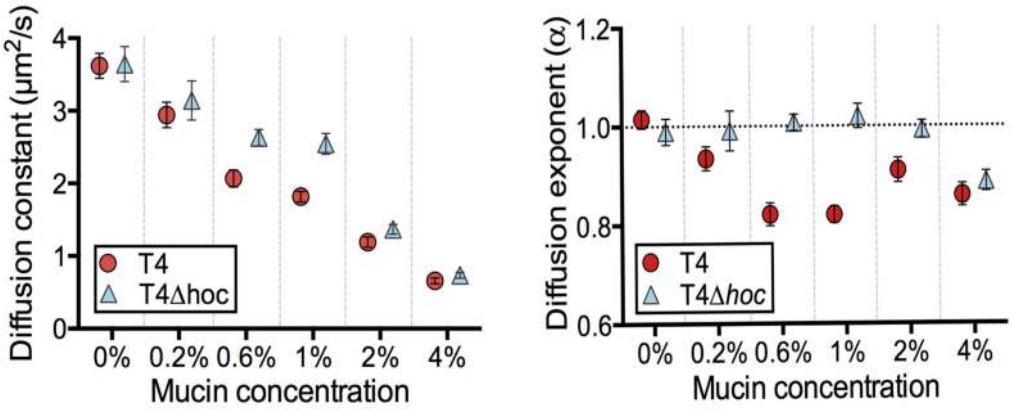

(a) (b)

Figure 2.1: Experimental results showing the decrease in diffusion coefficient (a) and subdiffusion exponent (b) of bacteriophage in mucus. Image reproduced from Barr *et al.* (2015), for illustration purposes only, under fair use for research.

The nature of the motion of phages within mucus was investigated by Barr *et al.* (2015) by observing the diffusion of T4 and T4Δ*hoc* in a range of physiologically significant mucin concentrations using high-speed multiple particle tracking. Fluorescently tagged phages in mucin solution were observed in concave slides under the microscope, and their trajectories were tracked manually by recording their diffusion for a span of a few seconds. The ensemble-averaged mean squared displacement of both phages was calculated using the relation given below:

$$\mathrm{MSD}(\tau) = K\tau^{\alpha} \tag{2.1}$$

where K is the effective diffusion constant and α is the diffusion exponent. It was observed that the effective diffusion constant for both phages decreased with increasing mucin concentration. At 0% mucin, T4 and T4Δ*hoc* had comparable values of K. But T4 showed a significant decrease in K compared to T4Δ*hoc*, especially at 0.6% and 1% mucin. This means that T4 exhibited slower diffusion at these concentrations. At 4% mucin, the two phages had similar diffusion constants (refer to Figure 2.1(a)).

The diffusion exponent α was extracted from the slopes of the line of best fit to the MSD data. T4Δ*hoc* showed a diffusive behaviour till 2% mucin after which the value of α became less than 1 ($\alpha = 0.89 \pm 0.02$). On the other hand, T4 has a diffusive behaviour like that of T4Δ*hoc* at 0% mucin, which then becomes subdiffusive with an increase in mucin concentration. α decreased to a value of 0.89 ± 0.02 at 0.6% mucin and $\alpha = 0.82 \pm 0.01$ at 1% mucin. At 4% mucin, both T4 and T4Δ*hoc* have comparable diffusion exponents.

2.1.5 BAM model

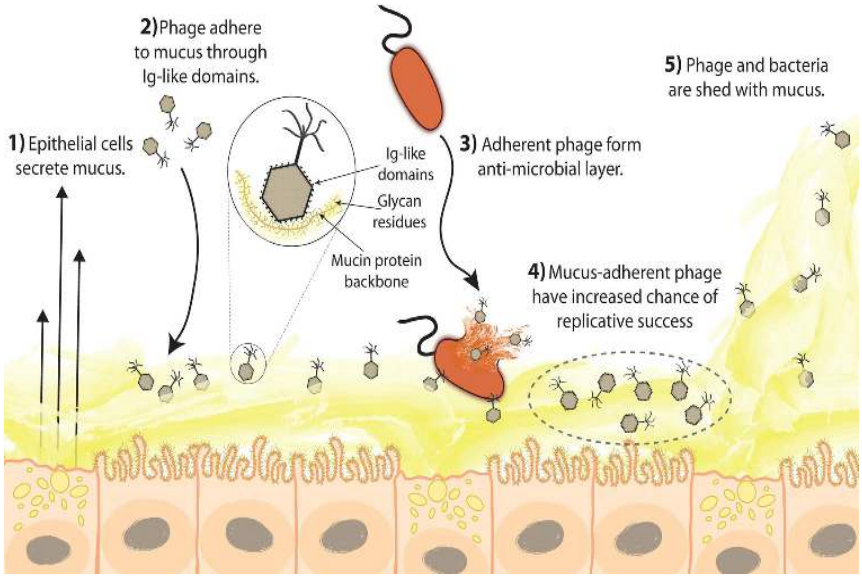

Figure 2.2: Bacteriophage Adherence to Mucus model predicts the binding interaction between phage and mucus. Image reproduced from Barr *et al.* (2013a), for illustration purposes only, under fair use for research.

Based on their experiments, which confirm the adherence of phages to glycans resulting in their subdiffusion and the subsequent protection of underlying cells from infection, Barr *et al.* (2015) proposed the Bacteriophage Adherence to Mucus Surface (BAM) model of immunity

(Figure 2.2). According to this model, mucus is produced continuously by the epithelium, which expands outward towards the lumen. Phages, found abundantly in the mucus layers, enter mucus and encounter larger mesh sizes due to the initial low mucin concentration due to which both phages (T4 and T4Δ*hoc*) have similar diffusive properties. As they move towards the epithelial layer, the mesh size decreases as concentration increases, slowing them down (diffusivity decreases). The adherent phages bind to the glycans present on mucin glycoprotein using Hoc proteins on its capsid. The glycan-Hoc interaction is avidity-based and the Hoc protein binds weakly to multiple glycans. This adherence causes them to be subdiffusive at critical mucin concentrations. As they move toward the epithelial layer, they get trapped due to smaller mesh sizes. However, due to the constant mucin network expansion, phages re-enter the subdiffusive region. The weak binding interaction gives adherent phage enough time to thoroughly search the mucus layer. This leads to a higher number of bacterial encounters. The progenies released from the lysis of host cells enter the subdiffusive zone. Hence there is always a higher chance of phage-host encounter in the subdiffusive region. This was not observed in the case of T4Δ*hoc* phage due to the absence of the adherence mechanism. With increasing mucin concentration, the mesh size of the mucin network decreases and becomes comparable to phage size. At 4%, the mucin network effectively traps both the phages resulting in subdiffusive motion. This phenomenon is usually observed in viscoelastic fluids like mucus. Due to the turnover dynamics of mucus, phage and bacteria are sloughed away into the lumen.

2.2 Nanoparticle diffusion

We now review results from the synthetic systems of nanoparticles in polymer matrices which is the closest to the physiologically significant system discussed above. Due to its applications in several fields, the diffusion of nanoparticles (NPs) in crowded environments has been studied extensively. A proper understanding of its interactions with the surroundings is essential for understanding processes like the transport of cargos through the cytoplasm and network of microtubules and actin filaments, diffusion of viruses in the extracellular matrix and biological processes like protein folding (Babayekhorasani *et al.*, 2016; Safi Samghabadi *et al.*, 2022; Smith *et al.*, 2021; Kumari *et al.*, 2020; Kozer *et al.*, 2007; Zhang *et al.*, 2024). Polymer matrices, both semidilute solution and networks, serve as a model system to mimic the viscoelastic, heterogeneous and dynamic environments encountered in biological and industrial contexts, offering a controlled platform to investigate nanoparticle behaviour. The semidilute polymer solution is a regime that lies between dilute and concentrated solutions, characterised by overlapping polymer chains but without the formation of a dense, entangled network as in concentrated solutions. The interplay between nanoparticle size, surface chemistry, polymer ar-

chitecture and matrix dynamics plays a crucial role in determining the diffusion characteristics of the nanoparticle (Ge, 2023, 2024).

The diffusivity of probe particles in simple viscous fluids is given by the Stokes-Einstein (SE) equation, which relates the diffusion coefficient of the particle to the viscous drag it experiences. In a complex fluid, like a polymer solution or network, the viscoelastic effects of the fluid are accounted for by the generalised Stokes-Einstein (GSE) equation (Mason and Weitz, 1995; Squires and Mason, 2010). However, the underlying assumption that the fluid is a continuum breaks down when the size of the particle is comparable to the characteristic length scales in the solution like the radius of gyration of the background chains, or the correlation length of the solution. As a result, the SE and GSE equations fail to describe the dynamics of such tracer particles (Ye *et al.*, 1998; Mackay *et al.*, 2003; Tuteja *et al.*, 2007; Maldonado-Camargo and Rinaldi, 2016; Grabowski and Mukhopadhyay, 2014).

It has been observed experimentally that the mobility of nanoparticles decreases with increasing concentration of polymers (Cheng *et al.*, 2002; Omari *et al.*, 2009; Kohli and Mukhopadhyay, 2012; Poling-Skutvik *et al.*, 2015; Yang *et al.*, 2020; Slim *et al.*, 2020; Smith *et al.*, 2021). Anomalous diffusion (subdiffusive) regimes were observed in the mean squared displacement versus time plots (Babayekhorasani *et al.*, 2016; Grabowski and Mukhopadhyay, 2014; Smith *et al.*, 2021) and the probability distribution functions of displacement was often non-Gaussian (Slim *et al.*, 2020; Smith *et al.*, 2021). Additionally, the terminal diffusivity showed either stretched exponential (Cheng *et al.*, 2002; Kohli and Mukhopadhyay, 2012) or power law (Poling-Skutvik *et al.*, 2015; Safi Samghabadi *et al.*, 2022) dependence on the ratio between its size and the correlation length of the solution. Recent advances in chemistry and biotechnology have led to the development of nanoparticles of desired size and shape. Some of the commonly used nanoparticles in experiments include gold nanoparticles (Kohli and Mukhopadhyay, 2012; Kohli *et al.*, 2013; Moncure *et al.*, 2022), polystyrene nanoparticles (Schuster *et al.*, 2013; Rodríguez-Suárez *et al.*, 2020; Slim *et al.*, 2020), nanorods (Molaei *et al.*, 2018; Poling-Skutvik *et al.*, 2018; Gratz and Tschope, 2019) and silica nanoparticles (You and Yu, 2019; Yang *et al.*, 2020). Similarly, the development of various types of polymer matrices with tunable stereochemistry, architecture and interactions along with the advancement of experimental techniques in scattering and microscopy has led to an explosion of research in this field.

The dynamics of nanoparticles in polymers have also been investigated using molecular simulations. Nanoparticles are usually modelled as a single rigid particle with a smooth surface (Sorichetti *et al.*, 2021; Chen *et al.*, 2017) or as a cluster of similar beads (Wang *et al.*, 2021; Karim *et al.*, 2016). For the polymer matrix, the popular coarse-grained bead-spring

chain models are used which accounts for the covalent backbone of a polymer as well as the weak inter-chain interactions.

To elucidate the observed characteristics of nanoparticle diffusion, analytical frameworks have been proposed, which can be broadly categorized into two classes: those addressing nanoparticles in semidilute polymer solutions and those examining nanoparticles in polymer networks.

2.2.1 Nanoparticle motion in semidilute polymer solutions

Over the years, various theoretical models have been developed to describe nanoparticle dynamics in semidilute polymer solutions. Starting from the initial studies that proposed a stretched exponential dependence of the reduced diffusion coefficient on solution concentration (Langevin and Rondelez, 1978; Cukier, 1984; Altenberger and Tirrell, 1984), efforts have been made to include a range of probe sizes, dynamics of the background chains and the coupling between the dynamics of nanoparticle and polymer chains. Two major recent theories explain the mobility of nanoparticles in semidilute polymer solutions: the Holyst model (Holyst *et al.*, 2009; Kalwarczyk *et al.*, 2015) and the coupling theory (Cai *et al.*, 2011). The former predicts a stretched exponential dependence of the nanoparticle terminal diffusivity on the ratio between an effective nanoparticle size to the correlation length (ξ) of the semidilute solution (defined subsequently in equation 3.10) given by

$$\frac{D}{D_0} = \exp\left[\frac{-\gamma}{RT}\left(\frac{R_{\text{eff}}}{\xi}\right)^a\right] \tag{2.2}$$

where $R_{\text{eff}}^{-2} = R_{\text{H}}^{-2} + R_{NP}^{-2}$, with R_{H} being the hydrodynamic radius of the polymer and R is the radius of the nanoparticle. $\gamma\,(\gamma > 0)$ and $a\,(a > 0)$ are system-dependent parameters and are reported in terms of an effective excess diffusion energy, $\Delta E_{\text{a}} = \gamma\,(R_{\text{eff}}/\xi)^a$, compared to that in pure solvent.

The coupling theory (Cai *et al.*, 2011) proposes a power law dependence for the terminal diffusivity, scaling as d_{NP}/ξ^{-2}, where d_{NP} is the diameter of the nanoparticle. The coupling theory also attempts to explain the observed subdiffusion of nanoparticles and predicts a constant exponent of 0.5 at intermediate times. Further details of these models are discussed in Chapter 5.

2.2.2 Nanoparticle motion in polymer networks

Similar to nanoparticle motion in polymer solutions, two major analytical theories predict the dynamics of nanoparticles within permanently crosslinked polymer networks. Both highlight the importance of the confinement parameter, $C = d_{\text{NP}}/\xi$, where ξ is the mesh size of the network which is equivalent to the correlation length in semidilute solutions. The first theory (Cai

et al., 2015) describes the diffusion of non-sticky hard spheres, predicting that nanoparticles larger than the mesh size experience ballistic motion initially, followed by subdiffusion and eventual trapping in polymer cages. At longer timescales, mobility arises through a hopping mechanism, governed by thermal fluctuations of the network strands, with the diffusivity scaling as

$$D_{\text{hop}} \approx (\xi^2/\tau_x)\frac{\exp(-C^2)}{C} \tag{2.3}$$

where τ_x is the Rouse relaxation time of a network strand a_x defined as $a_x \approx bN_x^{1/2}$, b is the Kuhn length and N_x is the number of monomers between two adjacent crosslinks.

The second framework incorporates the attractive interactions between nanoparticles and the network, proposing a critical confinement parameter, C_c, beyond which hopping dominates nanoparticle mobility. The diffusivity in this regime is expressed as

$$D_{\text{N}} \approx \Delta_h^2/\tau_h \tag{2.4}$$

where Δ_h represents the mean jump length and τ_h is the mean hopping time. Despite differences in their predictions, both theories provide a comprehensive understanding of nanoparticle dynamics, validated through simulation studies (Sorichetti *et al.*, 2021). Further details of these models are discussed in Chapter 7.

Due to the significance of tracer transport in various fields, numerous simulation studies have been conducted to understand the effect of matrix parameters on solute diffusion. Early models represented the network as an array of fixed obstacles (Netz and Dorfmüller, 1997), while recent ones have incorporated aspects such as network connectivity, flexibility (Kumar *et al.*, 2019), disorder and polydispersity (Sorichetti *et al.*, 2021) in their models. Most of these models place crosslinks at the vertices of a regular lattice (Lu and Hu, 2021) or connect them via springs (Zhou and Chen, 2009), thereby neglecting the effect of strands connecting crosslinks, like entanglement and strand dynamics. Moreover, real hydrogels are polydisperse systems with disorder. Recent simulation studies have accounted for these factors and compared them with theoretical predictions (Kamerlin and Elvingson, 2016; Cho *et al.*, 2020; Sorichetti *et al.*, 2021).

2.2.3 Polymer topology and stiffness

A key factor affecting nanoparticle dynamics is the topology of the background polymers. Studies have explored the impact of non-concatenated ring polymers versus linear chains as the polymer matrix. Based on the scaling predictions by Cai *et al.* (2011) for nanoparticles in linear polymer matrices, a theory was developed for ring polymer melts according to which,

the behaviour of nanoparticles larger than the characteristic length scales in ring polymer melts demonstrate qualitative agreement with that in linear polymers (Ge *et al.*, 2017). They exhibit subdiffusion at intermediate times, with the subdiffusion exponent larger than that observed in linear chains. The fact that the mobility of nanoparticles is less hindered in ring polymers due to the absence of an entangled network is reflected in their terminal diffusivities. Another computational study observed that nanoparticle dynamics in semidilute solutions of linear chains are comparable to those in ring polymer solutions (Chen *et al.*, 2021). The stiffness of the background polymers is also a significant factor influencing nanoparticle dynamics. Chain stiffness is typically implemented by adding a bending potential between adjacent bonds on a chain. Both in a semidilute solution (Chen *et al.*, 2019) and a network (Xu *et al.*, 2021; Kumar *et al.*, 2019), semiflexibility increases the polymer relaxation time, which leads to a stronger subdiffusion of the nanoparticle due to trapping. The terminal diffusivity deviates from the expected scaling laws for flexible chains (Chen *et al.*, 2021; Kumar *et al.*, 2019).

2.2.4 Topology of nanoparticles

Over the years, researchers have also explored varying nanoparticle topologies, ranging from tethered nanoparticles (also referred to as hairy colloids) to nanorods, each exhibiting distinct diffusion dynamics. For tethered nanoparticles in polymer melts, the dynamics are governed primarily by the number and length of tethered or grafted chains. This system has been analysed based on scaling theory (Ge and Rubinstein, 2019), and computational studies (Ge *et al.*, 2020) have validated this model. According to Ge *et al.* (2020), three distinct regimes exist: Regime I in which the terminal diffusion of loosely tethered particles is governed by the nanoparticle and there exists no hydrodynamic coupling between the tethered chains. Regime II, where chain-dominated diffusion arises as the tethered chain friction exceeds the nanoparticle friction. However, there is no hydrodynamic coupling between the tethered chains. Regime III is characterised by a non-draining layer around the nanoparticle due to hydrodynamic coupling between tethered chain segments, and diffusion is dominated by these chains. Notably, simulations have also identified the presence of two subdiffusive regimes in the MSD of loosely tethered nanoparticles in the tail-dominated regimes: the first is similar to that of the bare nanoparticle dynamics, and the second one is due to the participation of the particle in the dynamics of the tethered chains. Experimentally, Poling-Skutvik *et al.* (2019) used X-ray photon correlation spectroscopy to measure the diffusivity of polystyrene grafted silica nanoparticles in semidilute solutions of polystyrene, finding that normalized diffusivity data for various grafted nanoparticles could be collapsed onto a master curve when scaled by the ratio of free to grafted polymer molecular weights. Additionally, both simulations and experiments have examined the impact of shape anisotropy of the probe particle on its diffusivity, which includes nanorods in entan-

gled and unentangled polymer melts (Wang *et al.*, 2021; Choi *et al.*, 2015) and filamentous viral particles in polymer solutions (Smith *et al.*, 2021).

2.2.5 Attractive nanoparticles

In the studies discussed thus far, the nanoparticle interactions with the polymer matrix were predominantly repulsive. There has been increasing interest over the past few years in nanoparticles that have attractive interactions with polymers, referred to as sticky nanoparticles (Carroll *et al.*, 2018; Yamamoto *et al.*, 2018; Bailey *et al.*, 2019). A theoretical framework developed by Yamamoto *et al.* (2018) suggests that the attraction between the nanoparticle and matrix polymers causes the latter to be adsorbed onto the nanoparticle surface. The mechanism of movement depends on the relative size of the nanoparticle to the size of the matrix polymers. Specifically, "core-shell" diffusion occurs when the nanoparticle and the adsorbed shell of polymers diffuse as a single entity and its size is more than the matrix polymers. A "vehicular" diffusion occurs when the nanoparticle (NP) uses the adsorption layer as a carrier for its movement and is expected when the matrix polymers are larger than the nanoparticles. The latter process is dependent on the desorption time. This theory has been evaluated in the case of small attractive octa(aminophenyl) polyhedral oligomeric silsesquioxane (OAPS) NPs (Carroll *et al.*, 2018; Bailey *et al.*, 2019). Recent simulations also highlight the role of the strength of the NP-polymer interaction on the dynamics of NPs in a network. The higher the interaction strength, the slower the mobility and stronger the subdiffusion of NPs (Kumar *et al.*, 2019). It should be noted that the Lennard-Jones potential has frequently been used to model nanoparticle-polymer attraction in computational studies. Both the analytical theories (Cai *et al.*, 2015; Dell and Schweizer, 2014) discussed above for the terminal diffusivity of nanoparticles in polymer network have been validated for repulsive and attractive nanoparticles by Sorichetti *et al.* (2021).

2.3 Research gap

In the experiments of phage diffusion in the mucus layer, it is observed that both T4 and T4Δhoc phages become subdiffusive at higher concentrations with similar diffusion exponents, owing to the fact that their size is greater than the mesh size. This holds even in the case of nanoparticles in polymer matrices with sizes larger than the characteristic length scales of the system. Existing theories for nanoparticle diffusion in polymer solutions and gels suggest that this observed subdiffusion is due to the trapping of nanoparticles within the polymer matrix at intermediate times. Similarly, the diffusion coefficient of phages decreases with increasing mucin concentration, a trend also seen in nanoparticles within polymer solutions and networks. While the BAM model, which is a phenomenological model, proposes that the subdiffusion of T4 bacteriophages

at low mucin concentrations is due to its adherence to glycans present on the mucus network, the strength of interaction between the Hoc protein on phage capsid and the glycans remain unclear. Additionally, the role of the mesh size of the mucus network and the exact mechanism by which phages tune their motion to increase their residence time in the bacteria-rich region is still unknown. A proper understanding of these mechanisms will enable researchers to effectively employ phages in various applications. Hence, there is a need for a comprehensive study of this system which incorporates the interaction between phages and mucus network as well as the viscoelastic nature of the mucus layer.

Theoretical and computational studies have investigated systems of nanoparticles that have both repulsive and weakly attractive interactions with polymer networks. Specifically, parameters such as nanoparticle size, surrounding polymer chain lengths, and nanoparticle "stickiness" have been extensively analysed (Yamamoto *et al.*, 2018). However, to our knowledge, most research on soft colloids, including tethered nanoparticles and star polymers, has been limited to the dynamics of these bodies in polymer melts of linear chains, with theoretical models and simulations providing insights into the mechanisms underlying observed behaviours. Therefore, it is crucial to analyse soft colloids in crosslinked polymer networks of linear polymers. Furthermore, the system of sticky soft colloids remains an open area yet to be explored. Among soft colloids, dendrimers represent a significant category, with star polymers forming the simplest dendrimeric structure. However, the mobility of dendrimers with repulsive and attractive interactions within semidilute solutions and crosslinked networks of linear polymers is not well understood. Key aspects such as the influence of dendrimer architecture, the concentration of the background polymer matrix and interaction strength between the dendrimer and the surrounding matrix are least studied. Apart from this, developing models of phages necessitates the inclusion of specific attractive interaction sites on the probe particle that interact with the surrounding network.

2.4 Proposed model

The model employed in this research uses associative linear polymers to simulate the mucus network and branched polymers (called dendrimers) to simulate phages. Associative polymers are those that have attractive groups (also called stickers) on them. The mucus layer is modelled as a network of linear polymers as illustrated in Figure 2.3. The network formation is achieved by the association of some stickers (red beads) on the linear polymers similar to the Cysteine-rich domains on the mucin glycoprotein molecule. Our choice of associative polymer network to model the mucus layer is based on work done previously in the group (Santra *et al.*, 2021; Robe *et al.*, 2024) where we observed signatures of gelation at interaction strengths of the order

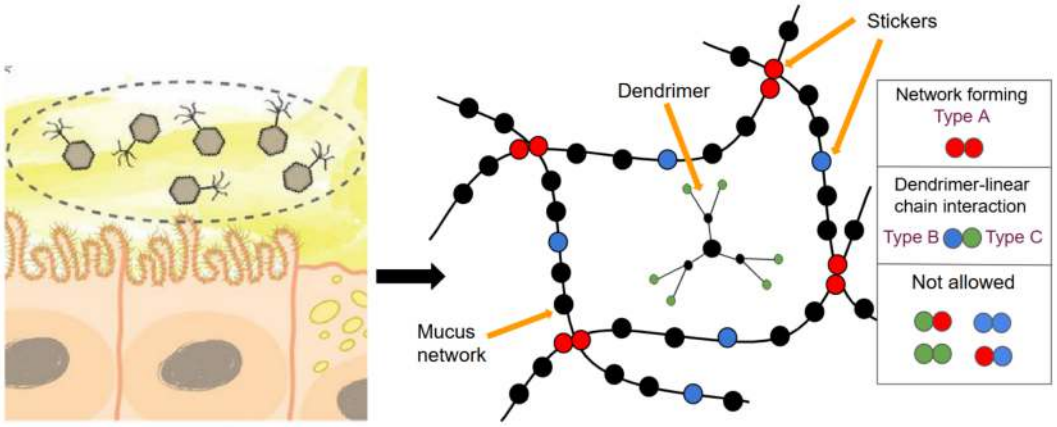

Figure 2.3: The schematic shows our proposed model for phages in the mucus network. The coloured beads are the stickers. Left (Image reproduced from Barr *et al.* (2015), for illustration purpose only, under fair use for research.)

of $10k_BT$ and concentrations of the order of the overlap concentration. Parameters like the concentration, chain length and mesh size of the network can also be easily controlled. The phages are represented as dendrimers or branched polymers. These are macromolecules, that have a central core bead with arms extending outwards. The stickers at the ends of the dendrimer arms (green beads) interact with certain stickers (blue beads) on the linear chains which are similar to the Hoc-glycan interaction between phage and mucus. The structure of dendrimers can be varied from being 'floppy' to globular by tuning a few parameters, thus enabling us to model soft colloids as well as nanoparticles. Another advantage of using dendrimers to model phages is that the number of interaction points (stickers) on their outer surface can easily be controlled by changing their structure-related parameters. Also, since the monomer beads on the dendrimers are considered point particles just like those on the background linear chains, the near-field hydrodynamics can be neglected unlike in the case of hard spheres.
A multi-species Brownian dynamics simulation algorithm has been developed for this purpose that can simulate polymers with arbitrary architectures and sticky interactions. To model the network formation and adherence between phage and mucus glycans, we consider three types of stickers in the system as shown in the inset of Figure 2.3:

1. Type A: These are the network-forming stickers (represented as red beads) and are present only on the linear chains. They are allowed to stick to each other and are similar to crosslinkers in experiments.

2. Type B: This type of sticker is interspersed between type A stickers on the linear chain (the blue beads in Figure 2.3) and represents the glycans on the mucus network. Therefore, they stick to the stickers on the dendrimers.

3. Type C: Representing the Hoc proteins on the phage capsid, type C stickers are present at the ends of the arms of dendrimers (green beads on the dendrimer in the schematic). They stick to type B stickers on the linear chains

The adherence between the phage and glycans is modelled using the association between stickers B and C. Therefore, we only allow A-A and B-C interactions in the system, while all the other interactions are prevented (Figure 2.3). By varying the concentration of the background linear polymers, interaction strength and number of stickers and dendrimer architecture, we aim to investigate the dynamics of phages under different mucin concentrations.
Discussed in the next section are the set of systems analysed in this research in the order in which they are reported in the upcoming chapters.

2.5 Heirarchy of problems

The system of a sticky dendrimer in a network of associative linear polymers has several complex interactions. Therefore, it is essential to break it down into a series of systems with increasing complexity. The static and dynamic properties of each of these systems were analysed and the results are reported in the subsequent chapters of this thesis. The systems considered are as follows:

1. A non-sticky dendrimer in a semidilute solution of linear polymers: The simplest system to examine is that of a dendrimer in a semidilute solution of linear homopolymers (Figure 2.4(a)). Recent studies have increasingly focused on the dynamics of nanoparticles, typically modelled as hard spheres, in semidilute polymer solutions with well-established analytical theories for these probe particles validated both experimentally and using simulations. A thorough analysis of how dendrimers, often referred to as soft colloids, of low generations behave in semidilute solutions has not been carried out so far. Chapter 5 focuses on the static and dynamic properties of this system and compares it with that of a nanoparticle.

2. A non-sticky dendrimer in a network of linear polymers: The T4Δ*hoc* phage in the experiments performed by Barr *et al.* (2015) is a non-adherent version of the T4 phage. In order to study its dynamics, it is essential to simulate a non-sticky dendrimer in a network of linear polymers. This means only the type A stickers are present on the linear chains which are responsible for the formation of a network (Figure 2.4(b)). Stickers of types B and C are absent. Chapters 6 and 7 discuss the static and dynamic properties of such a system, respectively, as a function of sticker strength, the distance between stickers and the concentration of linear chains.

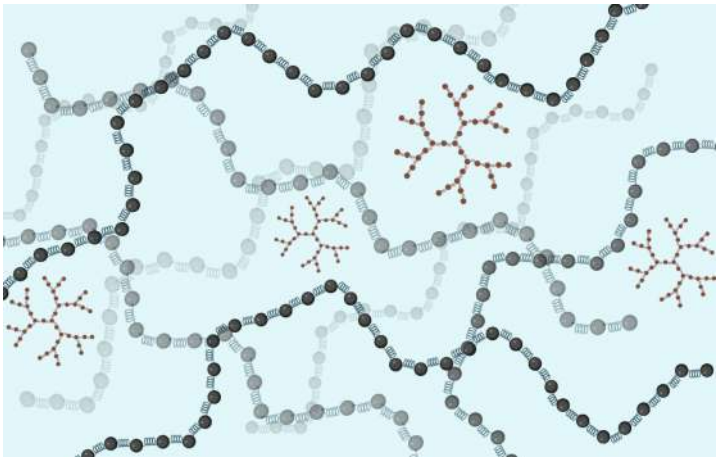

(a)

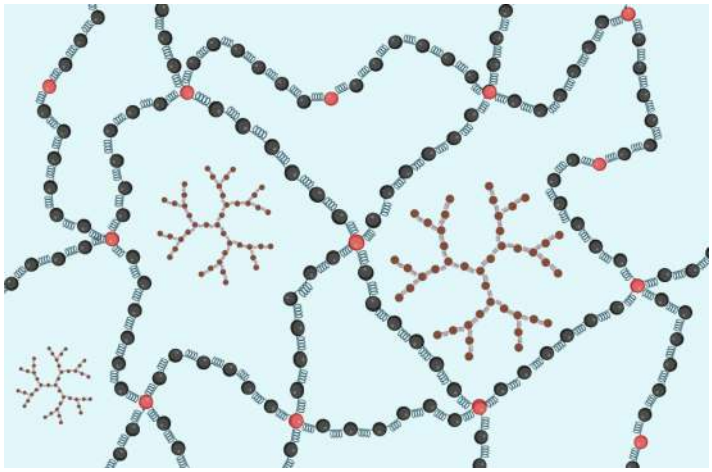

(b)

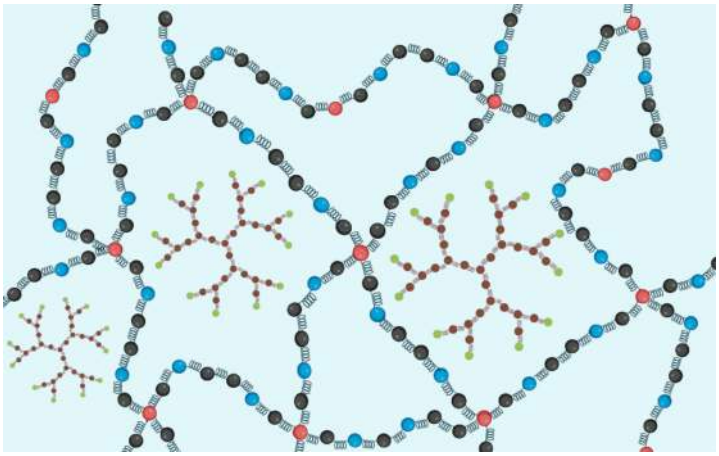

(c)

Figure 2.4: Schematic representation of dendrimers in a solution of linear chains (a), non-sticky dendrimers in a network (b) and sticky dendrimer in a polymer network (c). The red beads are the network-forming stickers and the blue beads on the linear chains stick to the green beads on the ends of the dendrimer. The black and brown beads are backbone monomers.

3. Sticky dendrimers in a network of linear polymers: According to the BAM model, the T4 phage in the animal body becomes subdiffusive due to its adherence to the mucus network. Hence, the next system to probe is that of a sticky dendrimer in a polymer network. In addition to the network forming stickers, there are stickers of type B (on the linear chain) and C (on the dendrimer) that only interact with each other (Figure 2.4(c)). Chapters 6 and 7 discuss the static and dynamic properties of this system as a function of sticker strength, the distance between stickers and the concentration of linear chains. Comparison with experiments of T4 phage is also carried out.

The properties of each of these systems are calculated and compared with analytical theories and experimental results available in the literature for similar systems of nanoparticles, high-generation dendrimers and polymer-tethered nanoparticles in semidilute polymer solutions and networks.

2.6 Rheology of associative polymers

The system of phages in the mucus layer is modelled using polymers with attractive groups on them, hence are called associative polymers (APs). Also referred to as sticky polymers, these are macromolecules capable of forming reversible physical bonds due to the presence of attractive groups (or stickers) (Rubinstein and Dobrynin, 1997; Rubinstein and Colby, 2003; Winnik and Yekta, 1997). These groups might be hydrophobic side groups, charged groups or functional monomeric units. The properties of associative polymers can be tuned by varying the number, strength and location of the attractive groups on them. Due to their tunable viscoelastic properties and stimuli-responsiveness, APs are used in a wide range of applications like adhesives, surfactants, rheology modifiers, coatings, absorbents and even in pharmaceutical delivery systems (Glass *et al.*, 1991; Rossow and Seiffert, 2015; Pancharoen, 2009; Layre *et al.*, 2009; Cadix *et al.*, 2015; Kostansek, 2006). Based on the arrangement of stickers along its backbone, associative polymers can be classified into telechelic APs, comb APs and types of copolymers. Sticker associations in APs are of two types: intra-chain association and inter-chain association. Intra-chain associations are observed in dilute solutions in which stickers on the same chain form bonds leading to the formation of loops and micelles. Inter-chain associations are usually found at higher concentrations and play a vital role in network formation (Rubinstein and Dobrynin, 1997). An example of an associative polymer is an ethylene oxide-urethane copolymer that has alternating sequences of hydrophobic and hydrophilic groups. At low concentrations, micelle formation takes place with hydrophobic groups forming the core and the hydrophilic groups forming the corona. As concentration increases, micelles join to form clusters and subsequently, a gel is formed.

Recent advances in the field of simulations of associative polymers have significantly enhanced the understanding of their complex behaviour. Computational approaches have progressed with the incorporation of multi-scale methods to capture both short-range molecular interactions and large-scale material behaviour. Molecular dynamics (MD) and Brownian dynamics (BD) simulations have been particularly useful in studying the phase behaviour, gelation and network formation kinetics, enabling the prediction of macroscopic properties like viscosity and elasticity in associative polymeric networks (Jiang *et al.*, 2021; Castillo-Tejas *et al.*, 2016, 2017; Xia and Olvera de la Cruz, 2024; Santra *et al.*, 2019, 2021; Robe *et al.*, 2024).

2.7 Structure and Properties of Dendrimers

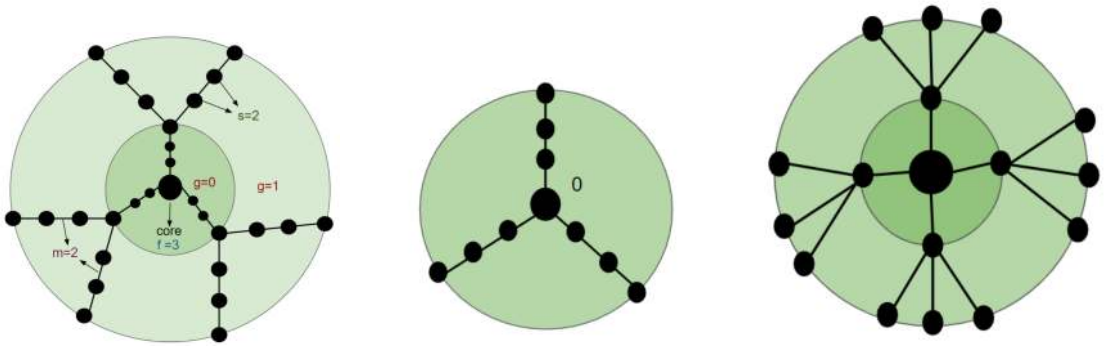

(a) (b) (c)

Figure 2.5: (a) Various parameters related to dendrimer structure. (b) Structure of a star polymer ($g = 0$) with functionality three ($f = 3$) and two spacer beads ($s = 2$). (c) A generation one ($g = 1$) dendrimer with functionality four ($f = 4$), order of dendra equal to three ($m = 3$) and no spacer beads ($s = 0$)

Our research utilises dendrimers to model bacteriophages. These are hyperbranched macromolecules that possess unique and exciting properties due to their architecture. These are monodisperse molecules built by adding short chains containing multifunctional groups on ends, starting from the central core (La Ferla, 1997). This unique class of polymers has a wide range of applications as their properties, mainly viscosity and diffusivity, differ from linear chains with similar molecular weights. They are used as rheology modifiers, additives and nanoscale building blocks apart from being employed as drug delivery vehicles and chemical catalysts (Nikzamir *et al.*, 2021; Najafi *et al.*, 2021; Bober *et al.*, 2022; Jaisingh and Nebhani, 2024). The structure of dendrimers is primarily characterised by their generation number (g), functionality (f) of the core, number of monomers between branching points (s) and order of dendra (m). An example of a symmetric first-generation dendrimer with a trifunctional core

and order of dendra two is shown in Figure 2.5(a). The simplest case of a generation zero dendrimer is a star polymer with a core and f linear chains attached to it (given in Figure 2.5(b)). The terminal groups of each arm are a potential branching point to which short linear chains can be attached, which will then constitute the next generation. Similarly, successive higher generations are constructed from previous generations. Thus, we can consider each generation to be a concentric shell about the core. A dendrimer is symmetric if each dendra ends in the same generation and all branches within a shell have the same length. Figure 2.5(c) shows a functionality four dendrimer without any spacer beads and order of dendra three.

The polymer scaling theory has been proven to work well in the case of linear chains, predicting the existence of a universal exponent for polymer size. Similar attempts have been made in the case of branched polymers like dendrimers, the macroscopic properties of which are dependent on factors like solvent quality and the presence of hydrodynamic interactions. The effect of these on dendrimer static and dynamic properties has been studied extensively both theoretically and experimentally. The initial theoretical investigation of dendrimers was conducted by de Gennes and Hervet based on the mean-field theory (de Gennes and Hervet, 1983). Subsequently, the Flory method was employed by Boris and Rubinstein to analyse the properties of dendrimers (Boris and Rubinstein, 1996; Ganazzoli *et al.*, 2000). La Ferla in his work extended the Rouse and Zimm approximations for these branched systems (La Ferla, 1997; Cai and Chen, 1997; Chen and Cai, 1999). The role of solvent quality in determining the structure of dendrimer molecules was studied by Sheng *et al.* (2002) and Timoshenko *et al.* (2002) using Monte Carlo simulations and using Brownian Dynamics simulations (Bosko and Prakash, 2008, 2011).

2.7.1 Effect of solvent quality on dendrimer size

Molecular Dynamics simulations by Murat and Grest were the earliest work done to investigate the effect of solvent quality on dendrimer size (Murat and Grest, 1996). They found that the radius of gyration of dendrimers scaled as $R_{\mathrm{g}} \sim N^{1/3}$ in athermal, theta and poor solvents, where N is the number of monomers per dendrimer molecule. Later, the effect of three-body interactions was incorporated into the Flory theory for dendrimers and a scaling law was derived for its radius of gyration in terms of the parameters g, s and N, in the good solvent conditions Sheng *et al.* (2002):

$$R_g \sim N^{1/5}(g+1)^{2/5}s^{2/5} \tag{2.5}$$

These exponents were validated using off-lattice Monte Carlo simulations. However, they failed to obtain the scaling law for θ solvent conditions due to the definition of θ point similar to that of linear chains. Giupponi and Buzza, using Monte Carlo simulations later showed that

the dendrimer segments do not behave ideally at θ point due to the presence of three-body interactions (Giupponi and Buzza, 2004). They assumed that the theta point coincides with the zero of the second virial coefficient and the two-body interactions vanish like in the case of linear chains, but the three-body interactions remain significant, leading to non-ideal behaviour. Thus they put forward the scaling law for branched polymers at theta point:

$$R_{\mathrm{g}}^{\theta} \sim N^{1/4}(g+1)^{1/4}s^{1/4} \tag{2.6}$$

Similar other attempts were made to study the structure of dendrimers in various solvent conditions (Lyulin *et al.*, 2004b; Kłos and Sommer, 2009; Kroger *et al.*, 2010; Bosko and Prakash, 2008, 2011; Kłos and Sommer, 2013). It is clear from the expressions for R_{g} in different solvent conditions that the topological parameters g and s play a significant role in determining the size of branched polymers. The accurate method for studying the scaling of the radius of gyration is by changing g, s and N. However, when g is fixed, equations 2.5 and 2.6 reduce to the scaling laws for the radius of gyration of linear chains. For example, by varying s, $R_{\mathrm{g}} \sim N^{3/5}$ and $R_{\mathrm{g}} \sim N^{1/2}$ are obtained for athermal and theta solvents respectively at a fixed generation number (Bosko and Prakash, 2011; Giupponi and Buzza, 2004). This is because, in the case of a large number of spacers, dendrimer arms are expected to exhibit the same scaling behaviour as that of linear chains in similar solvent conditions.

The size of symmetric dendrimers in theta state with fixed values of s and m was exactly calculated by La Ferla (1997). The analytical expression for the mean squared radius of gyration of freely jointed symmetric dendrimers with $s = 1$ and $m = f - 1$ is given below:

$$\left\langle R_{\mathrm{g}}^2 \right\rangle = b_k^2 \frac{f[c^2(fhm - fh - f - m) + c(2f + fh - fhm - h + m^2h) - f + m]}{(fc - f + m - 1)^2(m-1)} \tag{2.7}$$

where $c = m^h$ and $h = g + 1$. b_k is the length of a spring given by $b_k^2 = 3\dfrac{b}{b+5}$.

Some of these theories have been validated for dendrimers in our simulations in Chapter 4. Due to their unique structure, tunable size and functionalities, dendrimers have been explored as carriers for targeted drug delivery, templates for synthesizing metal nanoparticles and in gene therapy. However, the movement of such tracers in complex environments has not been studied extensively. Rather most research focuses on the usage of nanoparticles as probe particles and several theories have been developed in this context, which are discussed below.

While the primary objective of this thesis is to compare the dynamics of bacteriophages in mucus with those of dendrimers within a polymer network, we have also analysed our results in the context of established theories for nanoparticles in similar environments. This comparison is achieved by varying dendrimer parameters, with our findings presented in Chapters 5 and 6.

The following chapter details the simulation algorithm, various interactions incorporated into our simulations and the properties evaluated in the subsequent chapters.

Chapter 3

Simulation details

In this chapter, the details of the governing equations, the various interactions included between polymer segments and the expressions for the various properties calculated are discussed.

3.1 Governing BD equations

Polymers in this study were modelled using the coarse-grained bead-spring chain model, with N_b beads connected by $N_b - 1$ springs (Bird *et al.*, 1987a). The simulated semidilute solution contains N_c^{lc} linear chain molecules with N_b^{lc} beads and N_c^{d} dendrimers with N_b^{d} beads, immersed in an incompressible Newtonian fluid. This system is contained in a cubic, periodic simulation box of length L and volume V, where $V = L^3$. The total monomer concentration in a simulation box is given by $c = N/V$, where N is the total number of monomers in the box given by $N = (N_c^{lc} \times N_b^{lc}) + (N_c^{d} \times N_b^{d})$. The Itô stochastic differential equation, which is the governing equation in Brownian dynamics simulations, provides the bead position vectors $\mathbf{r}_\mu$ ($\mu = 1, 2, ..., N$) as a function of time. The Euler integration algorithm form of this equation is given below:

$$\mathbf{r}_\mu(t + \Delta t) = \mathbf{r}_\mu(t) + \frac{\Delta t}{4} \sum_{\nu=1}^{N} \mathbf{D}_{\mu\nu} \cdot (\mathbf{F}_\nu^{s} + \mathbf{F}_\nu^{SDK}) + \frac{1}{\sqrt{2}} \sum_{\nu=1}^{N} \mathbf{B}_{\mu\nu} \cdot \Delta\mathbf{W}_\nu \tag{3.1}$$

Here the length and time non-dimensionalization factors are $l_H = \sqrt{k_B T/H}$ and $\lambda_H = \zeta/4H$, respectively, where k_B is the Boltzmann constant, T is temperature, H is the spring constant, and $\zeta = 6\pi\eta_s a$ is the Stokes friction coefficient of a spherical bead with radius a and η_s is the solvent viscosity. In equation 3.1, $\boldsymbol{D}_{\nu\mu}$ is the diffusion tensor, defined as $\boldsymbol{D}_{\nu\mu} = \delta_{\mu\nu}\boldsymbol{\delta} + \boldsymbol{\Omega}_{\mu\nu}$, where $\delta_{\mu\nu}$ is the Kronecker delta, $\boldsymbol{\delta}$ is the unit tensor, and $\boldsymbol{\Omega}_{\mu\nu}$ is the hydrodynamic interaction tensor. $\boldsymbol{B}_{\mu\nu}$ is a non-dimensional tensor whose evaluation requires the decomposition of the diffusion tensor and $\Delta\boldsymbol{W}_\nu$ is a non-dimensional Wiener process with mean zero and variance Δt. If $\mathcal{D}$ and $\mathcal{B}$ are block matrices consisting of $N \times N$ blocks each having dimensions of 3×3, with the (μ, ν)-th

block of $\mathcal{D}$ containing the components of the diffusion tensor $\boldsymbol{D}_{\mu\nu}$, and the corresponding block of $\mathcal{B}$ being $\boldsymbol{B}_{\mu\nu}$, the decomposition rule for obtaining $\mathcal{B}$ is then given by $\mathcal{B} \cdot \mathcal{B}^{\mathrm{T}} = \mathcal{D}$.
The spring force exerted on individual beads is represented by $\mathbf{F}_{\nu}^{\mathrm{s}}$. We have used finitely extensible nonlinear elastic (FENE) springs and the spring potential is given by,

$$U_{\mathrm{FENE}} = -\frac{1}{2}Q_0^2 \ln\left(1 - \frac{r^2}{Q_0^2}\right) \tag{3.2}$$

where Q_0 is the dimensionless maximum stretchable length of a single spring, and $k_B T$ is used to non-dimensionalize energy.

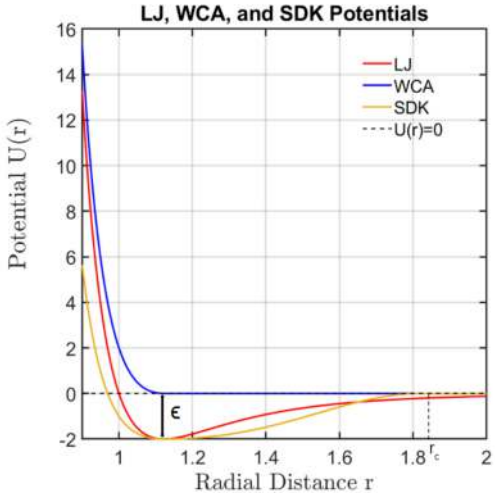

Figure 3.1: A comparison between the LJ, WCA and SDK potentials with well depth, $\epsilon = 2$, $\sigma = 1$ and cut off radius, $r_c = 1.82$ for SDK.

The force due to the excluded volume interactions between bead pairs is denoted by $\mathbf{F}_{\nu}^{\mathrm{SDK}}$ and is calculated using the Soddemann-Dünweg-Kremer (SDK) potential (Soddemann *et al.*, 2001), U_{SDK}, given below (plotted in Figure 3.1):

$$U_{\mathrm{SDK}} = \begin{cases} 4\left[\left(\frac{\sigma}{r}\right)^{12} - \left(\frac{\sigma}{r}\right)^{6} + \frac{1}{4}\right] - \epsilon; & r \leq 2^{1/6}\sigma \\ \frac{1}{2}\epsilon\left[\cos\left(\alpha\left(\frac{r}{\sigma}\right)^{2} + \beta\right) - 1\right]; & 2^{1/6}\sigma \leq r \leq r_c \\ 0; & r \geq r_c \end{cases} \tag{3.3}$$

Here, ϵ is the well depth of the potential which controls the interaction strength between bead pairs and the non-dimensional distance σ is fixed as 1 in this study. The repulsive part of this potential is modelled by a truncated Lennard-Jones (LJ) potential and the attractive part is modelled using a cosine function. The constants α and β are determined from boundary conditions, $U_{\mathrm{SDK}} = 0$ at $r = r_c$ and $U_{\mathrm{SDK}} = -\epsilon$ at $r = 2^{1/6}\sigma$ which is the minima of the potential.

The cut-off radius r_c was taken to be 1.82σ, following the discussion in work by Santra *et al.* (2019). The advantage of using the SDK potential is that by varying a single parameter ϵ, a range of solvent qualities can be studied and it affects the attractive part of the potential without altering the repulsive force. Also, the short-ranged attractive tail of this potential smoothly approaches zero, unlike the LJ potential. At $\epsilon = 0$, the SDK potential reduces to the purely repulsive Weeks-Chandler-Anderson (WCA) potential. A comparison between the LJ, WCA and SDK potentials is shown in Figure 3.1. Note that in this study, $\epsilon = 0$ for all the repulsive interactions (athermal conditions) and $\epsilon > 0$ for attractive (between stickers) interactions.
We use the regularized Rotne-Prager-Yamakawa (RPY) tensor to compute hydrodynamic interactions (HI),

$$\mathbf{\Omega}_{\mu\nu} = \mathbf{\Omega}(\mathbf{r}_{\mu\nu}) \tag{3.4}$$

where $\mathbf{r}_{\mu\nu} = \mathbf{r}_\mu - \mathbf{r}_\nu$ and the function $\mathbf{\Omega}$ is

$$\mathbf{\Omega}(\mathbf{r}) = \Omega_1 \boldsymbol{\delta} + \Omega_2 \frac{\mathbf{rr}}{r^2} \tag{3.5}$$

with

$$\Omega_1 = \begin{cases} \dfrac{3\sqrt{\pi}}{4}\dfrac{h^*}{r}\left(1 + \dfrac{2\pi}{3}\dfrac{h^{*2}}{r^2}\right) & \text{for} \quad r \geq 2\sqrt{\pi}h^* \\ 1 - \dfrac{9}{32}\dfrac{r}{h^*\sqrt{\pi}} & \text{for} \quad r \leq 2\sqrt{\pi}h^* \end{cases}$$

and

$$\Omega_2 = \begin{cases} \dfrac{3\sqrt{\pi}}{4}\dfrac{h^*}{r}\left(1 - \dfrac{2\pi}{3}\dfrac{h^{*2}}{r^2}\right) & \text{for} \quad r \geq 2\sqrt{\pi}h^* \\ \dfrac{3}{32}\dfrac{r}{h^*\sqrt{\pi}} & \text{for} \quad r \leq 2\sqrt{\pi}h^* \end{cases}$$

The hydrodynamic interaction parameter h^* gives the dimensionless bead radius in the bead-spring model and is defined as $h^* = a/(\sqrt{\pi k_B T/H})$. The Brownian Dynamics (BD) simulation code used in this work is based on the GPU-accelerated Python package named HOOMD-Blue, developed at Michigan University (Anderson *et al.*, 2020) for the study of colloidal suspensions. It has been modified recently to study the dynamics of associative polymer solutions (Robe *et al.*, 2024) and branched polymer architecture (Mariya *et al.*, 2024) along the lines of an earlier in-house BD code based on the Molecular Modelling ToolKit (Jain *et al.*, 2012, 2015; Santra *et al.*, 2021). The decomposition of the diffusion tensor, which is computationally demanding, has been efficiently implemented recently using the Positive Split Ewald algorithm (PSE) (Fiore *et al.*, 2017), which is available as a plugin to HOOMD-Blue.

3.2 Sticker parameters

There are three important interaction parameters related to each sticker in the simulation:

- Sticker strength: The strength of interaction between two stickers is determined by the well depth (ϵ) of the SDK potential. A higher well depth implies a stronger sticker as shown in Figure 3.2.

- Sticker functionality: The maximum number of stickers to which a reference sticker can adhere is referred to as its functionality. In this study, the functionality of all stickers is set to one.

- Sticker species: As mentioned in the model description, there are 3 types of stickers in our simulations. The stickers that interact, i.e. A-A and B-C types, have a finite well depth for the SDK potential, ϵ_N and ϵ_d respectively. The homopolymer beads and non-interacting stickers repel each other, hence the well depth of the potential, $\epsilon_{bb} = 0$.

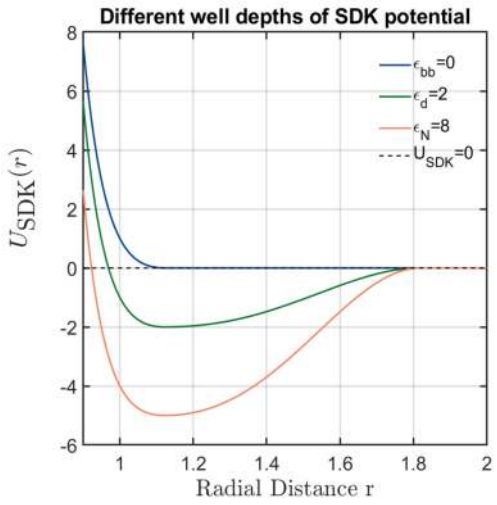

Figure 3.2: A comparison between the well depth of SDK potential for various stickers. ϵ_{bb} is the well depth for all the EV interactions, A-B, A-C, B-B and C-C sticker interactions. ϵ_N and ϵ_d are for A-A and B-C interactions respectively.

The process of binding and unbinding of stickers is determined using a simple Monte Carlo (MC) process. This is applicable only in the case of sticker pairs A-A and B-C. When two unstuck stickers are within the cutoff radius, the energy change (ΔE) due to a potential association is calculated. If a pseudo-random number, drawn between 0 and 1 from a uniform distribution, is less than the Boltzmann factor $\exp(-\Delta E/k_B T)$, the stickers are allowed to bind. Bond breakage is also attempted similarly in the update sweep. If at least one of the 2 stickers within the cutoff radius is stuck already, new bond formation is not attempted. The MC and BD steps are carried out alternately, and care has been taken to maintain detailed balance. This algorithm is similar to that developed by Robe *et al.* (2024).

Using the multi-species Brownian Dynamics algorithm developed, we calculated several properties related to the linear chains and dendrimers. The expressions for the static and dynamic properties studied are described below.

3.3 Definition of static and dynamic properties

Radius of gyration and correlation length

The radius of gyration of dendrimers and linear chains in the solution is calculated using the expression

$$R_g^2 = \frac{1}{N_b}\langle \sum_{i=1}^{N_b} (\mathbf{R}_i - \mathbf{R}_{CM})^2 \rangle \; ; \; N_b \in \{N_b^d, N_b^{lc}\} \tag{3.6}$$

where R_{CM} is the centre of mass of the molecule given by

$$\mathbf{R}_{CM} = \frac{1}{N_b} \sum_{i=1}^{N_b} \mathbf{R}_i \tag{3.7}$$

We introduce a quantity χ, which is the ratio of the radius of gyration of dendrimer (R_{g0}^d) to that of the linear chain (R_{g0}^{lc}) in the background, both in the dilute limit, given by $\chi = \left(R_{g0}^d / R_{g0}^{lc}\right)$. The overlap concentration, c^*, of a polymer solution is defined in terms of the radius of gyration of the polymer in the dilute limit, given by $c^* = \left(N_b/(4/3)\pi R_{g0}^3\right)$. In this study, the solution contains polymers of two architectures. Therefore, c^* can be estimated separately for each of them (c_d^* for dendrimers and c_{lc}^* for linear chains) given by:

$$c_d^* = \frac{N_b^d}{\frac{4}{3}\pi (R_{g0}^d)^3} \tag{3.8}$$

$$c_{lc}^* = \frac{N_b^{lc}}{\frac{4}{3}\pi (R_{g0}^{lc})^3} \tag{3.9}$$

Another important length scale in the solution is the correlation length (ξ). It is defined in terms of the radius of gyration in the dilute limit, the overlap concentration of linear chains, and the total monomer concentration in the solution (Colby and Rubinstein, 2003),

$$\xi = R_{g0}^{lc} \left(\frac{c}{c_{lc}^*}\right)^{\frac{-\nu}{(3\nu-1)}} \tag{3.10}$$

where ν is the Flory exponent, assumed here to be equal to 0.588. Note that the total monomer concentration c, includes monomers of both species in the system.

Relative shape anisotropy and the universal ratio U_{RD}

This work aims to compare the dynamics of dendrimers to nanoparticles, and therefore, it is essential to understand the influence of dendrimer parameters on their shape and compactness. Two important measures that can be used to probe these are the relative shape anisotropy (κ^2) and the dimensionless ratio U_{RD}.

The relative shape anisotropy, one of the shape functions, has been used to understand the asymmetry in the shape of polymer molecules. It is defined in terms of the eigenvalues, $\lambda_1^2, \lambda_2^2, \lambda_3^2$, of the gyration tensor $\mathbf{G}$ given by

$$\mathbf{G} = \frac{1}{2N^2} \sum_{\mu=1}^{N} \sum_{\nu=1}^{N} \mathbf{r}_{\mu\nu} \mathbf{r}_{\mu\nu} \tag{3.11}$$

Here $\lambda_1^2, \lambda_2^2, \lambda_3^2$ are arranged in ascending order. The relative shape anisotropy κ^2 is defined as (Theodorou and Suter, 1985; Bishop and Michels, 1986; Kumari *et al.*, 2020):

$$\kappa^2 = 1 - 3 \left[\frac{\langle I_2 \rangle}{\langle I_1^2 \rangle} \right] \tag{3.12}$$

where $I_1 = \lambda_1^2 + \lambda_2^2 + \lambda_3^2$ and $I_2 = \lambda_1^2\lambda_2^2 + \lambda_2^2\lambda_3^2 + \lambda_1^2\lambda_3^2$. $\kappa^2 = 0$ for a spherically symmetric molecule while it is equal to one for a rod-shaped molecule.

U_{RD}, which is a measure of the hard sphere-like behaviour of molecules, is given by

$$U_{\mathrm{RD}} = \frac{R_{\mathrm{g}}}{R_{\mathrm{H}}} = \frac{4\,D\,R_{\mathrm{g}}}{h^* \sqrt{\pi}} \tag{3.13}$$

where R_{H} is the hydrodynamic radius of the molecule related to its long time diffusivity, D, by $R_{\mathrm{H}} = \dfrac{h^* \sqrt{\pi}}{4D}$. For a polymer chain, U_{RD} is approximately 1.4 (Kröger *et al.*, 2000; Sunthar and Prakash, 2006; Pan *et al.*, 2014) while for a hard sphere, it is 0.77 (Guinier *et al.*, 1955).

Intra-molecular bead density

The internal bead density, obtained from the arrangement of beads about the centre of mass of the molecule, leads to an understanding of its internal structure. It is calculated by counting the number of beads along the major axis of the gyration tensor in intervals of fixed length and binning them. This requires all polymer configurations in the simulation ensemble to be aligned along their respective major axes. The linear bead number density obtained is given by:

$$\rho_{\mathrm{l}}(r) = \frac{n_{\mathrm{b}}(x + \Delta x) - n_{\mathrm{b}}(x)}{\Delta x} \tag{3.14}$$

where $n_{\mathrm{b}}(x)$ is the number of beads of a molecule within a distance x along the major axis, and Δx is the length of the fixed interval.

Mean squared displacement and diffusivity

The mean squared displacement of the centre of mass of the polymer molecules in solution is calculated using the following expression

$$\mathrm{MSD}(\Delta t) = \langle |\mathbf{R}_{\mathrm{CM}}(t + \Delta t) - \mathbf{R}_{\mathrm{CM}}(t)|^2 \rangle = 6\, D\, t^{\alpha} \tag{3.15}$$

where $\mathbf{R}_{\mathrm{CM}}(t)$ and $\mathbf{R}_{\mathrm{CM}}(t + \Delta t)$ are the position vectors of the centre of mass of the molecule at times t and $t + \Delta t$ respectively, D is the diffusion coefficient and α is the diffusion exponent. $\alpha = 1$ for normal diffusion and the molecule exhibits subdiffusion if $\alpha < 1$. The long time diffusivity, D is estimated from the slope of the mean squared displacement versus time plots at longer times.

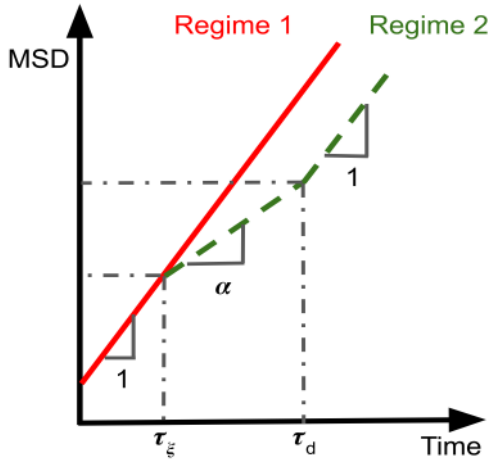

Figure 3.3: Schematic representation of the diffusive nature of dendrimers belonging to different size regimes. τ_{ξ} and τ_{d}, defined by eqn (3.16) and eqn (3.17), are the transition time scales to subdiffusive and diffusive behaviour respectively, for dendrimers with size larger than the solution correlation length (Regime-2). The exponents of time are indicated in the figure.

Cai *et al.* (2011) have identified several regimes for nanoparticles in entangled systems based on their size relative to the solution correlation length and the tube diameter. However, in the study of dendrimers in semidilute polymer solution, there are only two regimes based on the relative sizes of the dendrimer and correlation length: Regime-1 in which the dendrimer is smaller than the solution correlation length ($2R_{\mathrm{g}}^{\mathrm{d}} < \xi$) and Regime-2 in which the dendrimer size is larger than the correlation length ($2R_{\mathrm{g}}^{\mathrm{d}} > \xi$). It is important to note that, unlike a nanoparticle that has a constant size at all polymer concentrations, the size of a dendrimer is a concentration-dependent quantity.

The dynamics of dendrimers in the two regimes are different due to the influence of the surrounding linear chains as shown schematically in Fig 3.3. Following the arguments proposed by Cai *et al.* (2011), the following dynamics are expected in the two regimes:

1. Regime-1: When the size of the dendrimer is less than the correlation length ($2R_g^d < \xi$), it can diffuse freely through the solution, without being affected by the background linear chains. The diffusivity of a dendrimer is expected to be that experienced by it in the dilute limit (D_0) and exhibit normal diffusion at all time scales with the diffusion exponent, $\alpha = 1$. As a result, the mean squared displacement, MSD = $6\,D_0\,t$.

2. Regime-2: When the dendrimer is larger than correlation length, ($2R_g^d > \xi$), its dynamics is influenced by the presence of linear chains. The mean squared displacement shows three scaling regimes based on the time scale at which it is probed. At short times, the dendrimer does not experience any hindrance to its motion and therefore, exhibits normal diffusion. This continues up to a time of the order of the relaxation time of the correlation blob, τ_ξ given by:

$$\tau_\xi \equiv \eta_s \xi^3 / k_B T \tag{3.16}$$

   At times higher than τ_ξ, the dendrimer is trapped in cages formed by the linear polymers, and its motion is expected to become subdiffusive. Its dynamics are coupled to the motion of the centre of mass of the polymer and the polymer segmental relaxation times. The mean squared displacement of dendrimers at these intermediate times is given by MSD = $6\,D_\alpha\,t^\alpha$, where $\alpha < 1$. The subdiffusive regime extends until $t \sim \tau_d$, which is equal to the relaxation time of a chain segment with a size equal to the size of the dendrimer given by:

$$\tau_d \equiv \tau_\xi \left(2R_g^d/\xi\right)^4 \tag{3.17}$$

   Beyond τ_d, the dendrimer is set free due to the relaxation of linear chains and therefore the mean squared displacement is given by MSD = $6\,D\,t$. The diffusivity, D, in this regime, is referred to as the long-time diffusivity of the dendrimer.

Probability distribution function of displacement

Apart from the long-time diffusivity, the probability distribution function of displacement gives additional insight into the dynamics of the polymer molecules. The probability of a molecule displacing by a distance Δx in a time Δt is given by

$$\mathrm{P}(\Delta x, \Delta t) = \langle \delta\left(\Delta x - |x_{\mathrm{CM}}(t + \Delta t) - x_{\mathrm{CM}}(t)|\right)\rangle \tag{3.18}$$

where $x_{\mathrm{CM}}(t)$ and $x_{\mathrm{CM}}(t + \Delta t)$ are the x-components of the centre of mass of the molecule at times t and $t + \Delta t$, respectively.

In the next chapter, the various steps involved and the validation studies conducted at each stage of code development are discussed.

Chapter 4

Code validation

The necessary feature of a Brownian Dynamics algorithm to model phages in mucus networks is its ability to simulate different 'species' of polymers with arbitrary architectures. According to our model, this includes linear chains and dendrimers that are capable of interacting with each other to form inter- and intra-chain associations. The development of such an algorithm involved various stages which are discussed below along with the code validation studies.

4.1 Development of a multi-species code

The code previously used by our group was limited to simulating a single species of linear chains. Therefore, the first step of code development was to modify the existing code to simulate a homologous series of linear chains. At each stage, the mean squared displacement (MSD) and diffusivity from simulations were compared to the analytical values and results of the original single species code. For simplicity, we consider only two species of polymers in the simulation box, referred to as species A and species B. It should be noted that the code is set up such that there can be any number of species, each with any number of molecules.

The simplest system simulated was a single polymer bead (species A) diffusing through a dilute solution of linear chains (species B), the diffusivity of which can be calculated analytically. In these simulations, the background linear chains were 25 beads long and at a concentration of $c = 10^{-6}c^*$, where c^* is defined using equation 3.9. Excluded volume and hydrodynamic interactions were neglected and the diffusivity of the bead was calculated from the MSD vs time plot (Figure 4.1(a)). The analytical diffusivity in dimensionless units is $D_{\text{ana}} = 1/4$ (Bird *et al.*, 1987b) while that obtained from simulations is $D_{\text{sim}} = 0.224 \pm 0.007$. As the next step, the bead was replaced with a dumbbell, 2 beads connected by a FENE spring. The dimensionless diffusivity of a dumbbell is given by $D_{\text{ana}} = 1/4N = 1/8$ (Bird *et al.*, 1987b). The diffusion coefficient obtained from simulations was $D_{\text{sim}} = 0.1261 \pm 0.0003$ (Figure 4.1(b)).

In the subsequent study, both species A and B were linear chains of 5 beads connected by FENE springs. As both the chains are identical, they are expected to have the same size and diffusivity. Figure 4.1(c) shows the MSD of both species A and B, compared to that of a system of 5-bead chains simulated using the single species code at overlap concentration ($c = c^*$). Hydrodynamic interactions were present ($h^* = 0.2$) and the solvent was in theta conditions. The diffusivities calculated using the two codes are in agreement. Note that in these simulations, there is just one chain of species B, and hence the larger error bars on the data for species B. The total number of chains in the single-species and multi-species systems are the same. In Figure 4.1(d), the MSD of 5 bead chains in dilute solution in athermal solvent conditions with hydrodynamic interactions is shown. Both species A and B agree with the single species code results.

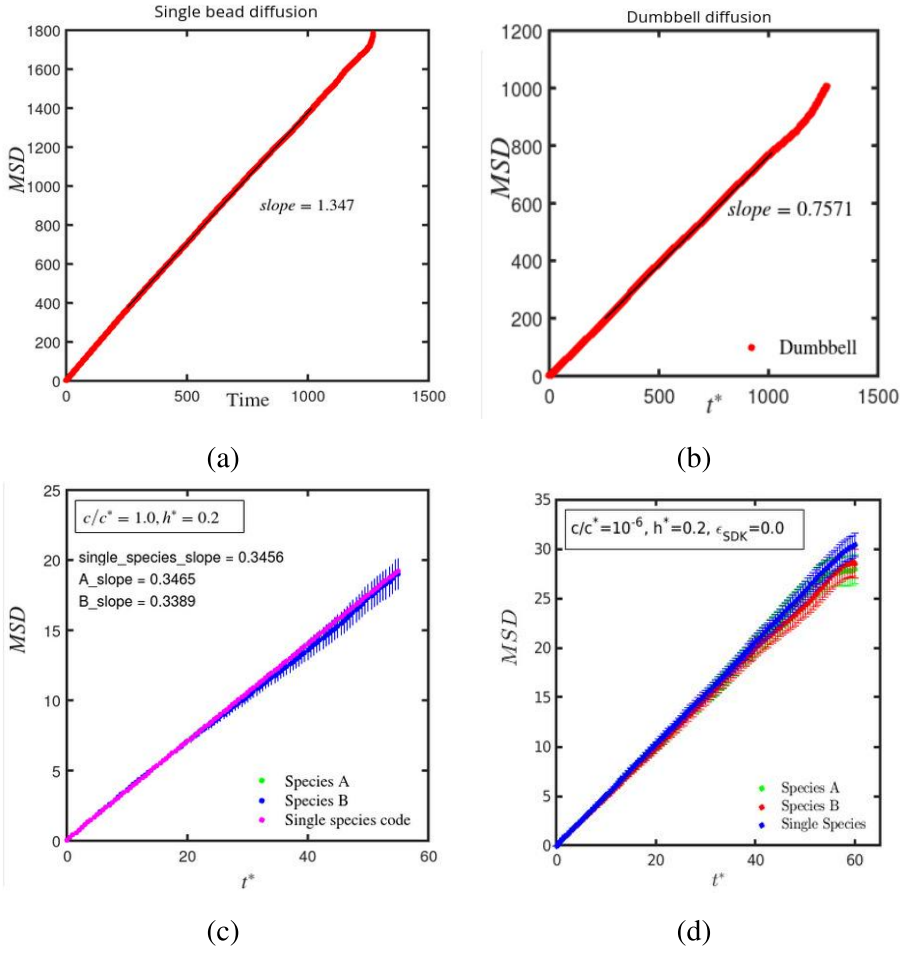

Figure 4.1: Code validations (a) The mean squared displacement of a single monomer bead through a dilute polymer solution. (b) The mean squared displacement of a dumbbell through a dilute polymer solution. (c) The mean squared displacement of a linear chain of type B in a semidilute solution of chains of type A under theta conditions. For simplicity, both the species have five beads each in them. (d) The mean squared displacement of two types of chains in dilute solution in athermal condition with hydrodynamic interactions. The results for the 2 species code in (c) and (d) are compared to results obtained using the single chain code.

4.2 Branched polymer architecture

The next step after obtaining a multi-species BD algorithm was to implement a branched polymer architecture. Every bead on the dendrimer molecule has a number tag. The central core bead is labelled zero. To assign bead numbers on a dendrimer, one of its arms is selected (tagged as arm 0). The beads along that arm are numbered sequentially, with continuous numbering within each 'generation shell'. The bead numbers for subsequent arms are obtained by adding the bead numbers on the first arm to the product of the number of springs on each arm ($N_{s,f}$) and the arm number. The bead numbering scheme along the dendrimer arms used in this model is shown in Figure 4.2. For example, in the figure, $N_{s,f} = 14$. The tag of bead equivalent to bead 6 on arm 2 is given by $6+(N_{s,f}\times\text{arm number}) = 6+(14\times2) = 34$. The preliminary simulation results obtained for dendrimers are compared to existing analytical theories discussed in Section 2.7.1 for such architectures. The two species code was used for all validations with one dendrimer type A and one of type B in solution, but both with the same architecture. Therefore, they are expected to have identical static and dynamic properties.

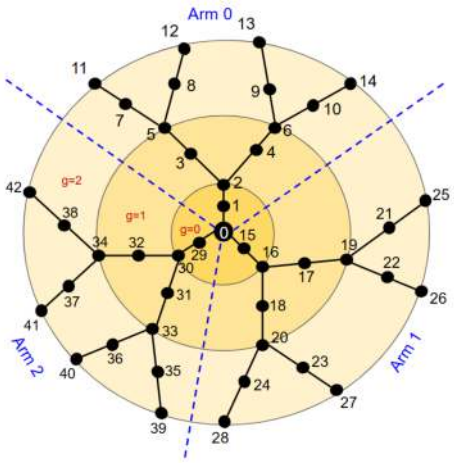

Figure 4.2: The figure shows the bead numbering in a generation two dendrimer with one spacer bead and functionality three.

4.2.1 Theta solvent

The theta solvent conditions can be achieved either by not including the excluded volume interactions (phantom chains) or by choosing well depth of the pairwise potential in such a way that the attractive forces are balanced by the repulsion between monomer beads. For linear chains, Santra *et al.* (2019) has shown that the well depth, $\epsilon_{SDK} = 0.45$, in the SDK potential gives theta solvent conditions. Experimental and computational studies in the past have shown that star polymers have the same theta temperature as that of their linear counterparts (Batoulis and

Kremer, 1988; Okumoto *et al.*, 1997, 1999; Bosko and Prakash, 2011). It is necessary to check if $\epsilon_{SDK} = 0.45$ produces theta conditions for dendrimers of all generations.

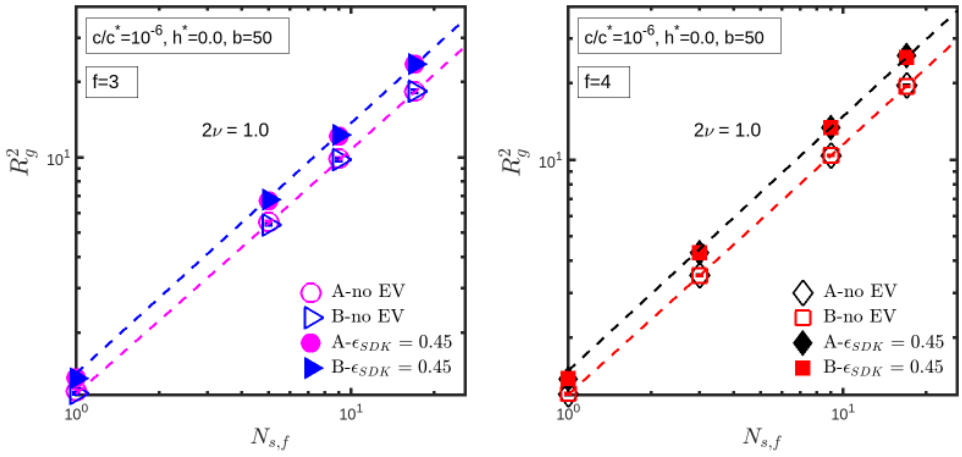

(a) (b)

Figure 4.3: Scaling of the radius of gyration of star polymers with functionality 3 (a) and 4 (b) as a function of $N_{s,f}$. The empty symbols represent the solution with no excluded volume interactions present (phantom chains), whereas the filled symbols represent the theta conditions simulated using the SDK potential at $\varepsilon_{SDK} = 0.45$. The red dashed line represents equation 4.1 and the black dashed lines represent scaling law with exponent 1.0.

The simplest dendrimer is a star polymer ($g = 0$), the number of monomers on which can be varied by changing the functionality or spacer length. In terms of these parameters, the radius of gyration of star polymer is as follows:

$$R^2_{g,\theta} = N_{s,f}\frac{(3f-2)(N_{s,f}+1)+1}{2f(N_{s,f}+1)} \tag{4.1}$$

In Figure 4.3, the radius of gyration of star polymers with functionality 3 and 4 obtained using the 2 species code for branched polymers is compared with the analytical expression given in equation 4.1. The theta conditions are simulated by not including the excluded volume interactions and using the SDK potential. It is evident from the values of the radius of gyration that star polymers are larger when SDK potential is used for θ conditions, which is expected. The black dashed line represents the scaling law $R^2_{g,\theta} \sim N^{2\nu}$ where $\nu = 0.5$, where N is the number of beads per molecule. This confirms that the θ temperature ($\epsilon_{SDK} = 0.45$) is the same for linear chains and star polymers in our simulations.

Similarly, in Figure 4.4, the radius of gyration of generation 1 and 2 dendrimers is plotted as a function of the total number of monomers in the molecule. Since g and m are fixed, N is varied by changing the spacer length s. Exact analytical expressions are not known for R_g as a function

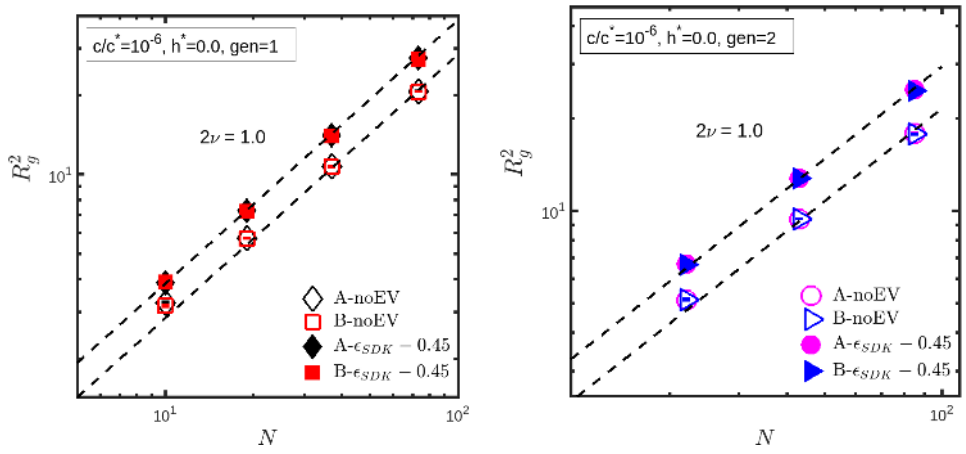

Figure 4.4: Scaling of the radius of gyration of dendrimers of generation 1 (a) and 2 (b) as a function of the total number of beads in a molecule in theta solvent conditions. The dashed lines represent scaling law with exponent 1.0.

of N for higher generation numbers, although the scaling is expected to be the same as that for linear chains in theta solvent (Bosko and Prakash, 2011).

Clearly, $\varepsilon_{SDK} = 0.45$ is the theta point for dendrimers similar to linear chains. In Figures 4.3 and 4.4, the size of the dendrimer is more when the theta state is obtained using the SDK potential compared to the case when EV is completely absent. This is because at the theta point of the SDK potential, the polymer monomer-monomer attraction is balanced by the excluded volume forces which results in an increase in size of the molecule compared to the completely collapsed state of phantom molecules. Also, the simulation results show a slight deviation from the scaling law (black and red dashed lines in Figure 4.4) at lower values of N due to finite chain effects.

As mentioned in Section 2.7.1, the size of a symmetric dendrimer can be exactly calculated using the La Ferla expression (equation 2.7). In Figure 4.5, the mean squared radius of dendrimers is plotted as a function of number of monomers in the molecule for $g = 0, 1, 2$. We have considered different functionalities ($f = 3, 4$) and FENE parameter ($b = 30, 70$). Agreement between the analytical predictions and simulation validates the model implemented in the code. Figure 4.6 shows agreement between equation 2.7 and simulations when the SDK potential is used to simulate theta conditions in the solution. The effect of the potential appears in the prefactor A in the expression $R_g = AN^{\nu}$. Therefore, we rescaled the simulation results with the ratio of prefactors, A^*, where $A^* = A_{noEV}/A_{SDK}$.

The dynamic properties of dendrimers in solution are primarily affected by hydrodynamic interactions. In the absence of HI, the drag experienced by a dendrimer molecule is equal to the

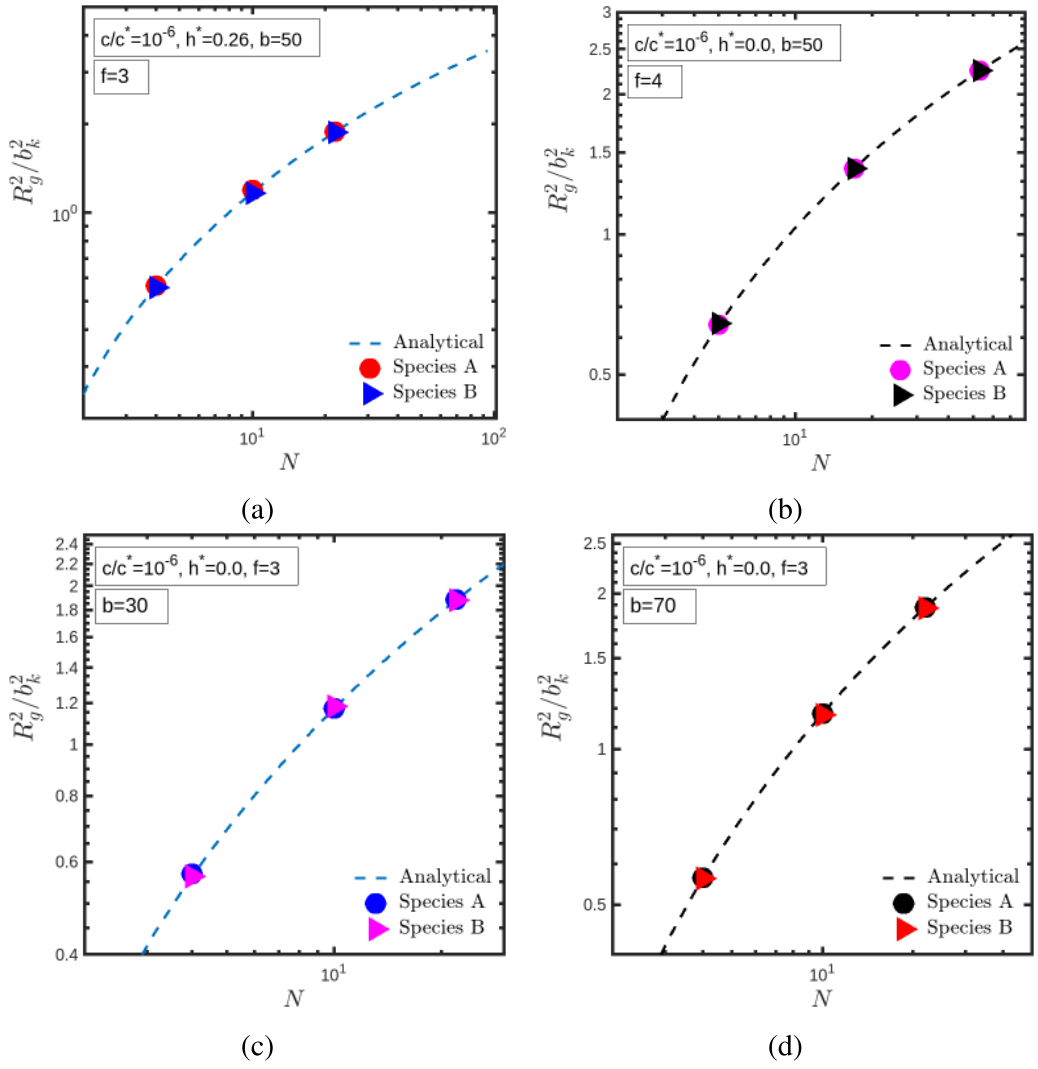

Figure 4.5: Comparison with La ferla expression for R_g of dendrimers. In the top panel, the FENE parameter $b = 50$, with functionality 3 (a) and 4 (b). In the bottom panel, the functionality is fixed ($f = 3$) and the FENE parameter is varied: $b = 30$ (c) and 70 (d). The dashed lines are the analytical expression 2.7.

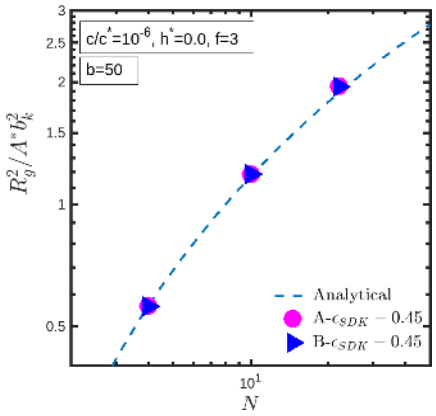

Figure 4.6: Comparison with La ferla expression for R_g of dendrimers with N using SDK potential for θ solvent condition. The three values of N correspond to $g = 0, 1, 2$.

sum of drag experienced by the individual beads in it. Therefore, self-diffusivity will scale as $D \sim 1/N$ (Bird *et al.*, 1987b). From Figure 4.7 it is clear that molecular topology does not play a role in determining the dynamics in the free-draining case. This is consistent with the computational results reported by Bosko and Prakash (2008).

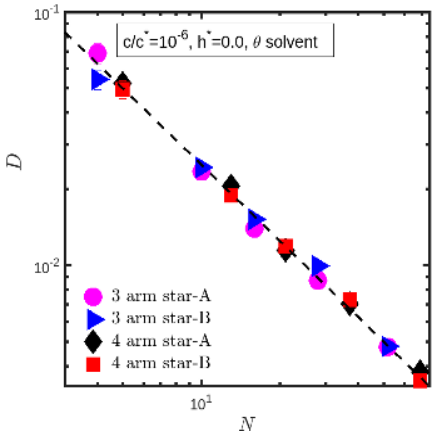

Figure 4.7: Scaling of D of star polymers of different functionalities in the free draining limit. The dashed line is the scaling law $D \sim 1/N$.

In the presence of hydrodynamic interactions, diffusivity scales as $D \sim N^{-0.5}$ for linear chains in theta solvent (Bird *et al.*, 1987b; Rubinstein and Colby, 2003). The same scaling is expected for star polymers with increasing arm length, keeping f fixed (Figure 4.8(a)). This is in agreement with Zimm predictions according to which the hydrodynamic radius scales as $R_H \sim N^{-0.5}$. However, dendrimers do not exhibit a single power law scaling when g is changed. Simulation results show that for smaller generation numbers, $D \sim N^{0.4}$ (Figure 4.8(b)) (Bosko and Prakash, 2008) which implies that the decrease in dendrimer diffusivity with molecular weight is slower than that observed in linear chains. The deviation from this scaling at higher generations is prob-

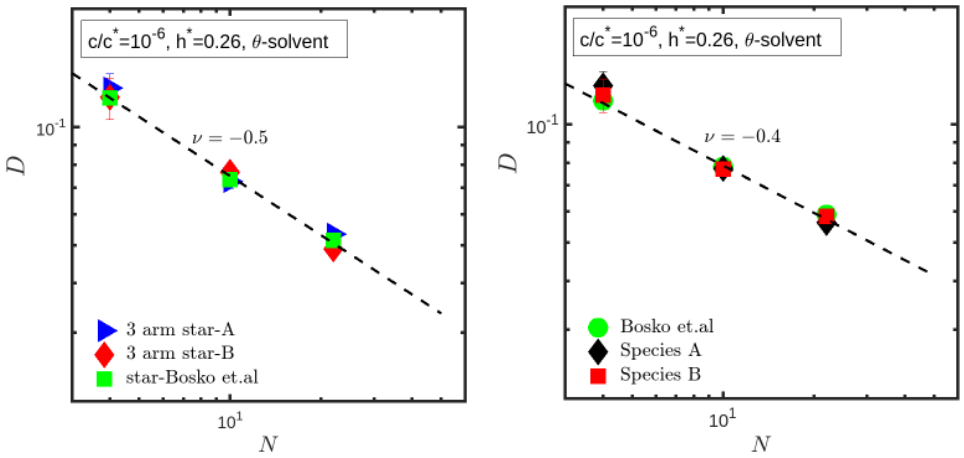

(a) (b)

Figure 4.8: Scaling of D of star polymers (a) and symmetric dendrimers (b) with N with hydrodynamic interactions ($h^* = 0.26$) in theta solvent conditions. Green symbols are the simulation results of Bosko *et al.*

ably due to the increased reduction in drag at higher generations (Bosko and Prakash, 2008). Similar values for the exponent have been reported by other experimental and computational works (Baille *et al.*, 2003; Rietveld and Bedeaux, 2000; Lyulin *et al.*, 2004a).

4.2.2 Athermal solvent

In a dilute polymer solution, the radius of gyration of linear chains exhibits a power law scaling with molecular weight, with the Flory exponent $\nu = 0.588$ for athermal solvent conditions. Even though a similar scaling law does not exist for dendrimers, it has been shown that with a fixed g and m, and varying spacer length, dendrimer size obeys the same scaling law (Bosko and Prakash, 2011). This has been attributed to the fact that with increasing spacer length, the shape of the dendrimer does not change. Instead, its size increases similar to linear chains as each segment in the dendrimer is essentially a linear chain of length s. This has been validated using our model as shown in Figure 4.9. The scaling of the radius of gyration of star polymers (Figure 4.9(a)), generation 1 and 2 (Figure 4.9(b)) is plotted as a function of a number of monomers per molecule. The athermal conditions are modelled using the SDK potential with well depth $\varepsilon_{SDK} = 0.0$ (Santra *et al.*, 2019). As expected, $R_g \sim N^{0.588}$ in athermal solvent. Note that the radius of gyration of a generation 2 dendrimer is smaller than that of a generation 1 dendrimer with a similar number of beads.

Similar to that in theta solvent conditions, the diffusivity of star polymers obeys a power law scaling with molecular weight, with an exponent similar to that of linear chains in an athermal

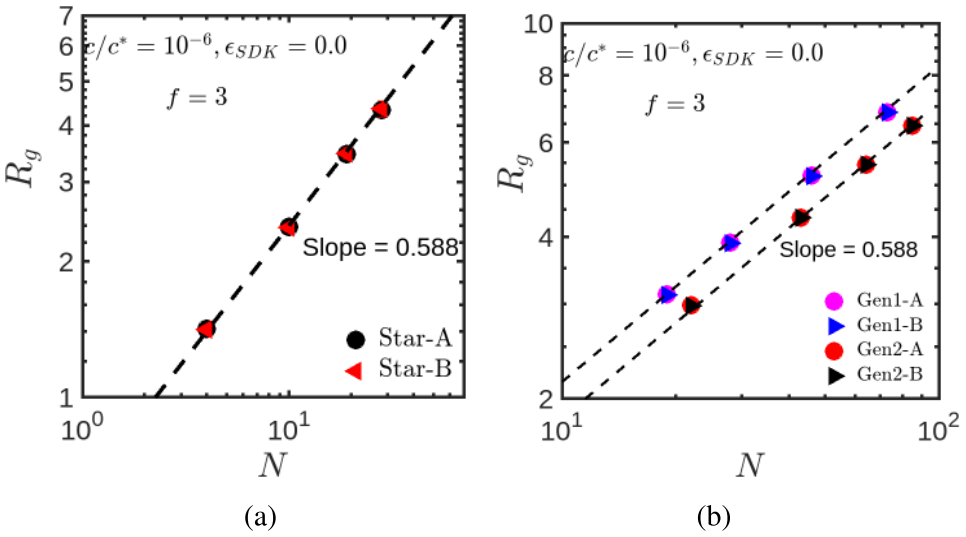

(a) (b)

Figure 4.9: Scaling of the radius of gyration of star polymers (a) and dendrimers (b) with N in athermal solvent. The functionality is 3 and order of dendra is 2 in all the cases reported. The dashed lines are scaling laws with exponent $\nu = 0.588$.

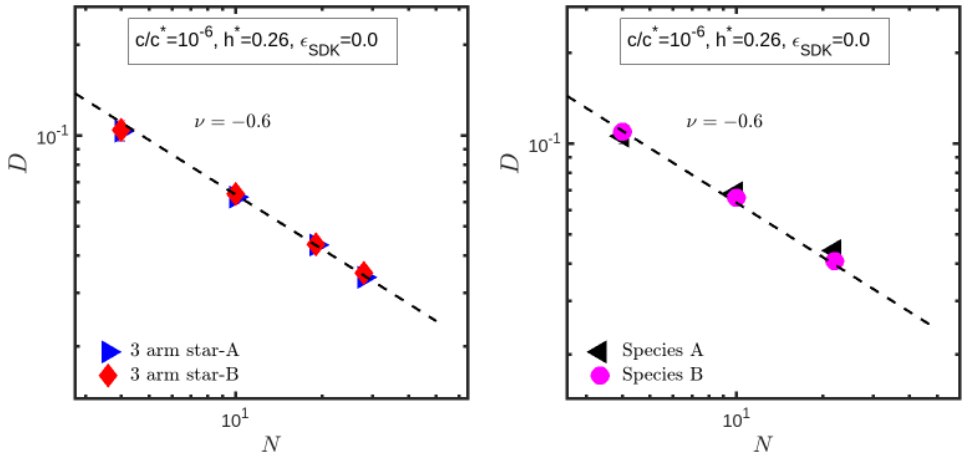

(a) (b)

Figure 4.10: Scaling of the diffusivity with the number of beads in a molecule in athermal solvent. (a) Star polymers with increasing spacer length. (b) Dendrimers with increasing generation number. The functionality is three in both the plots. The dashed line is the scaling law with exponent -0.6.

solvent. Therefore, $D \sim N^{-\nu}$ where ν is the Flory exponent equal to 0.588. However, with increasing generation number at a fixed f and m, the exponent is smaller than 0.588. It has been observed that the rate of decrease of D is less compared to that in linear chains due to branching in dendrimers (Bosko and Prakash, 2011). In Figure 4.10, the diffusivity is plotted as a function of number of monomer beads per molecule for a star polymer (at fixed f and varying s) and dendrimers of different generations (at fixed f and m). Our simulation results concur with those reported by Bosko and Prakash (2011).

4.3 Multi-sticker interactions

The code validation upto this point was carried out using the newly developed two-species code with two identical species. However, since the ultimate goal of this research is to have a mixture of linear chains and dendrimers, species 1 in the system was assigned as linear chains and species 2 as dendrimers. Finally, sticky beads were introduced on both the linear chains and dendrimers, which was implemented in 2 steps:

1. Formation of network: The type A sticker, which is responsible for forming a network, was included first. To validate this code, we compared the mean squared displacement of a dendrimer in solution with that in a network with the well depth $\epsilon_N = 0, 1$. At $\epsilon_N = 0$, the SDK potential is purely repulsive; therefore, the system is equivalent to a homopolymer solution. The dendrimer behaves the same in both systems as expected (shown in Figure 4.11 (a)). The well depth is so small at $\epsilon_N = 1$ that the stickers bind and unbind frequently. The dendrimer diffuses through the network as if no stickers were present even when the distance between stickers was reduced to less than the correlation length in the system calculated using equation 3.10 (Figure 4.11 (b)).

2. Interaction between dendrimers and linear chains: Stickers of types B and C, which are present on the linear chains and dendrimers respectively, interact with a sticker strength ϵ_d. In order to test the implementation of these stickers, we calculated the radius of gyration and mean squared displacement of sticky dendrimers at lower sticker strengths and compared it with that of a non-sticky dendrimer in homopolymer solution and network. The sticky and non-sticky dendrimers had the same values of radius of gyration (Figure 4.12 (a)) and mean squared displacement at similar concentrations (Figure 4.12 (b) and (c)), thus validating the code. In the figure, solution refers to $\epsilon_N = 0$ and network means $\epsilon_N = 6$.

The algorithm developed for polymers of arbitrary architectures interacting via sticky interactions has thus been validated. This algorithm was used to study three main systems: Non-sticky

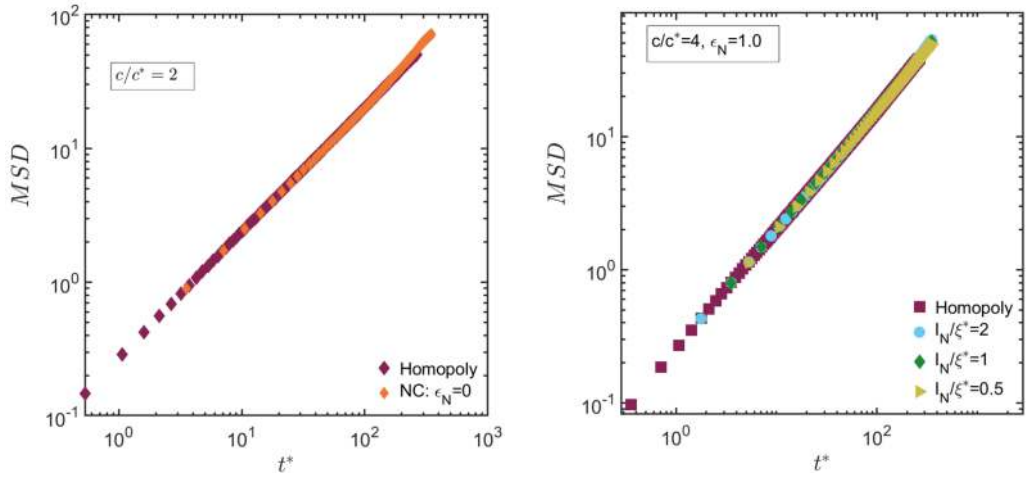

(a) (b)

Figure 4.11: The mean squared displacement of dendrimers in a network with sticker strength $\epsilon_N = 0$ (a) and $\epsilon_N = 1$ (b). 'NC' stands for new code which has stickers of 3 types and 'Homopoly' stands for a homopolymer dendrimer in solution.

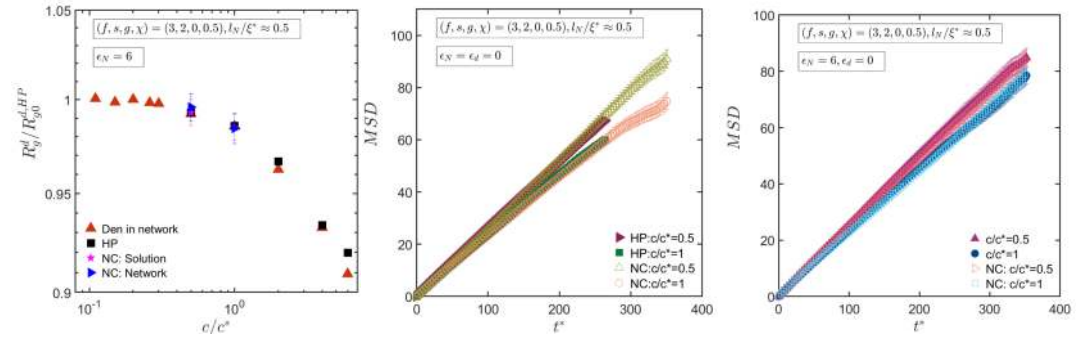

(a) (b) (c)

Figure 4.12: (a) The radius of gyration of sticky dendrimer in the network compared to a non-sticky dendrimer in network and solution. 'NC' stands for new code which has stickers of 3 types and 'HP' stands for a homopolymer dendrimer in solution. The sticker strength of B-C interaction, $\epsilon_d = 1$. The mean squared displacement of a sticky dendrimer in solution (b) and network (c) compared to that of a non-sticky dendrimer.

dendrimer in solution, non-sticky dendrimer in network and sticky dendrimer in network. The major findings of each of these investigations have been discussed in the following chapters of this thesis. In the next chapter, the static and dynamic properties of a non-sticky dendrimer in a semidilute solution of linear polymers obtained using the BD algorithm developed are discussed.

Chapter 5

Universal scaling of the diffusivity of dendrimers in a semidilute solution of linear polymers

The movement of tracer particles through crowded environments is an area of active research due to its applications in medicine and nanotechnology (Amblard *et al.*, 1996; Alai *et al.*, 2015; Salata, 2004; De *et al.*, 2008; Gomez-Solano *et al.*, 2016; Patteson *et al.*, 2015). Most research till date has focused on employing rigid nanoparticles as the tracer particle (Stark *et al.*, 2015; Kesharwani *et al.*, 2018; Aghebati-Maleki *et al.*, 2020; Mitchell *et al.*, 2021). However, recent biotechnological advances have enabled the use of dendrimers as drug delivery agents (Liu and Fréchet, 1999; Gillies and Frechet, 2005). Polymers of varying topology and soft colloids have also been used in biology where they diffuse in complex environments such as semidilute polymer solutions and networks of polymer chains (Baghbanbashi and Kakkar, 2022; Lee *et al.*, 2005). The movement of such tracers through crowded media has not been studied extensively. In this chapter, we use dendrimers as prototypical soft colloids, and examine their structural and dynamic properties when dissolved in a semidilute unentangled polymer solution shown schematically in Figure 5.1(a). By systematically varying the dendrimer architecture and the concentration of the background solution, the similarities and differences with previously reported behaviour of rigid nanoparticles in a similar environment are studied.

Dendrimers are often referred to as soft colloids as they act like a bridge between the floppy linear chains and hard spheres (Harreis *et al.*, 2003). The transition from linear chain-like behaviour to hard spheres is controlled by f, s, g and m (Vlassopoulos, 2004; Likos *et al.*, 1998). The molecular mass dependency of the self-diffusivity and intrinsic viscosity of low-generation dendrimers of fixed architecture follows the same power law scaling as for linear chains in dilute solution (Bosko and Prakash, 2011).

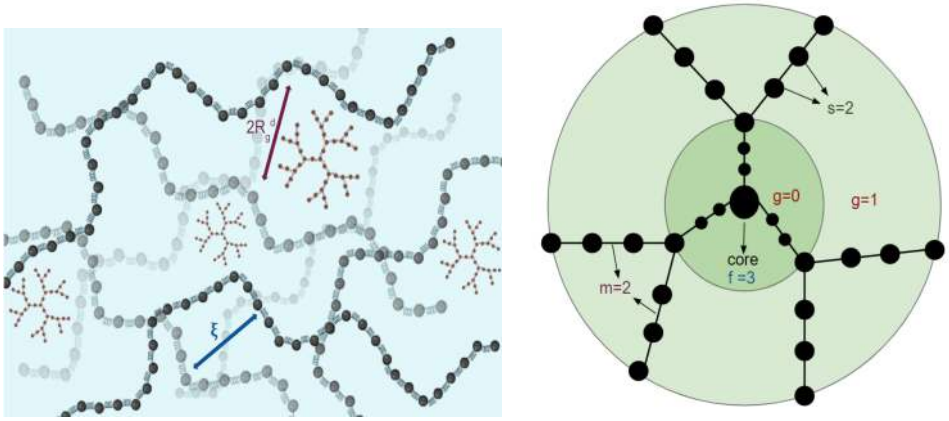

(a) (b)

Figure 5.1: Dendrimers in a solution of linear chains (a) Schematic representation of dendrimers in a solution of linear chains. The correlation length of the solution (ξ) and the size of dendrimer($2R_g^d$) are indicated. (b) A generation one ($g = 1$) dendrimer with functionality three ($f = 3$) and two spacer beads ($s = 2$). The order of dendra ($m = f - 1$) is two ($m = 2$). Beads belonging to each generation are included in a concentric circle.

Several theories have been developed over the past few years to describe the dynamics of nanoparticles in semidilute polymer solutions (Ge, 2023). Early theoretical studies of the diffusion of hard spheres in linear polymer solutions proposed a stretched exponential dependence of the reduced diffusion coefficient of the probe on the concentration of solution (Langevin and Rondelez, 1978; Cukier, 1984; Altenberger and Tirrell, 1984). This was modified by Phillies *et al.* (1989) to include the effect of size of the probe and the molecular weight of the linear polymers to obtain the generalized scaling relation $D/D_0 = \exp(-bR^u M^x c^y)$, where D and D_0 are the diffusion coefficients of the probe in the polymer solution and in the pure solvent, R is the size of the probe, M is the molecular weight of the polymer, c is the solution concentration, with exponents $u = 0 \pm 0.2$, $x = 0.8$ and y ranging from 0.5 to 1.0. However, these models do not account for the fluctuations in the mesh size and the size of the probe relative to the correlation length of the solution. Based on the works by de Gennes (1979) and Tong *et al.* (1997) which highlighted these factors, a scaling relation was proposed for probe diffusion through semidilute polymer solutions $D/D_0 = \exp\left[-\beta (R/\xi)^\delta\right]$ by Cheng *et al.* (2002). Here β is 2.2, δ is 0.95, and ξ is the correlation length of the polymer solution. Even though this theory could explain several experimental results, the regime with the size of the nanoparticle being comparable to that of the radius of gyration of the background polymers could not be captured.

Holyst and coworkers (Holyst *et al.*, 2009; Kalwarczyk *et al.*, 2015) introduced an effective size for the nanoparticle, which is a combination of its radius and the hydrodynamic radius of the polymers that determines its dynamics in this crossover regime. The scaling law for the long-

time diffusivity proposed by them is given by equation 2.2. According to this model, the length-scale of hydrodynamic flow in the solution determines the viscosity experienced by the probe particle and is equal to R_{eff}. The Holyst model has been validated by experiments (Kalwarczyk *et al.*, 2011; Sozański *et al.*, 2013) and simulations (Chen *et al.*, 2017).

Coupling theory, on the other hand, takes into account the coupling between the probe particle dynamics and the relaxation of the surrounding polymers (Cai *et al.*, 2011). According to this theory, probes larger than the correlation length of the solution get trapped in a polymer cage, thus leading to its subdiffusion at intermediate time scales. At longer times, the particle is set free as the polymer relaxes, with the diffusion coefficient scaling as d_{NP}/ξ^{-2}, where d_{NP} is the diameter of the nanoparticle. Recent experiments on nanoparticle diffusion in a partially hydrolyzed polyacrylamide solution indicate that the long-time diffusivity and short-time dynamics of particles larger and smaller than the correlation length show agreement with the predictions of the coupling theory (Poling-Skutvik *et al.*, 2015). However, the diffusion exponents of particles with a size comparable to the characteristic length scale of the solution were much higher than the predictions of the coupling theory. This discrepancy was resolved in a recent Multi-Particle Collision Dynamics (MPCD) study in which the dynamics of nanoparticles were found to be coupled to the dynamics of the centre of mass of the polymers, thus giving it an additional mechanism to move through the polymer solution (Chen *et al.*, 2018). The diffusion exponents of the nanoparticle and the polymer centre of mass were found to be correlated even in the absence of many-body hydrodynamic interactions. Coupling theory has also been supported by simulations (Chen *et al.*, 2018) and experiments (Poling-Skutvik *et al.*, 2015) on various systems.

The behaviour of dendrimers in a semidilute solution of linear polymers has not been studied extensively. Experiments have shown that the size of higher generation dendrimers does not change significantly with concentration (Cheng *et al.*, 2002) and, therefore, can be considered as a hard sphere. The dynamics of such dendrimers were shown to follow the Holyst model in semidilute solutions of linear chain polymers (Cheng *et al.*, 2002; de Kort *et al.*, 2015). However, the question of whether these theories can be applied to a low generation dendrimer, whose size is a function of the solution concentration, has not been addressed so far. In the current study, we have simulated low generation dendrimers in unentangled semidilute solutions of linear chain polymers in athermal solvent conditions using Brownian dynamics simulations. Dendrimer parameters like the generation number, functionality, and number of spacer beads were varied to understand their effects on the shape and internal bead arrangements of dendrimers in dilute solutions. We also studied the effect of the concentration of linear chains on the size and dynamics of dendrimers in semidilute solutions. It should be noted that the focus of this work is semidilute unentangled polymer solutions in which hydrodynamic interactions

(HI) are significant. To understand its effect on the dynamics of dendrimers, we have performed simulations with and without HI. The algorithm used in this work is not appropriate for entangled concentrated systems since entanglements have not been taken into account. In the concentrated-entangled regime, hydrodynamic interactions are screened and there is no need to incorporate them in the simulation algorithm. Several studies on nanoparticles in entangled and concentrated polymer solutions(Cai *et al.*, 2011) and networks(Cai *et al.*, 2015) reported characteristic features which cannot be derived directly from the results in this work. However, there is very little literature on the dynamics of these systems, especially for dendrimers, where HI plays an important role.

5.1 Details of the simulation parameters

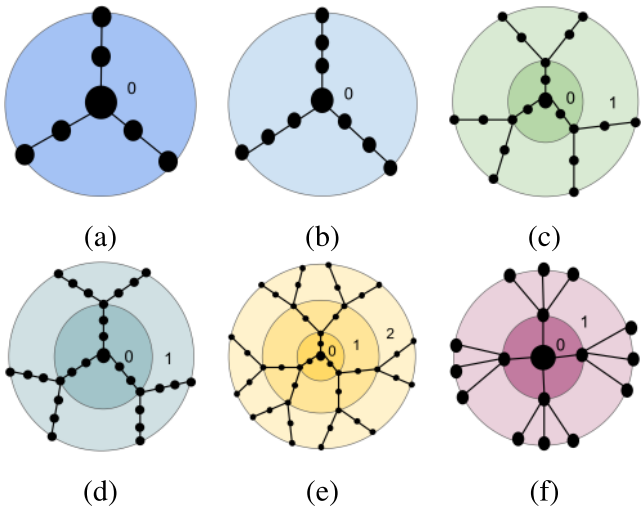

Figure 5.2: The various dendrimer architectures simulated in this study. The specific simulation parameters corresponding to the topologies (a) to (f) are given in Table 5.1

To choose the simulation system, we fixed the dendrimer architecture first and calculated the number of beads (N_b^d) on each dendrimer molecule. The various architectures chosen are given in Figure 5.2. The radius of gyration of dendrimers was determined by carrying out simulations in the dilute limit, and the values are reported in Table 5.1. Depending on the choice of the ratio between the radius of gyration of the dendrimer and linear chain, χ, we calculated the radius of gyration of the linear chain. The number of beads on the linear polymer was then estimated by running simulations in the dilute limit and reading off the value of N_b^{lc} from the R_g^{lc} vs N_b^{lc} plot (see Figure A.1). The simulation box length, L was chosen to be $L \geq 2R_e$, where R_e is the end-to-end distance of linear chains in the solution. This ensures that the molecules do not wrap around themselves. Simulations were carried out keeping the dendrimer concentration fixed and

Table 5.1: List of dendrimer parameters and linear chain lengths used in each system. g is the generation number, f is the functionality, s is the number of spacer beads, N_b^d is the number of beads in a dendrimer molecule, R_{g0}^d is the radius of gyration of the dendrimer in the solvent, χ is the ratio between the radius of gyration of dendrimers and linear chains in dilute limit, N_b^{lc} is the number of beads in the background linear chain, R_{g0}^{lc} is the radius of gyration of the linear chain. Note that dendrimer topologies in (c) and (h) are identical, but have different χ.

	f	s	g	N_b^d	R_{g0}^d	χ	N_b^{lc}	R_{g0}^{lc}
a	3	1	0	7	1.90	0.50	19	3.90
b	3	2	0	10	2.40	0.50	26	4.80
c	3	1	1	19	3.12	0.46	43	6.23
d	3	2	1	28	3.88	0.46	61	7.77
e	3	1	2	43	4.34	0.50	74	8.68
f	4	0	1	17	2.49	1.0	9	2.49
h	3	1	1	19	3.12	1.0	13	3.12

adding linear chains to the simulation box to increase the concentration of the solution. Hence, the resulting solution is always dilute in dendrimer concentration and semidilute in linear chains. The list of chain lengths, dendrimer parameters, and number of chains in each simulation are given in Table 5.1. All the dendrimers simulated in this study were symmetric, $m = f - 1$.

One special case we studied is a $f = 4, g = 1, s = 0$ dendrimer. By increasing the number of arms and reducing the spacer beads, we expect it to be more closely packed compared to the rest of the dendrimers, and thus behave qualitatively more like a nanoparticle. The concentration of linear chains was varied from 0.5 to $6c^*$. All simulations were carried out in athermal solvent conditions ($\epsilon = 0$) and the hydrodynamic interaction parameter, $h^* = 0.2$. When hydrodynamic interactions are not present (the free draining case), h^* is set equal to zero, so the RPY tensor is not invoked and the diffusion tensor simplifies to $\boldsymbol{D}_{\mu\nu} = \delta_{\mu\nu}\boldsymbol{\delta}$. The maximum stretchable length of each spring, $Q_0^2 = 50.0$, for all simulations. Every independent trajectory had an equilibration phase of 8 relaxation times followed by a production phase of 10 relaxation times with non-dimensional time step, $\Delta t = 10^{-3}$ to 10^{-4}. The dynamic properties were calculated as a function of time in the production phase of individual trajectories. Ensemble averages and

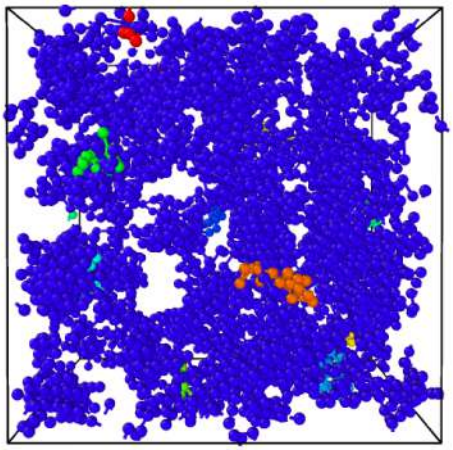

Figure 5.3: Snapshots from simulation of $f = 3, s = 1, g = 1$ dendrimer with $\chi = 0.46$ at $c/c^*_{\mathrm{lc}} = 1$. The blue beads belong to linear chains and other coloured beads belong to dendrimers.

error estimates were calculated over 700 to 2000 independent trajectories. Figure 5.3 shows a snapshot of a simulation box containing generation 1 dendrimers and linear chains at $c/c^*_{\mathrm{lc}} = 1$.

5.2 Results and Discussion

5.2.1 Radius of gyration

According to the blob theory for polymers, the radius of gyration of linear chain polymers reduces with an increase in concentration and follows the scaling law (Daoud *et al.*, 1975; Doi *et al.*, 1988; Huang *et al.*, 2010):

$$R^{\mathrm{lc}}_{\mathrm{g}} = R^{\mathrm{lc}}_{\mathrm{g0}} \left(\frac{c}{c^*_{\mathrm{lc}}} \right)^{\frac{1-2\nu}{2(3\nu-1)}} \tag{5.1}$$

On plotting the ratio $R_{\mathrm{g}}/R_{\mathrm{g0}}$ of dendrimers and linear chains as a function of the total monomer concentration, c, in solution normalized by the overlap concentration of linear chains, c^*_{lc}, dendrimers seem to shrink at a slower rate compared to the linear chains (inset to Figure 5.4(a)). However, if the normalizing factor for monomer concentration is the overlap concentration for each species, the normalised radius of gyration of dendrimers of all architectures and linear chains in the background collapse onto a universal curve as shown in Figure 5.4(a). Thus, the factor that determines the size of a polymer molecule is the number of monomers it interacts with in its neighbourhood. In other words, the concentration of monomers relative to its overlap concentration if all the monomers in the solution had belonged to its own architecture is what determines its shape. The fact that the solution has molecules of different architectures is unimportant.

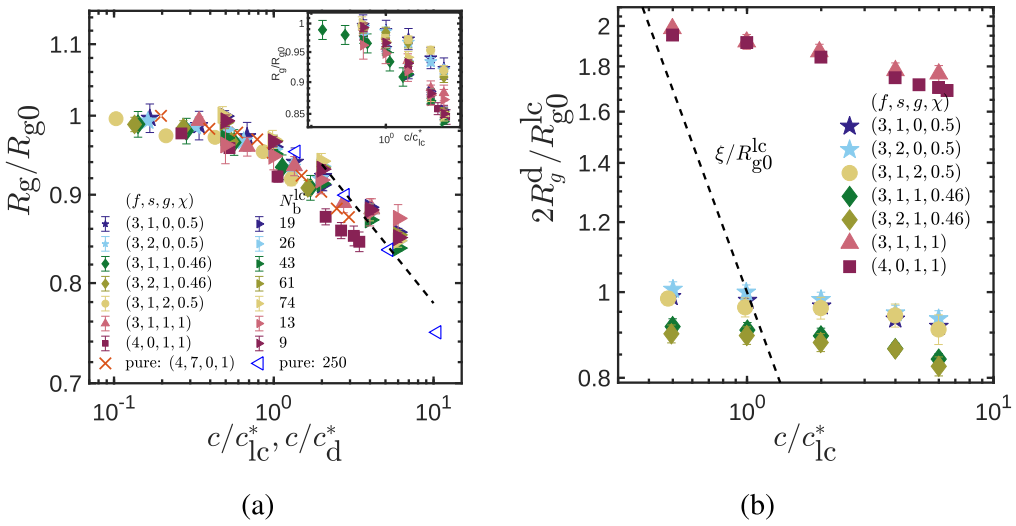

Figure 5.4: Radius of gyration of dendrimers in solution and different size regimes (a) Universal behaviour of radius of gyration of dendrimers and linear chains. The normalized radius of gyration of polymers is plotted as a function of the ratio of monomer concentration normalized by the respective c^* of each species. The dendrimer architecture is included in the order (f, s, g, χ) and N^{lc}_b is the number of beads on a linear chain. The same coloured symbols belong to one simulated system. Data from work on pure linear chain solutions by Huang *et al.* (2010) (empty triangles) and our simulation data for pure star polymer solutions (orange x-mark) are included. The dashed line is the scaling law given by equation 5.1. Inset: Normalised radius of gyration of dendrimers and linear chains in the solution as a function of the ratio of monomer concentration normalized by the overlap concentration of linear chains, c^*_{lc}. (b) Size regimes based on relative sizes of polymers and correlation length of the solution. The dendrimer architecture is included in the order (f, s, g, χ). The y-axis is the ratio between the size of the dendrimer and the radius of gyration of the linear chain in the dilute limit in each simulation system. The dashed line represents the scaling of ξ with concentration given by equation 3.10.

At lower concentrations, the correlation length of the solution is large compared to the size of polymers (Regime-1). With an increase in concentration, the size of dendrimers, linear chains, and the correlation length decreases given by equation 3.10 and 5.1. However, the correlation length ξ decreases faster than the diameter of the dendrimer $2R_g^d$ and after a certain concentration, the dendrimers in solution become bigger than correlation length, $2R_g^d > \xi$ (Regime-2). Thus there is a crossover from Regime-1 to Regime-2 with increasing concentration (see Figure 5.4(b)).

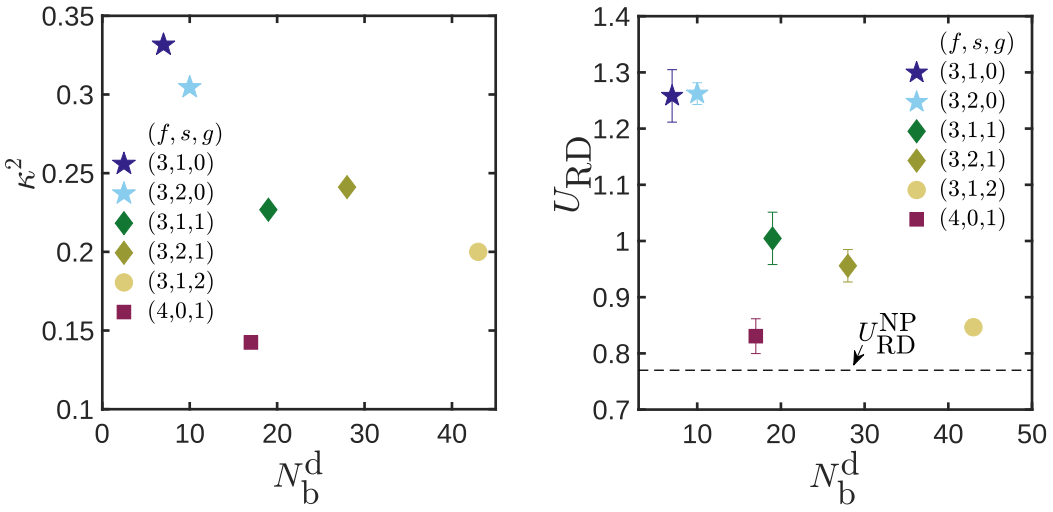

Figure 5.5: Relative shape anisotropy and U_{RD} of dendrimers. (a) Effect of different architectures on the relative shape anisotropy of dendrimers in dilute solution as a function of the number of beads in a dendrimer molecule. The symbols represent dendrimer topology given by the combination f, s, g. (b) U_{RD} of dendrimers in dilute solution as a function of the number of beads in a dendrimer molecule. The dashed line is the value of U_{RD} for a nanoparticle. The symbols represent dendrimer topology given by the combination f, s, g.

5.2.2 Relative shape anisotropy and U_{RD}

In Figure 5.5(a), the relative shape anisotropy of dendrimers of different architectures in dilute solution, calculated using equation 3.12, is plotted as a function of the number of beads per molecule. As the generation number (g) increases at constant f and s, κ^2 decreases. The number of beads inside and on the outer shell of a molecule is more for a dendrimer with higher g. Due to the excluded volume interactions, the internal beads spread out, and the molecule with higher g becomes more spherical compared to its lower-generation counterpart. The relative shape anisotropy of a functionality 4 dendrimer with $g = 1$ and $s = 0$ (Figure 5.2(f)) is much lower than that of the other architectures. With no spacers, every internal bead in the molecule is a branching point connected to 4 other beads. This gives it less chance of conformational

fluctuations and hence behaves more like a compact sphere (Cannon *et al.*, 1991). This is clear from the distribution of radius of gyration of dendrimers in dilute solution (see Figure A.2). The number of spacer beads appears not to have a significant effect on the shape of dendrimers. Along with the relative shape anisotropy, asphericity (B) is also a measure of the shape and compactness of molecules. It shows a similar trend as that of the κ^2 for dendrimers in our simulations supporting the argument of a spherical and compact structure (see Figure A.3(a)). Interestingly, κ^2 and B are unaffected by the concentration of the solution as shown in Figure A.3(b) and (c). In Figure 5.5 (b), the ratio U_{RD} for dendrimers of different architectures in the dilute limit is plotted as a function of the number of beads in the molecule. Similar to the behaviour of relative shape anisotropy, U_{RD} decreases with increasing g when f and s are fixed. Our simulation results are in line with the previous experiments (Tande *et al.*, 2001) and simulations (Bosko and Prakash, 2011) for dendrimers in dilute solution. The $f = 4, g = 1, s = 0$ (Figure 5.2(f)) dendrimer has a value of U_{RD} very close to that of a hard sphere even though the number of beads in it is almost the same as that of a $f = 3, g = 1, s = 1$ (Figure 5.2(c)) dendrimer. Thus, by increasing g and f, dendrimers can be seen to transition from 'fractal-like' to a 'nanoparticle-like' structure.

5.2.3 Bead density distribution

Figure 5.6(a) shows the linear bead density distribution along the major axis of the radius of the gyration tensor of linear chains and dendrimers in a dilute solution. Linear chains have a dip in the density distribution at the centre of the molecule (Kumari *et al.*, 2020) implying that in an athermal solution, beads near the centre have a higher effective excluded volume repulsion. The density distributions of dendrimer molecules, on the other hand, are peaked at the centre of mass. The linear number density is the density of the projected coordinates of the beads along the major axis. A higher functionality f of a dendrimer leads to the localisation of beads closer to the core, increasing the linear core density. The other factor responsible for higher core linear density is the presence of a larger number of beads in the molecule (the projected coordinates of which are likely to be higher near the core). The other characteristic feature of the linear number density of dendrimers is the presence of a non-Gaussian shoulder region midway between the core and periphery. We do not have a simple geometrical explanation for this behaviour. The linear bead density distribution of $f = 3, s = 1, g = 1$ in theta solvent conditions shows a Gaussian distribution, with a significantly high core density compared to that in athermal conditions. This could be due to the folding back of the dendrimer arms to the core due to the absence of the excluded volume interactions.

The density distribution is different along the 3 axes of the gyration tensor, with the internal bead distribution being more clearly non-Gaussian along the major axis (see Figure A.4(a)) and

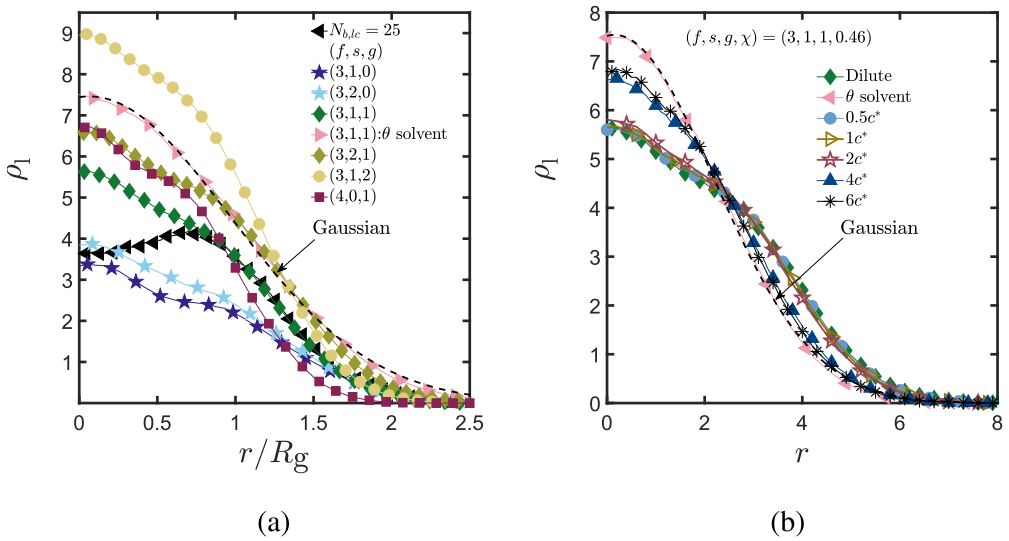

(a) (b)

Figure 5.6: Linear bead density distribution of dendrimers (a) Effect of architecture on the internal bead density distribution of dendrimers along the major axis in dilute solution. Black triangles represent linear chain with 25 beads and dendrimers are represented using the combination f, s, g. The pink triangle represents a $f = 3, s = 1, g = 1$ dendrimer in theta solvent conditions. The dashed line is a Gaussian fit to this data. (b) Effect of concentration on the bead density distribution of $f = 3, s = 1, g = 1$ dendrimer in a semidilute solution of linear chains with $\chi = 0.46$. The pink triangles represent dendrimer in theta solvent conditions and the dashed line is a Gaussian fit to this data.

Gaussian-like along the minor axes. The effect of increasing solution concentration on the bead density distribution along the major axis of generation-1 dendrimer is plotted in Figure 5.6(b). Due to the excluded volume interactions in an athermal solution, dendrimer molecules tend to swell, resulting in a lower core density. The shoulder that is present in the density distribution in the dilute case decreases as the concentration of the background linear chains increases. As is well known, at higher concentrations, the excluded volume interactions are screened in the molecule, and the onset of this is revealed in the figure. Thus, the molecule is shrinking, bringing beads closer to the centre of mass. After $2c^*$, the distribution approaches Gaussian, which corresponds to the theta solvent conditions. It should be noted that all simulation results reported in this manuscript for theta solvents have been obtained with the well depth set to $\epsilon = 0.45$ in the SDK potential.

The bead density distribution in concentric shells of equal volume, referred to as volumetric bead density, was also calculated (see Figure A.4(b) and (c)). All dendrimer architectures show a high core density in dilute solutions, which monotonically decreases towards the periphery.

As the solution concentration increases, the volumetric bead density approaches that in theta solvent conditions, similar to linear bead density.

5.2.4 Mean squared displacement

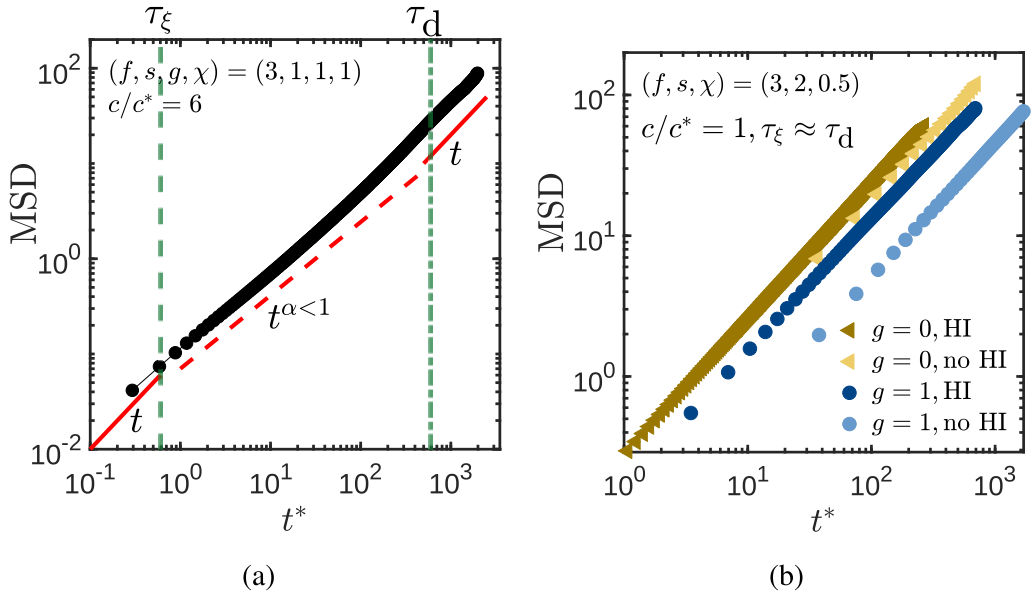

Figure 5.7: Mean squared displacement of dendrimers as a function of time (a) The mean squared displacement of a dendrimer with $f = 3, s = 1, g = 0, \chi = 0.5$ in a solution of linear chains of concentration $6c^*$. The vertical dashed and dashed-dotted lines are τ_ξ and τ_d, respectively. (b) Effect of hydrodynamic interaction on the mean squared displacement of dendrimers. The same symbol shapes represent identical systems. The concentration is fixed at $1c^*$ and $f = 3$ for all dendrimers. For the star polymer, $s = 1, \chi = 0.5$ and for generation one dendrimer, $s = 2, \chi = 0.46$.

According to the coupling theory (Cai *et al.*, 2011) for the diffusion of nanoparticles in a polymer solution, the particle dynamics is dependent on its size relative to the solution correlation length. Nanoparticles in Regime-1 pass smoothly through the polymer mesh, whereas particles larger than ξ get locally trapped and become subdiffusive at intermediate time scales, with the diffusion exponent $\alpha^{\mathrm{NP}} = 0.5$. However, a recent MPCD study (Chen *et al.*, 2018) has shown that α^{NP} gradually decreases from unity to 0.5, with an increase in solution concentration due to its coupling to the polymer centre of mass motion. To understand the behaviour of soft dendrimers in polymer solutions, the mean squared displacement of dendrimers was plotted as a function of time as shown in Figure 5.7(a). The system in the figure corresponds to Regime-2 ($2R_{\mathrm{g}}^{\mathrm{d}} > \xi$). The dendrimer is observed to be diffusive ($\alpha^{\mathrm{d}} = 1$) at times less than τ_ξ. It then becomes subdiffusive at intermediate times ($\tau_\xi < t < \tau_{\mathrm{d}}$) with $\alpha^{\mathrm{d}} < 1$, followed by normal diffusion at long times ($t > \tau_{\mathrm{d}}$), similar to the behaviour of a nanoparticle in the polymer solution.

With increasing concentration, the mean squared displacement of dendrimers decreases and the subdiffusive regime increases(Figure 5.7(a)). This is because τ_ξ (equation 3.16) decreases and τ_d (equation 3.17) increases with increasing concentration (see Tables A.1, A.2 and A.3). Therefore, dendrimers remain subdiffusive for a longer span at higher concentrations.
To understand the role of hydrodynamic interactions (HI) in determining the dynamics of dendrimers, simulations were performed with and without HI. From the mean squared displacement versus time plots, it is observed that HI promotes the movement of the dendrimers in the solution, thus leading to a higher MSD (Figure 5.7(b)). This is in line with earlier observations for nanoparticles in polymer solutions(Chen *et al.*, 2017). The architecture of dendrimers also affects its mean squared displacement because its size increases with generation number, keeping f and s fixed. At a constant concentration, a generation 2 dendrimer will experience more hindrance to its motion compared to a simple star polymer ($g = 0$), causing the former to diffuse slower than the latter (see Figure 5.7(b)). However, we can collapse MSD for different architectures by following a simple scaling relation as shown in Figure 5.7(c).

5.2.5 Diffusion exponent

As mentioned earlier, dendrimers that are larger than the solution correlation length become subdiffusive at intermediate time scales. We have extracted the diffusion exponents for dendrimers of different architectures at intermediate times ($\tau_\xi < t < \tau_\mathrm{d}$). Since this gives the minimum value of diffusion exponent in the entire trajectory, diffusion exponent at intermediate times is referred to as α_min. This quantity is plotted as a function of the ratio of their diameter to the correlation length (Figure 5.8(a)). Dendrimers smaller than correlation length (Regime-1) exhibit diffusion with $\alpha^\mathrm{d}_\mathrm{min} = 1$, whereas dendrimers larger than correlation length (Regime-2) experience hindrance to its movement and becomes subdiffusive $\alpha^\mathrm{d}_\mathrm{min} < 1$. It is remarkable that the diffusion exponents of all dendrimers collapse onto a universal curve independent of the architecture of dendrimers. The figure also contains the minimum diffusion exponent of nanoparticles from MPCD simulations carried out by Chen *et al.* (2018). Dendrimers have a higher value compared to a hard sphere with the same d_NP/ξ value in regime-2, where d_NP is the diameter of the nanoparticle. This may be due to the concentration-dependent size of the dendrimer, unlike that of a nanoparticle, which is a hard sphere. A dendrimer trapped in a polymer mesh can move out of it due to its own fluctuation along with fluctuations of the mesh-forming strands. It is consequently more diffusive compared to a nanoparticle of comparable size. Instantaneous diffusion exponents also can be obtained by taking the time derivatives of mean squared displacement. It was observed that α thus obtained at intermediate times is similar to that calculated from the time exponent of MSD between τ_ξ and τ_d. It starts increasing beyond τ_d and tends to unity (see Figure A.7).

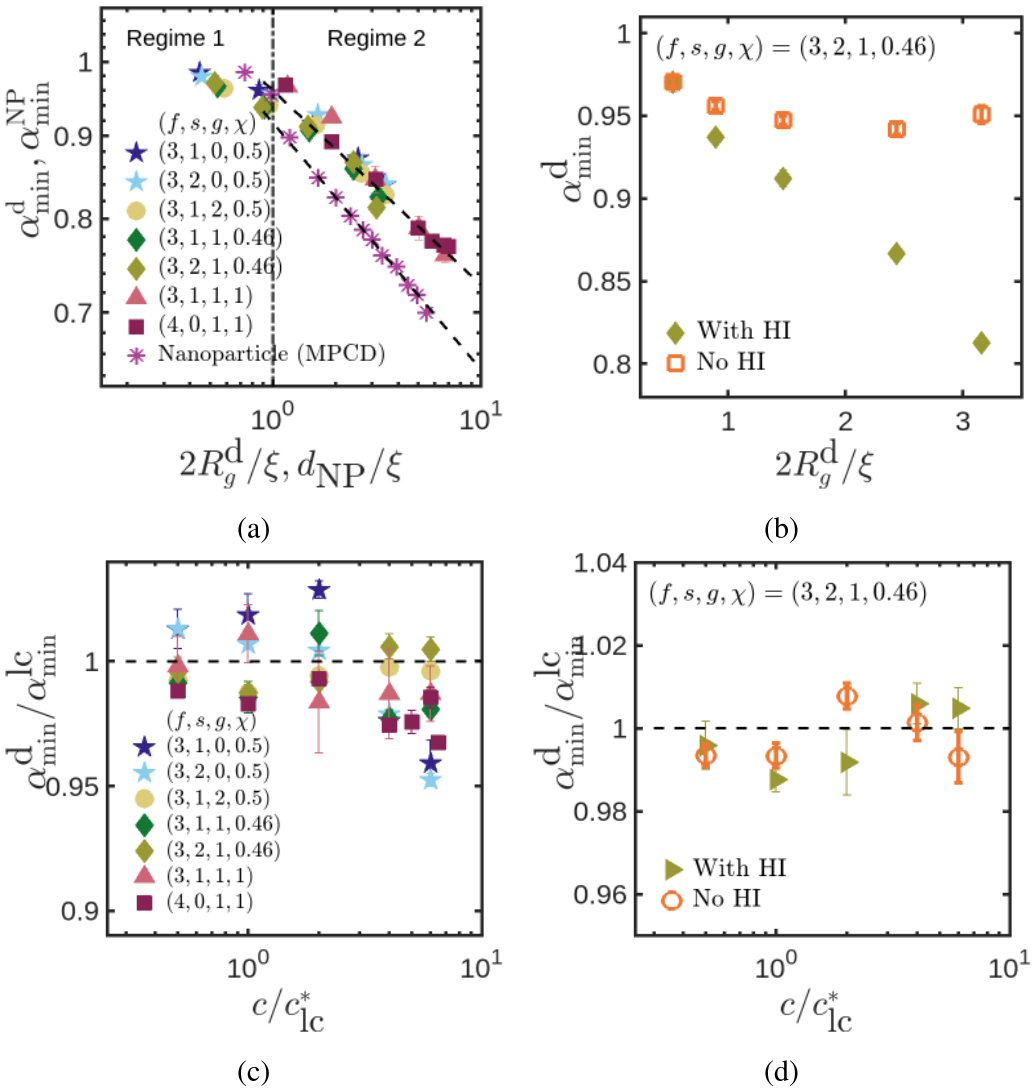

Figure 5.8: The minimum diffusion exponents (a) The minimum diffusion exponent of dendrimers of different architectures is plotted as a function of the ratio of its size to the correlation length in the two regimes. Data from work by Chen *et al.* (2018) for a nanoparticle in semidilute polymer solution of linear chains is included. The dashed lines are a guide to the eye and the vertical line demarcates the two regimes. (b) The minimum diffusion exponent of $f = 3, s = 2, g = 1$ dendrimers in solutions with and without hydrodynamic interactions with $\chi = 0.46$. (c) The ratio of the minimum diffusion exponents of dendrimers to that of linear chains in its background as a function of concentration for dendrimers of different architectures. The dashed line is equal to unity. The symbols represent dendrimers in the solution with topological parameters $f, s, g, \chi,$. (d) The ratio of the minimum diffusion exponents of dendrimers to that of linear chains in solutions with and without hydrodynamic interactions. The system considered is the same as that in (b).

Figure 5.8(b) shows the influence of hydrodynamic interactions on the minimum diffusion exponents of dendrimers in a solution. The exponent $\alpha^{\mathrm{d}}_{\mathrm{min}} = 1$ for both cases as dendrimers exhibit pure diffusion at low concentrations. As concentration increases, the minimum diffusion exponent of dendrimers with HI decreases monotonically, while that without HI levels off. The diffusion exponent of nanoparticles in semidilute solutions has also been studied using MPCD simulations. While an earlier study (Chen *et al.*, 2017) indicated behaviour different from that observed here, the observations of a more recent study by Chen *et al.* (2018) are in agreement with our results. Paradoxically, HI seems to slow down the motion of dendrimers in the intermediate times as shown by the decreasing values of the diffusion exponent, while, as seen earlier, it enhances the long-time diffusivity. This is perhaps due to the backflow caused by HI that prevents the escape of dendrimers from polymer 'cages' at intermediate times. However, at long times, HI enhances its motion through polymer-mediated motion as shown by the MSD plots (Figure 5.7(c)). A better insight into the effect of HI at different time scales is obtained from the velocity field due to HI about the dendrimer molecule (see Figure A.8). At a length scale comparable to dendrimer size, which corresponds to intermediate times, each monomer on a dendrimer molecule experiences a force of different magnitude and direction at every instant in time due to its configuration. This causes the molecule to change shape and move in random directions, thus slowing its diffusion process. Whereas, when viewed from larger length scales, which corresponds to $t > \tau_d$, the dendrimer is like a particle placed at its centre of mass. Its diffusion is enhanced by the unidirectional flow due to HI.

We also examined the dynamics of linear polymer chains in the background solution at intermediate time scales. Similar to dendrimers, linear chains also enter a subdiffusive regime at intermediate times, and the minimum diffusion exponents of both species are highly correlated as shown in Figure 5.8(c). This is similar to the observation made by Chen *et al.* (2018) for nanoparticles. The correlation has been attributed to the coupling of nanoparticle motion to the centre of mass of the linear chains in the solution along with the segmental relaxation time of polymer, which results in the gradual decrease of diffusion exponent from 1 to 0.5 (Figure 5.8(a)), unlike the predictions of coupling theory (Cai *et al.*, 2011) which predicts a constant value of 0.5 as the diffusion exponent of nanoparticle. It appears that the correlation is lost for some of the architectures at higher concentrations, however, the scatter is due to insufficient statistics. Since the difference across the entire range of concentrations considered is less than 5%, the correlation exists at all concentrations and across all architectures.

The coupling of the motion of dendrimers and linear chains would at first sight be attributable to the presence of long-range hydrodynamic interactions. However, the strong correlation between the minimum diffusion exponents of both species exists even in the absence of HI as shown in

Figure 5.8(d). This confirms that the correlation is due to comparable time scales of relaxation between the dendrimers and linear chains, and not due to the many-body HI (Chen *et al.*, 2018).

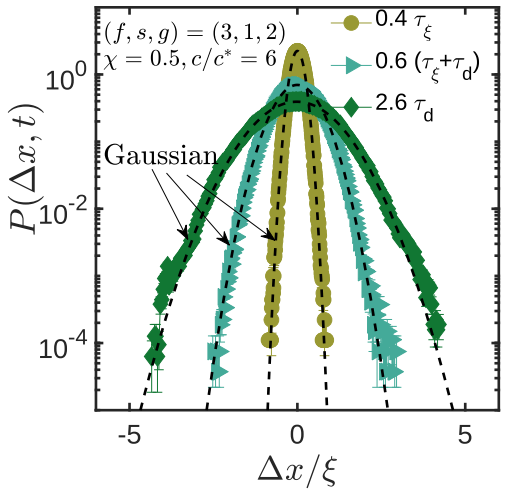

Figure 5.9: Probability distribution function of displacement for a generation two dendrimer ($f = 3$, $s = 1$,$\chi = 0.5$) at concentration $c = 6c^*$ at different times (at $t = 0.4\tau_\xi$, $0.6(\tau_\xi + \tau_d)$, $2.6\tau_d$).

5.2.6 Probability distribution function of displacement

To get a better insight into the characteristic features of dendrimer dynamics, we analyzed its probability distribution function of displacement at various time intervals (Figure 5.9). The displacements are normalized by the correlation length as it is the length scale at which the dendrimer experiences the presence of linear chains. It is clear from the distribution function that even though dendrimers become subdiffusive at intermediate time scales, they demonstrate Gaussian probability distributions. On the other hand, many systems of nanoparticles in complex environments exhibit non-Gaussian distributions (Phillies, 2015; Kumar *et al.*, 2019). There has been an increasing interest in studying Fickian systems with non-Gaussian probability distributions over the past few years (Wang *et al.*, 2012, 2009; Slim *et al.*, 2020; Smith *et al.*, 2021). In these systems, the observed deviation from Gaussian behaviour has been attributed to the temporal (Lampo *et al.*, 2017; He *et al.*, 2016) or spatial (Jee *et al.*, 2014; Guan *et al.*, 2014) heterogeneities in the complex environment leading to a distribution of diffusivities, due to the shape anisotropy of the tracer (Smith *et al.*, 2021) or due to activated hopping mechanisms (Xue *et al.*, 2016).

Subdiffusive motion has been explained using two mathematical models: the continuous-time random walk model (CTRW) (Montroll and Weiss, 1965) and fractional Brownian motion (FBM) (Mandelbrot and Van Ness, 1968). While the former has a series of trapping and discrete jumps leading to subdiffusion and non-Gaussian probability distribution functions, the latter is a

Gaussian process in which successive steps are correlated (non-Markovian). An analysis of the motion of the centre of mass of the dendrimer molecule confirms the absence of long waiting times and hopping (shown in Figure A.6). Therefore, it appears from the MSD plots and the probability distribution of displacements that the subdiffusive yet Gaussian behaviour of dendrimers mimics fractional Brownian motion rather than continuous time random walk motion. Similar results were obtained for polymer-grafted nanoparticles in a recent molecular dynamics study (Chen *et al.*, 2022).

Figure 5.9 shows the probability distribution functions (PDD) for a $f = 3, s = 1, g = 2$ (Figure 5.2(e)) dendrimer at different time scales at a fixed concentration. When $t < \tau_\xi$ and $t > \tau_d$, dendrimers exhibit normal diffusion and hence the PDD is expected to be Gaussian. However, in the intermediate time scales when the dendrimer is subdiffusive, they have a Gaussian PDD. Note that the correlation length, τ_ξ and τ_d are concentration and architecture-dependent quantities. The probability distributions remain Gaussian at all concentrations irrespective of the architecture and the time (see Figure 5.9).

5.2.7 Diffusivity as a function of concentration

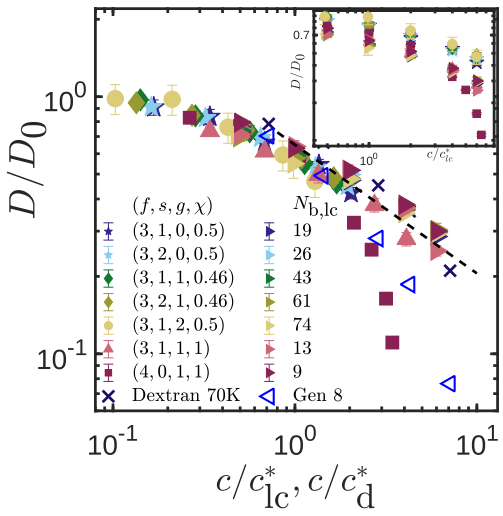

Figure 5.10: Universal behaviour of normalised diffusivity of dendrimers and linear chains as a function of the ratio of monomer concentration normalized by the respective c^* of each species. The dendrimer architecture is included in the order (f, s, g, χ) and N_b^lc is the number of beads on a linear chain. Symbols in the same colour belong to the same system, with right triangles representing linear chains. The dashed line is the scaling law given equation 5.2. Experimental data for generation 8 dendrimers and dextrans from Cheng *et al.* (2002) is included. Inset: Normalised diffusivity of dendrimers and linear chains in the solution as a function of the ratio of monomer concentration normalized by the overlap concentration of linear chains, c^*_lc.

The diffusivity of linear chains in semidilute polymer solutions is known to follow a universal scaling law given by (Doi *et al.*, 1988)

$$D^{\mathrm{lc}} = D_0^{\mathrm{lc}} \left(\frac{c}{c^*_{\mathrm{lc}}} \right)^{\frac{\nu-1}{3\nu-1}} \tag{5.2}$$

To understand the long-time dynamics of the simulated hybrid system, we calculated the long-time diffusivity of dendrimers and linear chains in the solution. The diffusivity, normalized by the respective dilute diffusivity, of dendrimers and linear chains decreases with an increase in concentration as shown in Figure 5.10. Dendrimers of functionality $f = 3$ and linear chains in the solution follow the universal scaling law for linear chains when the monomer concentration (c) is normalized with respect to the overlap concentration of each species. However, the diffusivity of a $f = 4$ dendrimer does not follow equation 5.2. Rather, it drops rapidly after $c/c^*_{\mathrm{d}} = 1$.

There is a remarkable collapse of diffusivity of dendrimers of several architectures in spite of having different anisotropies. Therefore it would appear that anisotropy does not affect their dynamics. We have also calculated the distribution of the radius of gyration of dendrimers in a dilute solution (shown in Figure A.2(a)) and examined the effect of concentration (Figure A.2(b) and (c)). This was obtained using the R_g^d from many trajectories at different instances in time and binning them. The variance of the distribution of R_g^d gives a measure of the size fluctuations. The $f = 4$ dendrimer has a significant decrease in variance compared to the $f = 3$ dendrimers in dilute solution. Note that the $(f, s, g) = (3, 1, 1)$ dendrimer has a similar number of beads per molecule to that of the $f = 4$ dendrimer, and indeed the $(f, s, g) = (3, 1, 2)$ and $(f, s, g) = (3, 2, 1)$ dendrimers have a higher number of beads. Yet the $f = 4$ dendrimer has a smaller variance of the distribution of R_g. This suggests that a decrease in the fluctuations in size might be a more important factor in determining the difference observed in the behaviour of the functionality four dendrimer, rather than its anisotropy. The variance in R_g^d seems to decrease rapidly with concentration for both the architectures that are displayed in Figure A.2(b) and (c). Our simulation results are compared with experimental data for a generation 8 dendrimer and Dextran molecules reported by Cheng *et al.* (2002). A generation 8 dendrimer is a dense and compact molecule with fractal dimension ≈ 3.1 whereas dextrans are slightly branched molecules with fractal dimension 2.3 (Cheng *et al.*, 2002). The diffusivities of $f = 3$ dendrimers and linear chains in our simulations behave similarly to Dextran molecules while the $f = 4$ dendrimer behaves more like the generation 8 dendrimer, confirming that the former has a more compact structure.

While dendrimers are just one example of soft colloids, there are other systems like microgels, multiarm stars, and hairy colloids that may also be considered as soft colloids. Our search of the literature seems to suggest that a systematic study of the dependence of diffusivity on the

concentration of the semidilute solution has not been reported for this variety of soft colloids, rather the effect of temperature and pH has been well studied. Therefore, we are unable to compare our results directly with data for a range of these systems. On the other hand, there is data by Poling-Skutvik *et al.* (2019) on polymer-grafted nanoparticles (PGNP) or hairy colloids on the dependency of its diffusivity on concentration. They have observed that the normalised diffusivity of a variety of PGNP-linear chain systems can be collapsed when represented in terms of $\left(c/c^*_{\mathrm{lc}}\right)\left(M_{w,f}/M_{w,g}\right)^{-1/8}$. In our simulations, since, c^*_{d} can also be represented in terms of c^*_{lc} (for a detailed derivation see Section A.9), the overlap concentration of dendrimers, c^*_{d}, can be written as $c^*_{\mathrm{d}} = c^*_{\mathrm{lc}}\left(a^{\mathrm{lc}}/a^{\mathrm{d}}\right)^3\left(N^{\mathrm{d}}_{\mathrm{b}}/N^{\mathrm{lc}}_{\mathrm{b}}\right)^{1-3\nu}$, where the constants a^{d} and a^{lc} are defined by $a^{\mathrm{d}} = R^{\mathrm{d}}_{\mathrm{g0}}/(N^{\mathrm{d}}_{\mathrm{b}})^{\nu}$ and $a^{\mathrm{lc}} = R^{\mathrm{lc}}_{\mathrm{g0}}/(N^{\mathrm{lc}}_{\mathrm{b}})^{\nu}$. Using this relation, the diffusivity of all the dendrimer architectures can be collapsed by plotting the data in Figure 5.10 in terms of $c^*_{\mathrm{lc}}\left(N^{\mathrm{d}}_{\mathrm{b}}/N^{\mathrm{lc}}_{\mathrm{b}}\right)^{-0.76}$. Note that the exponent of the normalisation factor is different from that reported by Poling-Skutvik *et al.* (2019). A comparison of the results displayed in Figure 5.10 for dendrimers with the data of Poling-Skutvik *et al.* (2019) for one of their systems, is shown in Figure A.10.

5.2.8 Scaling law for dendrimer diffusivity

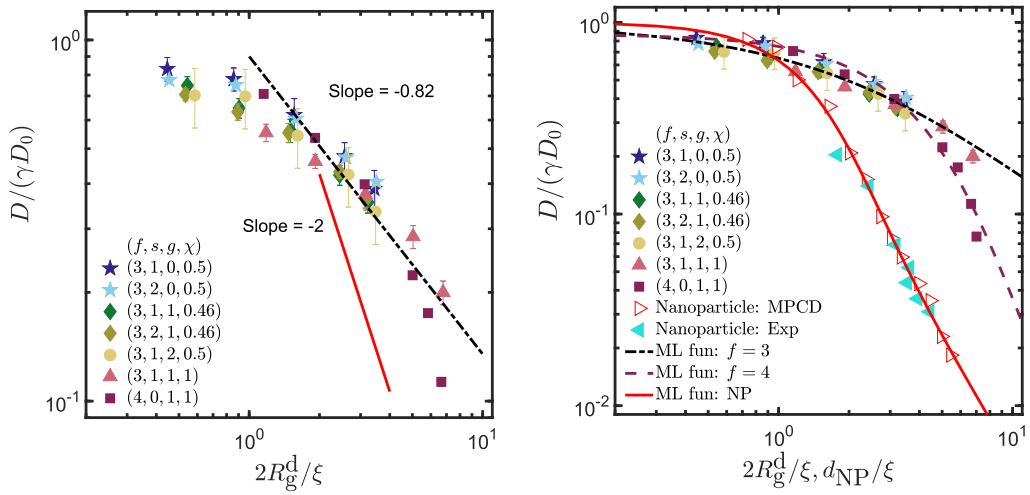

Figure 5.11: (a) Normalised diffusivity for dendrimers of all architectures in the solution of linear chains as a function of the ratio of its size to the correlation length of the solution. Symbols represent dendrimers with topological parameters in the order f, s, g, χ. The dashed line represents the scaling law derived for dendrimers (equation 5.3) and the solid line represents the predictions of coupling theory (Cai *et al.*, 2011). (b) Normalized diffusivity for dendrimers of all architectures along with MPCD (Chen *et al.*, 2018) (red empty triangles) and experimental data (Kohli and Mukhopadhyay, 2012) (cyan filled triangles) from literature for nanoparticles. The lines are Mittag-Leffler fits (ML fun) to various systems with parameters *m*,*a* and *p* given in Table 5.2.

Table 5.2: Values of parameters used in the Mittag-Leffler fits to various data sets in Figure 5.11(b)

System	m	a	p
$f = 3$	−0.43	0.59	0.82
$f = 4$	−0.11	0.79	1.40
Nanoparticle	0.45	0.78	2.00

Dendrimers are soft polymers, the size of which changes with the concentration of the background solution (Figure 5.4(a)), unlike nanoparticles that have a fixed size. The theories that govern nanoparticle dynamics in homopolymer solutions are consequently not directly applicable to dendrimers. Combining equation 5.1 and 5.2 for dendrimer radius of gyration and diffusivity, and equation 3.10 for correlation length, a new scaling law for the dynamics of dendrimers in semidilute polymer solutions can be derived. The normalized diffusivity of dendrimers as a function of the ratio of its size to the correlation length of the solution is given by (for detailed derivation see Section A.10):

$$\frac{D^{\mathrm{d}}}{D_0^{\mathrm{d}}} = \gamma \left(\frac{2R_{\mathrm{g}}^{\mathrm{d}}}{\xi} \right)^{2(\nu-1)} \tag{5.3}$$

where $\gamma = \left(\frac{\beta^{\mu}}{2\chi^{(1+3\mu)}} \right)^{2(\nu-1)}$ with $\beta = \frac{N_{\mathrm{b}}^{\mathrm{d}}}{N_{\mathrm{b}}^{\mathrm{lc}}}$.

Figure 5.11(a) shows our simulation data fitted with the scaling law for dendrimer diffusivity given by equation 5.3. As expected, the normalized long-time diffusivity is equal to 1 in the dilute limit and a crossover to the semidilute regime happens when the size of the dendrimer is comparable to the correlation length ($2R_{\mathrm{g}}^{\mathrm{d}} \approx \xi$). Data for functionality 3 dendrimers collapse to a universal curve when divided by the factor γ, which depends on χ and β. However, the $f = 4$ (Figure 5.2(f)) dendrimer does not follow this power law at sufficiently high concentrations. In equation 5.3, the exponent $2(\nu - 1) = -0.82$ when $\nu = 0.588$. The -2 power law from coupling theory for nanoparticles is also displayed for comparison.

In the case of nanoparticles, two competing theories predict different scaling behaviour for diffusivities: the hydrodynamic model gives a stretched exponential dependence of the normalized long-time diffusivity of nanoparticles on its size relative to the system correlation length, whereas the coupling theory predicts a power law dependence with an exponent -2. These theories have been well supported by experiments and simulations (Chen *et al.*, 2017, 2018; Kohli and Mukhopadhyay, 2012; de Kort *et al.*, 2015; Poling-Skutvik *et al.*, 2015). Since the diffusiv-

ity is normalized by its dilute value, in both cases, the ratio tends to one at low concentrations. It is interesting to consider the disparity in scaling predictions with the help of the Mittag-Leffler (ML) function, which is unique as it becomes a stretched exponential at small values of its argument x, while it is a power law at large values of x (Mainardi, 2020; Jaishankar and McKinley, 2013). In this study, we are using a modified version of the ML function ($E_{a,b}\left(mx^p\right)$), given by:

$$E_{a,b}\left(-mx^p\right) = \sum_{k=0}^{\infty} \frac{(-m)^k x^{pk}}{\Gamma\left(ak+b\right)} \tag{5.4}$$

where m, p, a and b are arbitrary constants. At small x, equation 5.4 is given by

$$E_{a,b}\left(-mx^p\right) = \exp\left(\frac{-mx^p}{\Gamma\left(a+b\right)}\right) \tag{5.5}$$

and at large values of x it becomes a power law, with p being the power law exponent:

$$E_{a,b}\left(-mx^p\right) = \frac{x^{-p}}{m\Gamma\left(b-a\right)} \tag{5.6}$$

The diffusivity as a function of the ratio of the size to the correlation length of dendrimers of all architectures and nanoparticles can be fitted using different values of m, a and p of the Mittag-Leffler function (details of the code can be found in Section A.11. Since $D/D_0 = 1$ in the dilute regime, $b = 1$, and the expression is given by:

$$D/D_0 = E_{a,1}\left(-m\left(\frac{2R_g^d}{\xi}\right)^p\right) \tag{5.7}$$

All dendrimers with $f = 3$ can be fitted using the modified Mittag-Leffler function (equation 5.7) with a power law exponent $p = -0.82$ as shown in Figure 5.11(b). The normalized diffusivity of nanoparticles from MPCD simulations by Chen *et al.* (2018), which follows the scaling law from coupling theory, is fitted with a power law exponent of $p = -2$. Experimental results for nanoparticles that were thought to have a stretched exponential dependence (Kohli and Mukhopadhyay, 2012) are also included (cyan triangles) for comparison. Interestingly, both these data sets can be fitted well with the same Mittag-Leffler function. The $f = 4$ dendrimers that do not follow the scaling law for diffusivity of linear polymers (equation 5.2) cannot be fitted with the same power law exponent of $f = 3$ dendrimers. Fitting this data using equation 5.4 gives $p = -1.4$, which is between the power law exponents for $f = 3$ dendrimers and hard spheres. Hence, there is a transition from the polymer-like behaviour to a hard-sphere due to the increased functionality, leading to a compact structure. The values of the various parameters used for fitting in Figure 5.11(b) are given in Table 5.2.

5.3 Conclusions

Through Brownian Dynamics simulations, we have examined a hybrid system of soft dendrimers in a semidilute solution of linear polymers. Our investigation focused on the effects of

solution concentration, dendrimer architecture, and hydrodynamic interactions on the static and dynamic properties of the dendrimers. We compared our findings to those of a rigid sphere in a semidilute polymer solution. Dendrimers with a mean R_g comparable to that of linear chains in the background were chosen for all simulations.

Our results showed that, unlike hard spheres, the size of dendrimers decreases as the solution concentration increases and follows the universal scaling law for linear chains represented by equation 5.1. In the dilute state, the shape functions of dendrimers decreased with increasing functionality and generation number but remained constant with concentration. Additionally, the internal bead density of all dendrimers was highest at the core and rapidly decreased towards the periphery of the molecule in a dilute solution. The higher functionality dendrimer showed a higher internal bead density compared to its counterpart with similar bead numbers. At higher concentrations, the bead density distribution approached a Gaussian distribution, similar to that of a polymer in theta solvent conditions. This is due to the screening of excluded volume interactions, which allows the overlap of dendrimer branches.

In the study, it was observed that dendrimers exhibit subdiffusion during intermediate times as they become trapped in cages formed by linear chains. However, the minimum diffusion exponent for dendrimers was found to be higher than that of their hard sphere counterparts at higher concentrations. This can be attributed to the additional fluctuation of dendrimers, which facilitates their motion out of the polymer cages. It was also observed that dendrimers and linear chains have similar diffusion exponents at all concentrations, regardless of the presence or absence of hydrodynamic interactions (HI). As time progresses, dendrimers become diffusive as a result of polymer relaxation. The study also found that HI enhances polymer dynamics at longer times and increases its mean squared displacement. However, the minimum diffusion exponents decrease with concentration when HI is present, unlike the free-draining case where there is no variation.

The long-time diffusivity of dendrimers decreased with increasing solution concentration, similar to that of the linear chains in the background, and collapsed onto a universal curve. However, the diffusivity of dendrimers does not follow theoretical predictions for nanoparticle diffusivity as a function of its size relative to the solution correlation length. From the analysis of the effect of concentration on dendrimer size and diffusivity, as well as the correlation length of the solution, we developed a scaling law for dendrimer diffusivity based on the ratio of its size to solution correlation length. We found that dendrimers with functionality three follow this scaling law, but more dense dendrimers with higher functionality ($f = 4$) do not obey it at higher concentrations. These dendrimers have a power law exponent that falls between that of $f = 3$ dendrimers and hard spheres. This shows with increasing functionality, dendrimers shift from polymer-like to hard sphere-like structures. Moreover, using the Mittag-Leffler function,

the crossover from the stretched exponential character at low concentrations to the power law behaviour at higher concentrations has been captured for both our simulation results and data from the literature for nanoparticles.
In the following chapter, the static properties of sticky and non-sticky dendrimers in a network of linear associative polymers is discussed.

Chapter 6

Static properties of a sticky and non-sticky dendrimer in polymer networks

In this chapter, the static properties of dendrimers in a network are analysed as a function of the concentration of the background chains and sticker-related parameters. This includes the evaluation of the radius of gyration and internal bead density distribution of both the sticky and non-sticky dendrimers as well as the mesh size distribution of the surrounding network.

The confinement parameter, C defined as σ_{NP}/ξ, emerges as the key factor governing the mobility of nanoparticles in polymer networks. Its significance has been independently established through theoretical predictions by Cai *et al.* (2015) and Dell and Schweizer (2014), both of whom demonstrated that terminal diffusivities exhibit a strong dependence on C. For dendrimers in semidilute polymer solutions, the preceding chapter demonstrated that their subdiffusive behaviour arises only when their radius of gyration exceeds the correlation length of the solution. For a nanoparticle of fixed size, the confinement parameter can be modulated solely by varying ξ of the network. However, dendrimers exhibit more complex behaviour, their size decreases along with ξ with increasing concentration. Due to its influence on the dynamics, it is crucial to analyse the size of sticky and non-sticky dendrimers in polymer networks. The presence of attractive interactions between dendrimers and linear polymer chains is expected to influence their static properties significantly. Changes in the radius of gyration will also be reflected in the arrangement of beads within the dendrimer molecule, captured by its internal bead density distribution.

Beyond the intrinsic properties of dendrimers, the structural characteristics of the polymer network, such as the mesh size, also critically influence dendrimer dynamics. A recent simulation study on nanoparticles in polymer networks has highlighted distortions in the network mesh due to the presence of nanoparticles. This is attributed to the interaction between the nanoparticle and the network. This raises important questions about the extent of such effects in the context

of dendrimers, particularly with varying interaction strengths. A detailed analysis of the radius of gyration and the bead density distribution of sticky and non-sticky dendrimers in polymer networks (as shown in Figure 2.4(b) and (c)) are presented in this chapter. It also examines the impact of dendrimer-network interactions on the mesh size of the polymer network under varying concentrations of linear polymers.

6.1 Details of the simulation algorithm

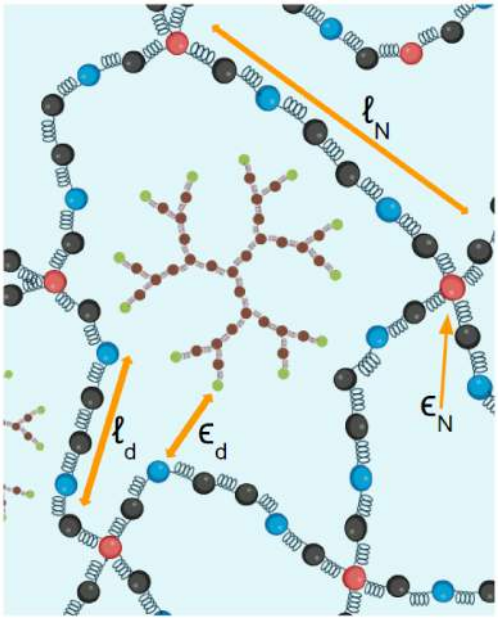

Figure 6.1: Schematic representation of sticky dendrimer in network. The various interaction parameters are indicated.

The SDK potential is employed to model both the sticker interactions and the repulsion between non-sticky beads. This is done by varying the well depth of the potential. For purely repulsive interactions, we set $\epsilon = 0$ and the solvent quality decreases with increasing ϵ. Unlike the conventional Lennard-Jones (LJ) potential, the SDK potential has a short-ranged attractive tail that smoothly goes to zero, making it a suitable choice for our simulations.

In this study, we have chosen two dendrimer architectures, a simple star polymer ($(f, s, g) = (3, 2, 0)$) and a generation one dendrimer ($(f, s, g) = (4, 0, 1)$) (refer to Section B.1). The order of dendra in both cases is given by $m = f - 1$. The size ratio between the radius of gyration of dendrimers ($R^{\mathrm{d}}_{\mathrm{g0}}$) and linear chains ($R^{\mathrm{lc}}_{\mathrm{g0}}$) in dilute limit ($\chi = R^{\mathrm{d}}_{\mathrm{g0}}/R^{\mathrm{lc}}_{\mathrm{g0}}$) was chosen to be 0.3 and 0.5. The length of linear chains was determined using the same methodology used in the previous chapter on dendrimers in a semidilute solution of linear polymers (given in Section 5.1).

The length of the simulation box $L \geq 2R_e$, where R_e is the end-to-end distance of linear chains in the solution so that molecules do not wrap around themselves. The concentration of the system refers to the monomer (or bead) concentration in the simulation box given by $c = N/V$, where N is the total number of monomers given by $N = (N_c^{lc} \times N_b^{lc}) + (N_c^{d} \times N_b^{d})$. The dendrimer concentration is always kept within the dilute limit and more linear chains are added to increase the overall concentration of the solution. The concentration range considered is from dilute to $6c^*$, where c^* is the overlap concentration defined in terms of the radius of gyration of the linear chains in the dilute limit (R_{g0}^{lc}), given by $c^* = N_b^{lc} / \left((4/3)\pi \left(R_{g0}^{lc}\right)^3\right)$.
The inclusion of stickers also introduces two important length scales (shown in Figure 6.1): l_N which is the distance between two A-type stickers and l_d which is the distance between two B-type stickers along the backbone of the linear chain. The details of the methodology to choose l_N and l_d is given in Section B.2. The C-type stickers are present at the ends of the dendrimer arms. The distance between stickers on the linear chain is always reported in terms of ξ^*, where the value of ξ at $c/c^* = 1$ is referred to as ξ^*. For example, $l_N/\xi^* = 1$ means there is an A-type sticker at every ξ^* along the linear chain. The parameter space for this study includes $\epsilon_N = 0, 1, 4, 6, 8, 12$, $\epsilon_d = 0, 1, 4, 8$, $l_N/\xi^* \approx 1, 0.5, 0.25$ and $l_d/\xi^* \approx 1, 0.5, 0.25, 0.1$. The exact values of l_N/ξ^* and l_d/ξ^* are reported in Table B.2. The interaction between any beads other than A-A and B-C stickers is purely repulsive and the well-depth of the SDK potential is zero. The dendrimer is referred to as 'non-sticky' when $\epsilon_d = 0$.

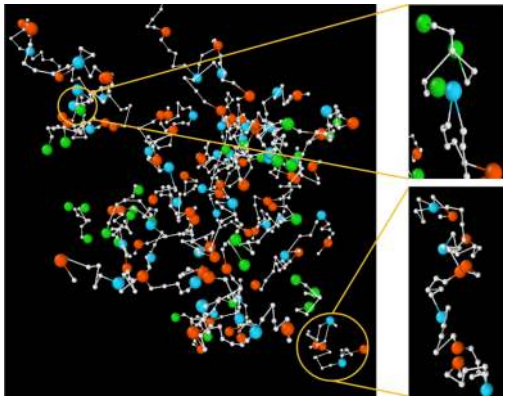

Figure 6.2: A snapshot from simulations of sticky star polymers (f, s, g, χ)=(3,2,0,0.5) in linear associative polymers at $c/c^* = 0.5$. The white beads in the system are the backbone monomers (non-sticky) and the coloured beads are stickers of type A (red), type B (blue) and type C (green). Type A stickers interact with themselves to form a network while types B and C represent the linear chain-dendrimer interaction.

The hydrodynamics interaction parameter is set at $h^* = 0.2$ and the maximum stretchable length of the FENE spring $Q_0^2 = 50.0$. Each simulation trajectory has an equilibration phase ($\approx 10\tau_R$) followed by a production run ($\approx 8\tau_R$), where τ_R is the Rouse relaxation time given by $\tau_R =$

$1/\left(2\sin^2\left(\pi/2N_b^{lc}\right)\right)$ (Bird *et al.*, 1987b). The time step of integration is $\Delta t = 10^{-3}$ to 10^{-4} in non-dimensional units. Properties were calculated from the ensemble averages of 700 – 3000 independent trajectories. Figure 6.2 shows a snapshot of a simulation box containing star polymers and linear chains at $c/c^* = 0.5$.

6.2 Results and discussion

6.2.1 Radius of gyration

The radius of gyration of dendrimers in a semidilute solution of linear chains was found previously to follow the scaling law for linear chains (refer to Section 5.2.1). To understand the effect of sticky interactions on the size of a dendrimer in a polymer network, we calculated the radius of gyration using the equation 3.6.

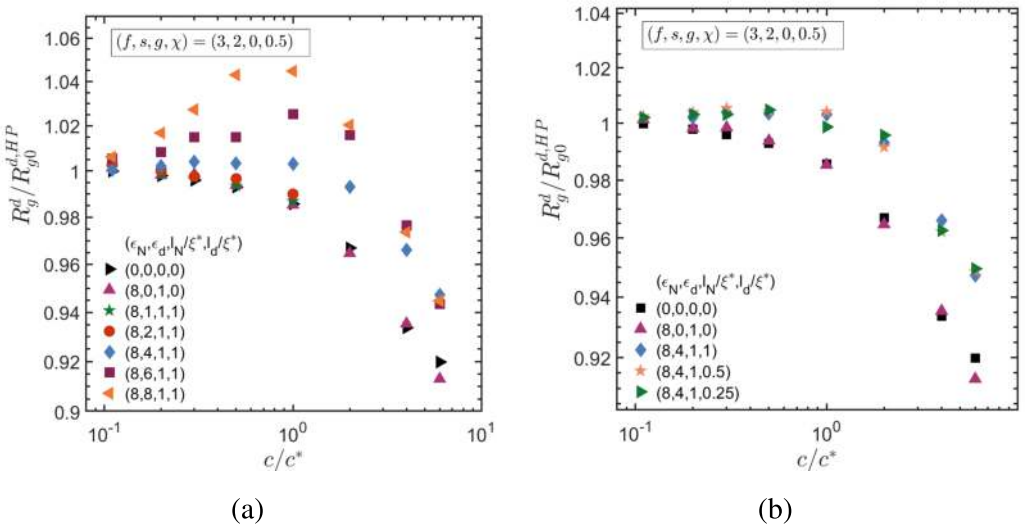

(a) (b)

Figure 6.3: (a) Effect of the sticker strength and concentration on the normalised radius of gyration of dendrimers. The right pointing and up pointing triangles are non-sticky dendrimers in solution and network respectively. The star and circle are sticky dendrimers with low sticker strengths, while the diamond, square and left pointing triangles are for higher sticker strengths. (b) Effect of distance between type B stickers and concentration on sticky dendrimers with $\epsilon_N = 8$ and $\epsilon_d = 4$. For comparison, data for homopolymers in semidilute solutions is also included.

Figure 6.3 shows the effect of sticker strength and the distance between type B stickers on linear chains (l_d) on the size of dendrimers in a polymer network. The radius of gyration is normalised by that in the dilute case (R_{g0}^d). For comparison, this ratio for the same dendrimer architecture in a semidilute solution of linear chains without network forming stickers is also included (black right pointing triangles denoted as (0,0,0,0)). The size of a non-sticky dendrimer (magenta

up pointing triangles denoted as (8,0,1,0)) and sticky dendrimers with low sticker strengths (ϵ_d = 1 and 2) (star and circle symbols respectively) decreases with increasing concentration and follows the scaling law for homopolymers in a semidilute solution given by equation 5.1 (Daoud *et al.*, 1975; Doi *et al.*, 1988; Huang *et al.*, 2010).

This implies that the state of the background chains (solution or network) does not affect the size of the dendrimer, rather the number of beads in its surroundings is what matters. For weak sticker interactions, which means low values of ϵ_d, the dendrimer binds and unbinds frequently to the network, which makes it similar to a non-sticky dendrimer. However, as the sticker strength increases, the dendrimer gets stuck to the network for a longer time. At low concentrations of the linear chains, there are fewer chains and hence fewer type B stickers available for the dendrimer to stick. Far-apart stickers of type B along with long sticking duration result in the stretching of dendrimer arms. Therefore, its normalised radius of gyration increases initially until $c/c^* = 1$ resulting in a maxima as shown in Figure 6.3(a) (refer to the diamond, square and right pointing triangles). Beyond $c/c^* = 1$, the chains come closer to each other, thus decreasing the distance between attachment points for the dendrimer. This, along with conventional Flory screening due to excluded volume (EV) effects leads to a decrease in dendrimer size. It is worth noting that there is a collapse of the normalised radius of gyration of sticky dendrimers with higher values of ϵ_d with increasing concentration.

In Figure 6.3(b), the effect of decreasing l_d on the normalised size of a sticky dendrimer is plotted as a function of concentration. The values of ϵ_N and ϵ_d are fixed at 8 and 4 respectively. The decrease in distance between dendrimer stickers on linear chains gives more available points of attachment to the dendrimer. However, it seems to not affect the dendrimer size.

6.2.2 Internal density distribution

The plot for the radius of gyration for dendrimers has shown that their size increases with increasing strength of adherence to the network due to a higher binding time. This would mean a decrease in the internal density near the core of the dendrimer. To test it, we calculated the internal bead distribution of the dendrimer along its major axis using equation 3.14.

Figure 6.4 shows the distribution of beads for dendrimers of two sticker strengths (ϵ_d = 4 in (a) and ϵ_d = 8 in (b)) with $(\epsilon_N, l_N, l_d) = (8, 1, 1)$. It is observed that irrespective of the strength of interaction between the dendrimer and the linear chain, dendrimers have a dense core. At lower sticker strengths, the bead density remains unaffected by concentration till $1c^*$ as shown in Figure 6.4(a). However, at higher sticker strengths in which a maxima in the radius of gyration was observed, the bead density away from the core of the dendrimer increases till $1c^*$ (Figure 6.4(b)). This is consistent with the increase in R_g^d till $1c^*$, beyond which the dendrimer starts shrinking and the core density increases.

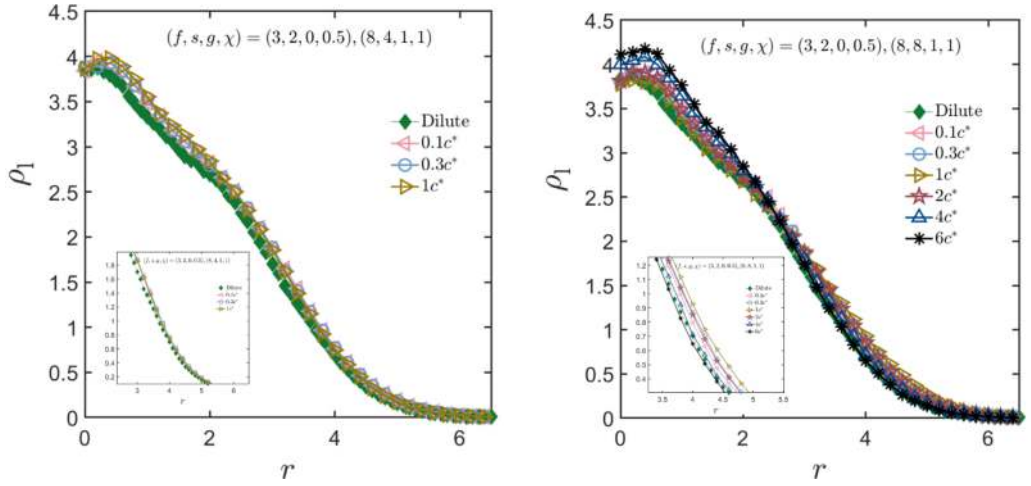

(a) (b)

Figure 6.4: (a) Effect of the concentration on the internal bead density of sticky dendrimers for $\epsilon_d = 4$ (a) and $\epsilon_d = 8$ (b). The system is a functionality three star polymer with $(\epsilon_N, l_N, l_d) = (8, 1, 1)$. Inset: Zoomed in version to show the difference in bead densities away from the core.

6.2.3 Distribution of mesh size

The distance between type A stickers, l_N, is an input to the simulation and to a certain extent, it is a measure of the 'ideal' mesh size. A more accurate measure of the mesh size can be obtained by calculating the mean spatial distance between stickers which is denoted here by a_x. The quantity a_x is defined as the mean squared distance between two adjacent stickers of type A that belong to the same linear chain and are stuck to a sticker on another chain. In other words, it is the distance between two stuck stickers on a linear chain that form an inter-chain association. The algorithm used to calculate a_x is discussed in Section B.3. An illustration of sample configurations is given in Figure 6.5. The bead pairs that contribute to mesh size calculation in (a) are 0-3 and 3-5 in the first chain (red beads) and 6-8 and 8-10 in the second chain (green beads) while in (b) they are 1-3, 3-5 and 6-10 and 10-11 (colours same as in (a)). The average over all chains at specific intervals of time during the entire production run gives an estimate of the actual distribution of mesh size a_x in simulation.

The mesh size of the network through which a probe particle diffuses affects the latter's dynamics to a great extent (discussed in Section 2.2.2 and Section 7.1.1) (Cai *et al.*, 2015; Dell and Schweizer, 2014). However, it is equally crucial to understand the influence of these particles on the mesh size of the network. Using the methodology mentioned in Section B.3, we calculated the distribution of mesh sizes in a network with dendrimers. Figure 6.6 presents the mesh size distribution in the network containing non-sticky dendrimers at two different concen-

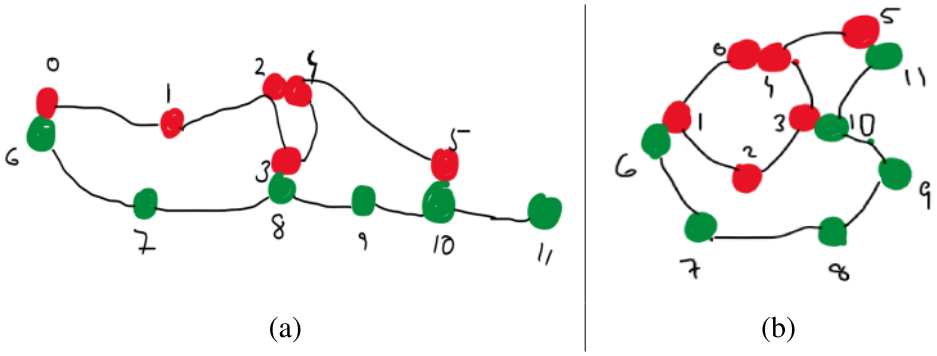

Figure 6.5: Two illustrations of mesh size calculation. Two linear chains with stickers (coloured beads) are shown. Only the stuck beads that form inter chain associations contribute to mesh size calculation. (a) In this figure, the eligible bead pairs are 0-3 and 3-5 in the first chain represented using red beads and 6-8 and 8-10 . (b) Here the bead pairs 1-3, 3-5, 6-10 and 10-11 are considered for mesh size calculation (colours same as in (a)).

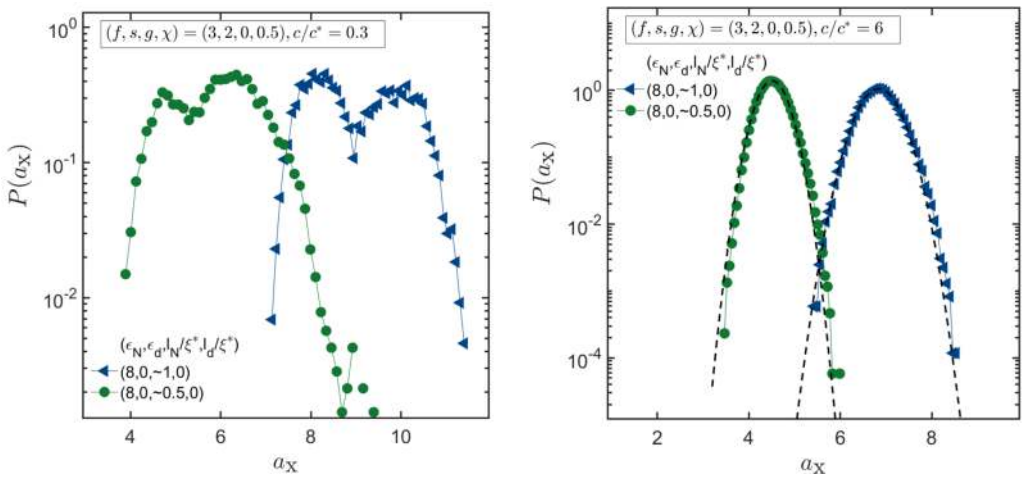

Figure 6.6: Effect of the distance between stickers and concentration on the mesh size distribution of the network. The system considered is ($\epsilon_N = 8$) with a star polymer with functionality three in it. Each figure has two values of l_N, $l_N = 1$ and 0.5. (a) and (b) correspond to $c/c^* = 0.3$ and 6 respectively. The dashed curve in (b) are Gaussian fits to the data.

trations ($c/c^* = 0.3$ in 6.6(a) and $c/c^* = 6$ in 6.6(b)) and each plot includes two values of l_N. For additional cases of l_N, refer to Figure B.4. At lower concentrations, the distribution of mesh size exhibits bimodality, with the local minima being more pronounced when $l_N = 1$ compared to the other values. As concentration increases, the distribution trends toward a Gaussian profile for all values of l_N.

To have a better understanding of the influence of dendrimers on the mesh size, we calculated the mesh size distribution for a network at similar concentrations, but without dendrimers. Figure 6.7 shows the distribution for $l_N = 1$ at $c/c^* = 0.3$. In the absence of dendrimers, the bimodality is absent and the distribution is Gaussian-like with a mean value similar to that of the network with dendrimers. The two peaks of the distribution are symmetrically spaced about the mean value of the no-dendrimer case, and the mean mesh size is around twice the diameter of the dendrimer calculated as $2R_g^d$. The vertical lines on the upper x-axis in Figure 6.7 indicates that the maximas occur at $a_x/2R_g^d = 1.7$ and 2.1, while the mean mesh size is equal to 1.9 times $2R_g^d$. The dashed curve is a Gaussian fit to the data.

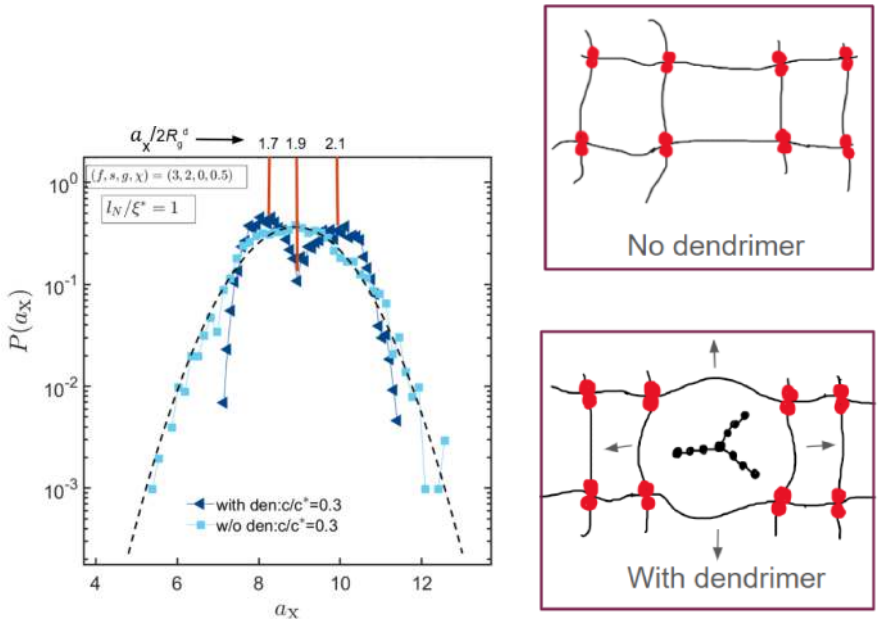

Figure 6.7: Effect of the presence of non-sticky dendrimers on the mesh size distribution for $l_N/\xi^* = 1$ at $c/c^* = 0.3$. The dashed curve is a Gaussian fit to the data and the vertical lines are guide to the eye for the peaks and minima in the distribution with respect to the size of the dendrimer. An illustration of the effect of dendrimers on the mesh size is shown on the left.

It is important to note that at low concentrations, the number of dendrimers and linear chains is comparable. When a dendrimer occupies a 'cage' in the mesh, the strands forming the cage expand due to repulsion from the dendrimer molecule, thus increasing the mesh size as shown

in the schematic in Figure 6.7. Consequently, if the adjacent cage is empty, it is likely to be compressed (as illustrated), leading to a higher probability of observing both larger and smaller meshes than the mean mesh size, thereby generating a bimodal distribution. However, as concentration increases, there are more stickers (Type A) available in the system, increasing their probability of binding to form a network with a large number of empty meshes, which are smaller. This is because the number of dendrimers which remain dilute has not changed. Therefore, the bimodality is absent at $c/c^* = 6$ (Figure 6.6(b)) and the maxima of the distribution has shifted to the left. This interpretation is further confirmed by simulations in which the number of dendrimers was increased, keeping the number of linear chains fixed (discussed in detail in Section B.4). As shown there, the double peaks vanish as the number of dendrimers is increased while the dynamics of dendrimers are unaffected by the presence of a bimodality in the distribution.

The presence of a sticky dendrimer also affects the network mesh size distribution, however, it does not lead to bimodality as shown in Figure 6.8. It should be noted that the distribution is broader in the presence of a sticky dendrimer relative to the non-sticky dendrimer case. In the latter, the interaction between the dendrimer and the network is purely repulsive. On the other hand, a sticky dendrimer, due to its attractive interaction with the network, pulls the network towards itself, thus leading to finite probabilities of having smaller and larger meshes, indicating increased pore heterogeneity and a broader network. The sticker strength ϵ_d seems to not affect the distribution. Note that the value of ϵ_d only determines the ease with which the dendrimer unbinds from the network which is a dynamic quantity.

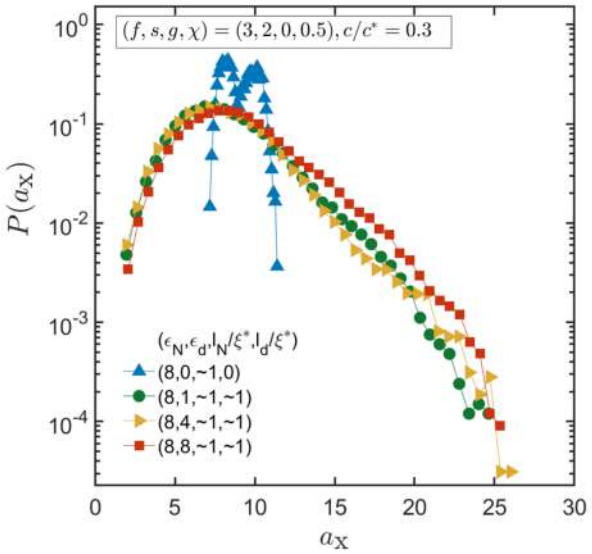

Figure 6.8: Effect of sticker strength ϵ_d on the mesh size distribution of the network. A range of ϵ_d is considered with a fixed value of $\epsilon_N = 8$.

Even though the methodology used is different, double peaks in the pore size distribution, $P(2r)$, of polydisperse polymer networks with spherical nanoparticles have been observed by Sorichetti *et al.* (2021) (shown in Figure 6.9). Here, r is the radius of the largest sphere containing the point without touching the network. The authors have considered repulsive and attractive nanoparticles referred to as RNPs and ANPs respectively. In both cases, the first peak is more pronounced and is located at the same r as that of a pure system with no nanoparticles. The second peak is a smaller one and is roughly located at $2r = \sigma_{\mathrm{NP}}$. Specifically, nanoparticles with repulsive interactions within the network, were found to broaden the distribution and the second peak is located at $\sigma_{\mathrm{NP}} + \delta$, where δ is a small shift. This is attributed to a larger effective diameter of the RNP due to its repulsion which also leads to a deformation of the surrounding network. On the other hand, the attractive nanoparticles have a sharp peak at σ_{NP} due to the 'cavity' it forms in the network. For smaller ANPs, they also observe a decrease in the mean mesh size due to the contraction of the network, a consequence of the attractive monomer-NP interaction.

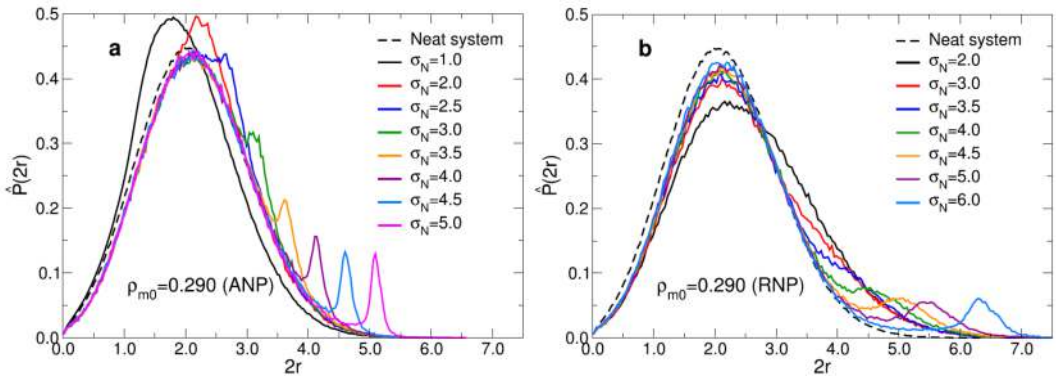

Figure 6.9: The pore size distribution of polydisperse polymer networks with spherical nanoparticles. Systems with attractive nanoparticles (a) and repulsive nanoparticles (b) with varying size. Image reproduced from Sorichetti *et al.* (2021), for illustration purposes only, under fair use for research.

Their observations for systems with RNPs are similar to the non-sticky dendrimers cases regarding the presence of double peaks. However, its location and amplitude are different. Also, we observe a single broad peak in the case of sticky dendrimers. These differences can be due to the ability of dendrimers to stretch and achieve any configuration and size, unlike nanoparticles.

6.3 Conclusions

The static properties of sticky and non-sticky dendrimers along with the mesh size distribution have been analysed. We find that the size of non-sticky dendrimers and sticky dendrimers of low sticker energies remains constant in the dilute regime and it decreases in the semidilute regime

following the same scaling law as that of linear chains and dendrimers in polymer solutions. Conversely, sticky dendrimers with high ϵ_d expand up to $1c^*$, after which they collapse, following a master scaling curve. Interestingly, the spacing between stickers on the linear chains did not affect dendrimer size. Consistent with this observation is the bead density distribution of sticky dendrimers. The density of beads away from the core increases till $1c^*$ and later drops with increasing concentration. Irrespective of the stickiness or concentration, all dendrimers have a dense core, with density dropping towards the periphery. On analysing the mesh size distribution of the network, it was observed that the non-sticky dendrimers create 'cavities' in the network, thus leading to a bimodal distribution of mesh sizes, while the sticky interaction between the dendrimer and the network stretches the meshes leading to a broader distribution. In the following chapter, the dynamic properties of sticky and non-sticky dendrimers in a network of linear associative polymers are discussed.

Chapter 7

Diffusion of sticky and non-sticky dendrimers in polymer networks

Anomalous diffusion of tracer particles in complex media is characterised by deviations from Brownian motion, where the mean squared displacement (MSD) has a power law dependence on time, $MSD = Dt^{\alpha}$ where D is the diffusion constant, α is the diffusion exponent with $\alpha \neq 1$ (Metzler and Klafter, 2000). This behaviour can be subdiffusive ($\alpha < 1$) or superdiffusive ($\alpha > 1$), depending on the properties of the medium and the interaction between the medium and tracer. Subdiffusion has been widely observed in systems like particle transport in the cytoplasm (Norregaard *et al.*, 2017), diffusion of proteins through the Nuclear Pore Complex (NPC) (Chatterjee and Cherayil, 2011; Ando and Gopinathan, 2017), virus diffusion in mucus (Barr *et al.*, 2013a, 2015), and nanoparticle diffusion in polymer solutions (Nahali and Rosa, 2018) and gels (Godec *et al.*, 2014). While much of the existing research focuses on hard-sphere tracers, the diffusion of soft colloids remains less understood despite their increasing use in drug delivery and catalysis due to their tunable properties. In this chapter, we investigate the dynamics of sticky dendrimers in an associative polymer network of linear chains (as shown in Figure 2.4(b) and (c)), to explore tracer diffusion through a polymer network. Our results are validated with analytical nanoparticle diffusion theories and experimental systems.

Two major analytical theories have been developed to describe nanoparticle dynamics within permanently crosslinked polymer networks. While the theory of hopping proposed by Cai *et al.* (2015) describes the diffusion of non-sticky hard spheres with a size larger than the network mesh size, the theory by Dell and Schweizer (2014) includes soft nanoparticles with attractive interactions with the network as well. Unlike in polymeric liquids, the constraint release mechanism is absent in dry networks or gels, making nanoparticle mobility completely dependent on the hopping process. Hopping occurs when one of the network strands confining the nanoparticle slips around it due to thermal fluctuations (Cai *et al.*, 2015). The significance

of the confinement parameter in determining the dynamics of nanoparticles has been independently predicted by Cai *et al.* (2015) and Dell and Schweizer (2014), although the two theories offer qualitatively different predictions regarding nanoparticle diffusivity as discussed in Section 2.2.2. Apart from diffusivity, several other properties have been studied for nanoparticles, including the diffusion exponent, the probability distribution function of displacements and velocity autocorrelation functions. However, there is a lack of research on the mobility of soft colloids in polymer networks (Ge, 2024) with hydrodynamic interactions included. The terminal diffusivity of dendrimers observed in our simulations is systematically compared with the theoretical frameworks for nanoparticles. Our findings indicate that the theoretical model proposed by Dell and Schweizer (2014) appears to be more appropriate for dendrimers.

As an attempt to bridge the gap in our understanding of soft colloid behaviour, we simulate dendrimers in an associative polymer network, with the inclusion of key interactions like the excluded volume and hydrodynamics interactions. We also aim to determine whether the sole cause of the observed differences between the behaviour of T4 and T4Δ*hoc* phage is the adherence between T4 capsid and mucus. By varying the linear polymer concentration, dendrimer architecture and sticker strength, we compare the dynamics of non-sticky dendrimers with established nanoparticle theories. The nature of diffusion and diffusivity of dendrimers interacting with the network is examined by varying the interaction strength, sticker spacing and the concentration of linear chains. These findings are then compared with the behaviour of phages. Note that the algorithm employed in this study does not account for entanglements and, hence cannot be used to study concentrated entangled systems where hydrodynamic interactions are screened.

7.1 Results and discussion

The dendrimer architectures and parameters used in this chapter are the same as those discussed in Section 6.1.

7.1.1 Effect of network-related parameters

As mentioned earlier, there are two main theoretical frameworks that explain diffusion processes of nanoparticles in crosslinked polymer networks. According to the analytical theory by Cai *et al.* (2015) based on scaling theory, probe particles in an unentangled permanently crosslinked network exhibit ballistic motion at short times, during which the particle does not experience the influence of the polymer strands. This behaviour continues until a characteristic timescale, τ_{bal}, after which the particle becomes subdiffusive (with a diffusion exponent of 0.5) due to the coupling of its motion to the segmental dynamics of the network strands (Cai *et al.*, 2011). At an

intermediate time, τ_a, the probe experiences confinement from the surrounding strands, causing it to become stationary until a further timescale, τ_w (shown in Figure 7.1). The stationary phase demarcates the trapping of such large particles in polymer cages. Beyond τ_w, there is a finite, though very small, probability for the particle to hop between adjacent cages. This hopping probability increases significantly after a timescale τ_{hop}, at which the mean squared displacement resulting from hopping becomes comparable to that caused by fluctuations of the nanoparticle within the confinement cage. Consequently, the nanoparticle becomes diffusive after τ_{hop}.

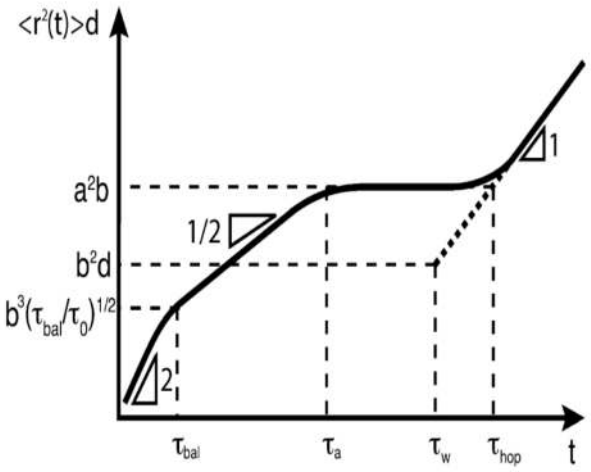

Figure 7.1: The mean squared displacement versus time plot for nanoparticles in network indicating the important timescales and various regimes. Image reproduced from Cai *et al.* (2015), for illustration purpose only, under fair use for research.

The alternative theoretical framework for nanoparticle diffusion in polymer network proposed by Dell and Schweizer (Dell and Schweizer, 2014) is based on the nonlinear Langevin equation and polymer reference interaction site model (PRISM) theory (Schweizer and Curro, 1997; Hall and Schweizer, 2008). Their predictions indicate that the onset of hopping occurs after a critical value of the confinement parameter, denoted as C_c. Beyond this threshold, the nanoparticle becomes confined within network cages, and hopping is the only process for nanoparticle mobility.

To investigate the effect of concentration, $\epsilon_{\text{N}}, l_{\text{N}}$ and a_{x} on dendrimer dynamics, we calculated the mean squared displacement of a non-sticky dendrimer under varying concentrations, l_{N} and ϵ_{N} using equation 3.15. Consistent with the behaviour of homopolymer dendrimers in semidilute solutions of linear chains, we found that the dendrimer remains diffusive as long as its size is smaller than the correlation length of the solution (ξ) (shown in Figure 7.2(a)). The concentration at which the onset of subdiffusion is observed depends on the size ratio between

the dendrimers and linear chains. For $\chi = 0.5$, this happens beyond $1c^*$, the concentration after which the size of the dendrimer is larger than ξ (refer to Section B.5). Note that the dendrimer is smaller than the mesh size a_x at all concentrations. This demonstrates that the dendrimer dynamics remain unchanged regardless of the state of surrounding polymers. Figures 7.2(b) and (c) demonstrate that variations in ϵ_N and l_N have minimal impact on the dynamics of non-sticky dendrimers at $c/c^* = 1$. A similar behaviour is observed in the case of sticky dendrimers dendrimers as well (shown in Section B.6).

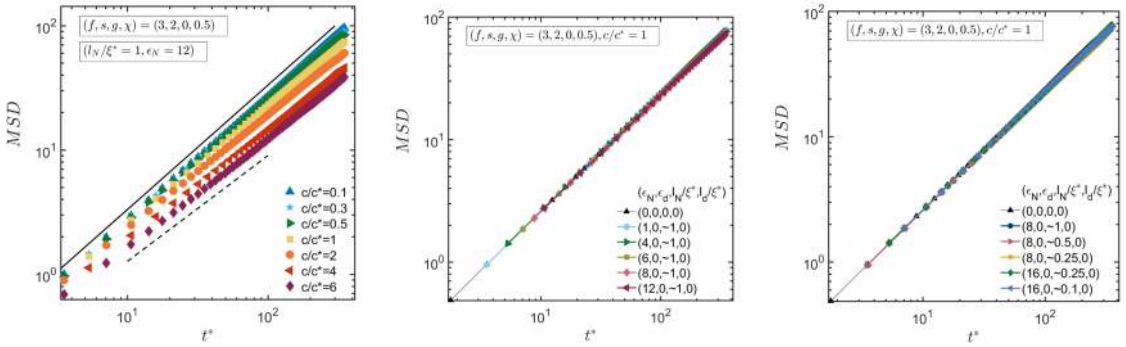

(a) (b) (c)

Figure 7.2: (a) Effect of concentration of linear chains on the mean squared displacement of a non-sticky dendrimer. The system considered is $(\epsilon_N, l_d/\xi^*)$=(12, 1). The straight line is a with slope=1 and the dashed line has a slope less than one. (b) Effect of the sticker strength of the network-forming stickers. (c) Effect of the distance between the network forming stickers.

7.1.2 Mean squared displacement of sticky dendrimers

The mobility of a sticky dendrimer in an associative polymer network is governed by the strength of interactions between dendrimer stickers and the surrounding polymer chains (ϵ_d) and the distance between the dendrimer interaction stickers (Type B) on the linear chain (l_d). Additionally, the concentration of the background chains also affects its dynamics, like in the case of non-sticky dendrimers.

At a fixed concentration, increasing the sticker strength has a profound impact on the MSD of the sticky dendrimer as shown in Figure 7.3(a). At short and long times, these dendrimers exhibit normal diffusive motion like nanoparticles and non-sticky dendrimers in a network. However, subdiffusion kicks in at intermediate times. At low sticker strengths (ϵ_d), the dendrimer behaves similarly to a non-sticky dendrimer, with almost no effect on its MSD. This behaviour parallels trends observed in the radius of gyration, where weak interactions do not significantly alter dendrimer size (shown in Figure 6.3). As ϵ_d increases, the number of binding and unbinding events is fewer and the dendrimer remains attached to the network for longer durations.

This extended residence time results in a slower diffusion rate. The onset of subdiffusion was observed even when the size of the dendrimer was smaller than the network correlation length (which is true at low concentrations) indicating that it is the dendrimer-linear chain interactions that primarily influence dendrimer dynamics. To understand the effect of the number of stickers, we varied l_d at a constant ϵ_d. Reducing l_d increases the number of potential binding sites available to the dendrimer. This leads to a decrease in the MSD, though the effect is less pronounced compared to changes in sticker strength (shown in Figure 7.3(b)). Further, the effect of background chain concentration was analysed. As the concentration of background polymer chains increases, the mean squared displacement (MSD) of sticky dendrimers decreases significantly, indicating slower diffusion. Interestingly, in contrast to nanoparticles that exhibit a region of constant MSD due to trapping in polymer cages followed by a hopping mechanism that leads to diffusion at longer times (Cai *et al.*, 2015), dendrimers—whether sticky or non-sticky—do not show such long-term confinement at any concentrations or architectures considered in this study. Both types of dendrimers transition from subdiffusive to diffusive regimes without evidence of persistent trapping. This behaviour may be due to the flexible architecture of dendrimers, allowing for shape fluctuations that facilitate their escape from polymer cages, unlike the rigid structure of nanoparticles. The effect of ϵ_d and l_d on sticky dendrimers is similar across different dendrimer architectures as shown in Section B.9.

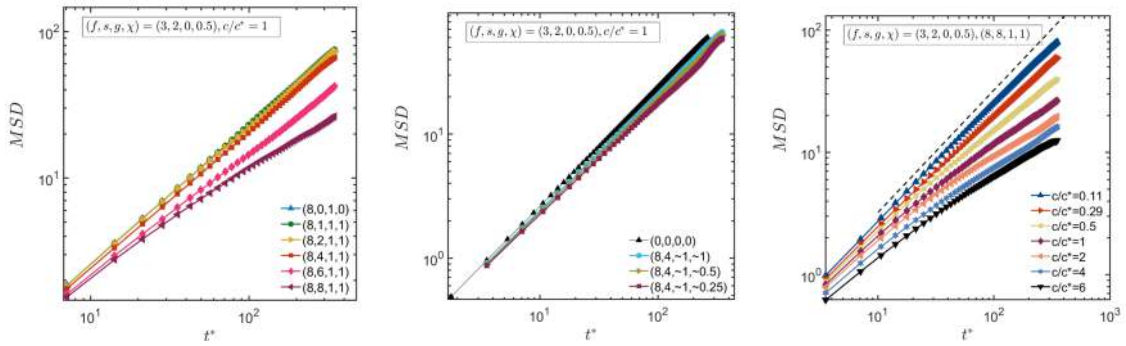

(a) (b) (c)

Figure 7.3: (a) Effect of the sticker strength ϵ_d on the MSD of sticky dendrimers. (b) Effect of the distance between the dendrimer interaction stickers l_d. (c) Role of concentration of linear chains on the mean squared displacement of a sticky dendrimer. The dashed line is a with slope=1.

7.1.3 Probability distribution function of displacement

Probe particles that exhibit subdiffusion are often characterised by non-Gaussian probability distribution of displacements, as a result of the hopping movement of the tracers and heterogenities of the environment (Phillies, 2015; Kumar *et al.*, 2019; Wang *et al.*, 2012; Smith *et al.*,

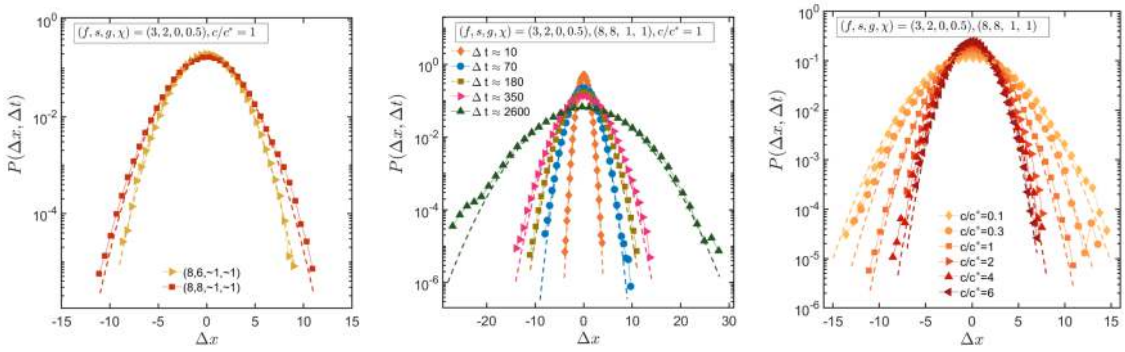

(a) (b) (c)

Figure 7.4: (a) Effect of the sticker strength of the network-forming stickers on the PDD. The times at which PDD is calculated are well into the subdiffusive regime. (b) The probability distribution functions calculated at different times. (c) Effect of concentration of linear chains on the probability distribution function of displacement of a sticky dendrimer. The dashed lines in all figures are Gaussian fits. The system considered in (b) and (c) is $(\epsilon_N, \epsilon_d, l_N/\xi^*, l_d/\xi^*)$=(8, 8, 1, 1).

2021; He *et al.*, 2016; Jee *et al.*, 2014). However, in the case of a homopolymer dendrimer diffusing in a solution of linear chains, the probability distribution of displacement remained Gaussian regardless of the time and concentration, even though subdiffusion was observed (section 5.2.6). This suggests that despite the restricted movement typical of subdiffusion, the homopolymer dendrimers experience relatively uniform interactions within the polymer solution. The probability distribution function of displacement of a molecule displaced by a distance Δx in a time Δt is given by equation 3.18. In the case of sticky dendrimers, which also exhibit subdiffusion, we observe slight deviations from Gaussian distributions particularly at intermediate times (shown in Figure 7.4(a)). This deviation becomes more pronounced at higher sticker strengths (ϵ_d), where the dendrimer adheres more strongly to the polymer network. At lower sticker strengths, the distribution remains closer to Gaussian, suggesting that dendrimer displacement is unaffected by such weak interactions. Initially, at short times, the diffusion of sticky dendrimers is Gaussian, indicative of free movement. However, as the system transitions to the subdiffusive regime, the distribution shifts towards non-Gaussian behaviour (refer to Figure 7.4(b)), highlighting the effect of the dendrimer's binding to the polymer network. Deviations from Gaussian distribution are also observed at higher concentrations of the polymer network at the intermediate times as shown in Figure 7.4(c). At these concentrations, the dendrimer experiences a greater degree of confinement, resulting in a higher likelihood of both smaller and larger displacements compared to what would be expected from a random walk. The smaller displacements occur when the dendrimer remains adhered to the network, limiting its movement. On the other hand, when the dendrimer unbinds from the network, it is free to

move freely for brief periods before getting attached again. This intermittent mobility resembles the continuous-time random walk model, where the particle alternates between periods of trapping and free movement (Montroll and Weiss, 1965).

7.1.4 Diffusion exponent

In the context of phage diffusion in mucus, the experiments of Barr *et al.* (2015) indicate that the difference between the T4 and T4Δhoc phages is at low concentrations when their sizes are smaller than the mucus mesh size. The T4 phage is subdiffusive while the T4Δhoc remains diffusive. However, at higher concentrations, the mesh size of mucin is smaller than the phage particle, and the diffusion exponents of both phages converge as they get trapped in the mesh. In semidilute solutions of linear chains, the diffusion dynamics of non-sticky dendrimers exhibited subdiffusion like those of rigid nanoparticles with a diffusion exponent higher than that of a hard sphere at similar concentrations. This indicates that dendrimers experience less confinement in these polymer environments due to their ability to deform and bypass the polymer cages 5.2.5. On introducing the network forming stickers in the background linear chains to create a network, the diffusive behaviour of non-sticky dendrimers remains largely unchanged. It remains diffusive at low concentrations with $\alpha = 1$, and subdiffusion is observed only when the size of the dendrimer is greater than the network correlation length irrespective of the values of ϵ_N and l_N. However, when the dendrimer begins to adhere to the network, it starts exhibiting subdiffusion even at lower concentrations. Both sticky and non-sticky dendrimers in our simulations encounter hindrance due to the cages formed by the polymer network, and the size and lifetime of these cages are influenced by the concentration of the network-forming linear chains, the sticker strength (ϵ_N), and the spacing between stickers (l_N) of type A.

A comparison between the mean squared displacement of sticky and non-sticky dendrimers of sizes smaller than the mesh size or the correlation length is shown in Figure 7.5(a). It is evident from this plot that the adhesion of the dendrimer to the network causes it to become subdiffusive, a phenomenon analogous to the behaviour of phages in mucus. However, the observed subdiffusion is restricted to intermediate times, with the dendrimers being diffusive at short and large times. To show the transition clearly, we have plotted the diffusion exponent as a function of the time of the dendrimer by computing the instantaneous derivative of the MSD as given below:

$$\alpha = \frac{d \log(\mathrm{MSD}(\tau))}{d \log \tau} \tag{7.1}$$

The non-sticky dendrimer exhibits diffusive behaviour across all observed timescales, with $\alpha \approx 1$ as shown in Figure 7.5(b). Whereas, the diffusion exponent of the sticky dendrimer begins

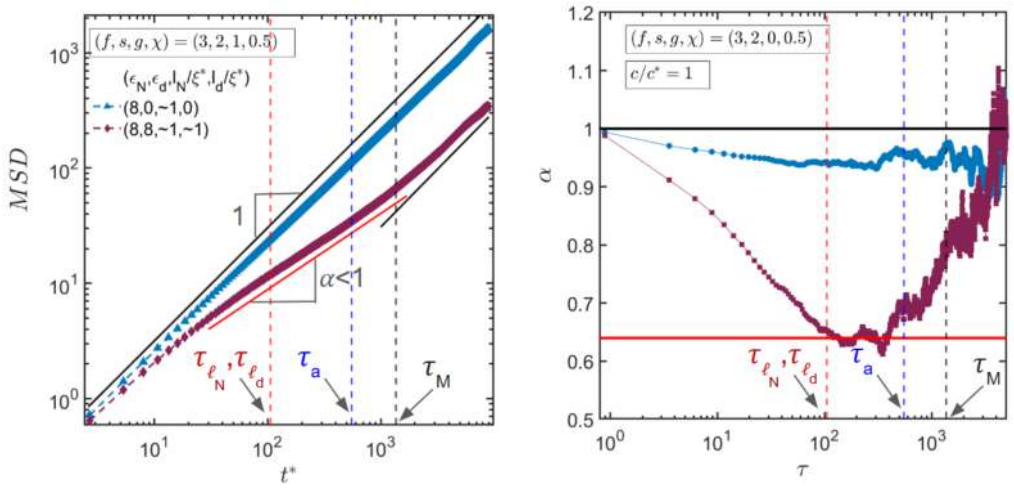

Figure 7.5: (a) The mean squared displacement of sticky and non-sticky dendrimers of identical architectures in polymer network at $c/c^* = 1$. (b) The diffusion exponent as a function of time for sticky and non-sticky dendrimers. The system considered is the same as that in (a). The dashed lines in both figures show the important timescales involved. The red horizontal line corresponds to $\alpha_{\min}$ for the sticky dendrimer.

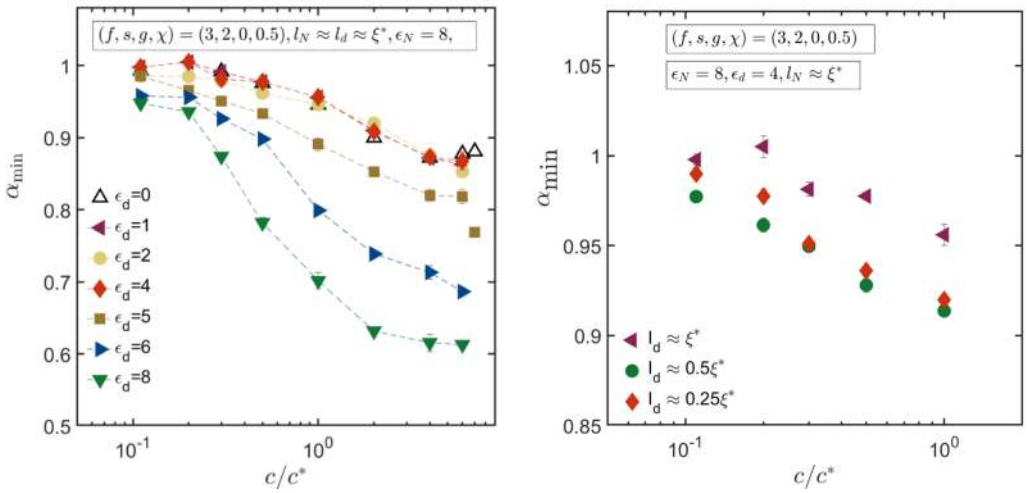

Figure 7.6: (a) Effect of the sticker strength and concentration on the minimum diffusion exponent of dendrimers. (b) Effect of distance between stickers and concentration on the minimum diffusion exponent of dendrimers.

near unity at short times, transitions to values less than one at intermediate times and eventually becomes one at long times. The inclusion of stickers introduces four important timescales in the system that significantly influence the dynamics of sticky dendrimers. These timescales are related to the characteristic distances and interaction strengths in the system, specifically l_{N}, l_{d}, ϵ_{d} and a_x ; and are named as $\tau_{l_{\mathrm{N}}}$, $\tau_{l_{\mathrm{d}}}$, τ_{M} and $\tau_{a_{\mathrm{x}}}$ respectively.

1. $\tau_{l_{\mathrm{N}}}$: This represents the relaxation time of a chain segment of length equal to l_{N}.
2. $\tau_{l_{\mathrm{d}}}$: This corresponds to the relaxation time of a chain segment of length l_{d}.
3. τ_{M}: The time for which a sticker remains bound to another sticker is referred to as τ_{M} and it increases exponentially with sticker strength (Rubinstein and Semenov, 2001; Robe *et al.*, 2024).
4. $\tau_{a_{\mathrm{x}}}$: This timescale corresponds to the relaxation time of a chain segment with length a_{x}.

The expressions used for the calculation of these timescales are given in Section B.8. The onset of subdiffusive behaviour in the sticky dendrimer happens around $\tau_{l_{\mathrm{d}}}$, which is the time required for the dendrimer to encounter stickers on the network. Due to the combined effect of sticking and trapping, the sticky dendrimer remains subdiffusive. To transition back to the diffusive regime, the dendrimer must either unbind from the network or be released through the fluctuations in the cage-forming strands. Consequently, this return to the diffusive regime typically happens approximately after τ_{a_x} and τ_{M} as shown in Figure 7.5(b).
The diffusion exponent is also calculated using power law fits to the MSD data in the intermediate times. This gives the minimum diffusion exponent (α_{min}) and is indicated using the red line in Figure 7.5. It systematically decreases with increasing sticker strength ϵ_{d} (shown in Figure 7.6(a)). Stronger interactions between dendrimers and linear chains lead to longer binding times, which slows the overall motion of the dendrimer resulting in $\alpha_{\mathrm{min}} < 1$. The minimum diffusion exponent also decreases with increasing concentration, similar to that in a semidilute solution.
Similarly, by reducing the distance between stickers on the polymer chains l_{d}, α_{min} decreases (Figure 7.6(b)). This is because of the increased interaction between the dendrimer and the network, thus damping its movement through the network. Similar trends have been observed in dendrimers of different architectures (refer to Section B.9).

7.1.5 Terminal diffusivity

Analytical theories for nanoparticle diffusion through polymer networks propose relations for the terminal diffusivity in terms of confinement parameter given by equation 2.3 and equation 2.4. Recently, using MD simulations, Sorichetti *et al.* (2021) have demonstrated that both

these theoretical frameworks hold true in the case of repulsive and weakly attractive nanoparticles in a crosslinked polymer network. Based on equation 2.3 from the hopping theory, they used the following relation to fit their simulation data for the terminal diffusivity D_{N}:

$$D_{\mathrm{N}} = A \exp[-(BC)^2]/BC \tag{7.2}$$

where A and B are fitting parameters, thus validating the hopping theory. By incorporating the dependencies of the mean jump length Δ_h on the confinement parameter C and considering the concept of free energy barrier in equation 2.4, they propose that D_{N} depends on C as follows:

$$D_{\mathrm{N}} = A' \exp[-(B'C)^{\delta}] \tag{7.3}$$

where A', B' and δ are fitting parameters. Using appropriate choice of the fitting parameters, Sorichetti *et al.* (2021) show that their simulations follow the analytical predictions of Dell and Schweizer (2014) as well. Equation 7.3 seems to be structurally similar to equation 7.2, however the two are different due to the latter's dependence on the confinement parameter in the denominator.

The normalised diffusivity of a number of gel-solute systems has also been studied based on the free volume and obstruction theories (Amsden, 1998; Masaro and Zhu, 1999; Axpe *et al.*, 2019). However, these approaches do not account for the effect of the flexibility of the network polymer chains, which has been recently identified as a crucial factor influencing nanoparticle dynamics (Kumar *et al.*, 2019; Godec *et al.*, 2014). Therefore, Quesada-Pérez *et al.* (2021) proposed a unified model for the relative diffusivity of nanoparticles in flexible, crosslinked hydrogels, expressed as a function of the parameter β:

$$D/D_0 = \exp\left(-1.77\beta^{1.07}\right) \tag{7.4}$$

where $\beta = \phi\left(1 + R_s/R_p\right)$, ϕ is the volume fraction of polymer solution, R_s is the radius of the solute and R_p is the radius of the polymer. A recent simulation study has validated this theory for solutes of varying sizes in polymer networks with different bond stiffness (Quesada-Pérez *et al.*, 2022). However, these simulations did not account for hydrodynamic interactions.

In Section 5.2.8, it has been shown that dendrimers, owing to their size fluctuations, do not follow the scaling law developed for terminal diffusivity of nanoparticles in semidilute polymer solutions. Instead, they have a different scaling exponent, which changes with increasing functionality. To investigate if the nanoparticle theories in the polymer network applies to floppy dendrimers, we calculated the terminal diffusivity of sticky and non-sticky dendrimers in the longtime diffusive regime. The confinement parameter for dendrimers is given below:

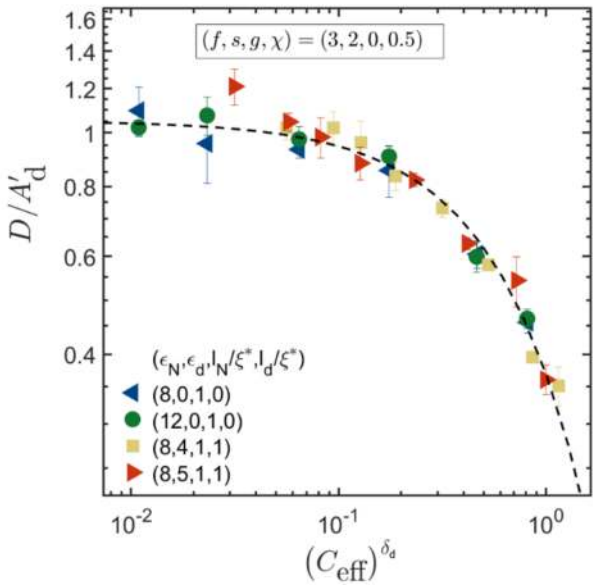

Figure 7.7: The normalised terminal diffusivity of non-sticky and sticky dendrimers as a function of normalised confinement paramter. The dashed line is equation 7.3

$$C_d = \frac{2R_g^d}{\xi} \tag{7.5}$$

Following the arguments of Sorichetti *et al.* (2021), the normalised diffusivity D/A'_d is plotted as a function of the normalised confinement parameter $(C_{eff})^{\delta_d}$, where $C_{eff} = B'_d C_d$. Both the non-sticky and sticky dendrimers having a range of sticker energies follow equation 2.4 as shown in Figure 7.7. The values of the various coefficients are given in Table 7.1. These are different from those reported by Sorichetti *et al.* (2021) for nanoparticles. There are deviations from equation 7.3 at lower $(C_{eff})^{\delta_d}$, which corresponds to small C_d. This is expected as the the-

Table 7.1: Values of fitting parameters used in Figure 7.7. Various systems are reported using a combination of $(\epsilon_N, \epsilon_d, l_N/\xi^*, l_d/\xi^*)$.

System	A'_d	B'_d	δ_d
$(8, 0, 1, 0)$	1.01	−0.25	2.00
$(12, 0, 1, 0)$	1.01	−0.25	2.00
$(8, 4, 1, 1)$	0.04	0.31	1.00
$(8, 5, 1, 1)$	0.03	0.27	1.14

ory is derived for higher confinement parameters. The fitting parameters for the two non-sticky dendrimer cases considered are the same since they exhibit similar diffusive dynamics at all concentrations as discussed in Section 7.1.1. However, sticky dendrimers show decreased mobility when the sticker strength ϵ_d is increased, hence they require different fitting parameters. Also, we have reported the terminal diffusivities of systems only for which we were able to acquire data in the terminal diffusive regime in the case of sticky dendrimers. Note that dendrimers in our simulations were not seen to not follow equation 7.2 and equation 7.4.

7.2 Comparison with phage experiments

Using particle tracking experiments, Barr *et al.* (2015) observed subdiffusion in T4 phage while the T4Δ*hoc* remained diffusive when its size was smaller than the surrounding mesh size. The transition to subdiffusive dynamics for T4Δ*hoc* phage occurs at high concentrations (beyond 2% mucin concentration) as they get trapped in the mesh. Similarly, in our simulations using dendrimers in semidilute polymer solutions as well as networks, it is observed that non-sticky dendrimers become subdiffusive when their size is greater than the system correlation length. The concentration at which this transition happens depends on the ratio between the radius of gyration of dendrimers and linear chains, defined as χ. A higher value of χ implies longer linear chains for a given dendrimer architecture and dendrimers remain smaller than correlation length till high concentrations. This delays the onset of subdiffusion in non-sticky dendrimers. In order to compare our results with experiments, we chose $\chi = 0.3$ so that the non-sticky dendrimer becomes subdiffusive around $2c^*$.

The experimental subdiffusion exponent was obtained by fitting a power law across the entire trajectory, in contrast to the analysis approach used in this study. To align with our analysis, a re-examination of the experimental data was performed, focusing on the intermediate time regime to obtain the diffusion exponent. This is particularly helpful as long timescales in some trajectories displayed noise. Initially, we fitted a best-fit line to the intermediate time data to obtain the subdiffusion exponent (refer to Figure B.9). The resulting value was found to be consistent with the mean of the instantaneous diffusion exponents in the intermediate regime as demonstrated in Figures B.10 and B.11. The subdiffusion exponent thus obtained and the values reported by Barr *et al.* (2015) are plotted in Figure 7.8 for comparison. The original values of α for T4Δ*hoc* phage agree with the values we obtained through this intermediate time fit, denoted as T4 Δ*hoc*-processed. However, there are discrepancies in the case of T4 phage, notably at 2% mucin concentration. It also appears that the diffusion exponent of T4 phage appears to level off at $\alpha = 0.85$ as shown in Figure 7.8. Note that the error bars on the processed diffusion exponents are large due to the noise in the mean squared displacement data.

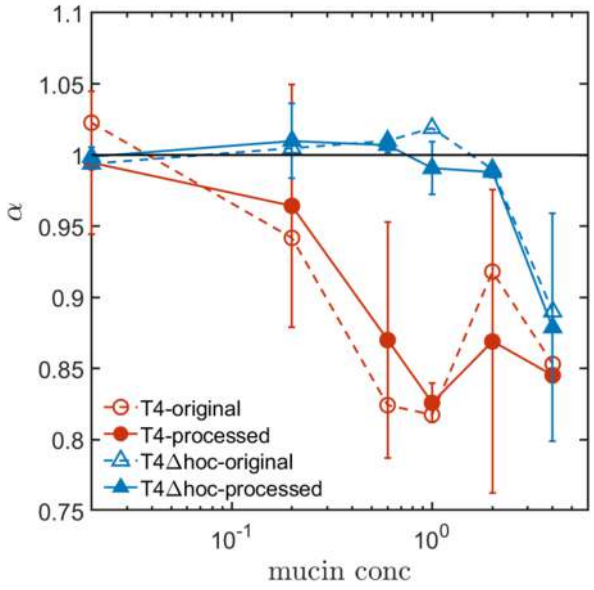

Figure 7.8: Diffusion exponent reported by Barr *et al.* (2015) and that processed from raw data to obtain $\alpha_{\min}$.

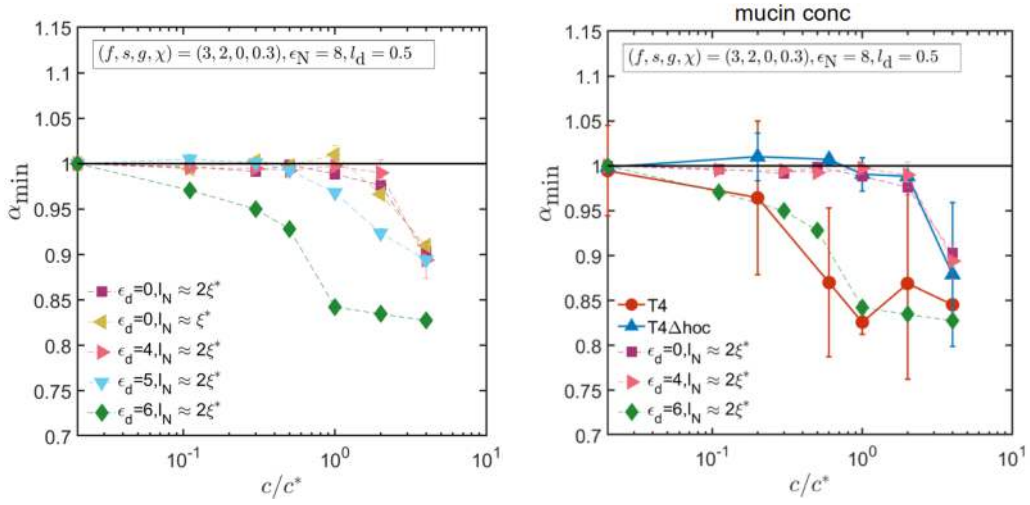

Figure 7.9: (a) Minimum diffusion exponents of sticky and non-sticky dendrimers with a range of sticker strengths and size ratio $\chi = 0.3$. (b) Comparison of the minimum diffusion exponents of sticky and non-sticky dendrimers (with $\chi = 0.3$) and T4 and T4Δ*hoc* phages. The processed data from 7.8 is used in (b).

Figure 7.9(a) shows the minimum diffusion exponents of both non-sticky and sticky dendrimers with different ϵ_d and $\chi = 0.3$. The overall trend of α_{min} with increasing concentration and ϵ_d remains the same as that of $\chi = 0.5$ case (shown in Figure 7.6). However, subdiffusion is delayed until $c/c^* \approx 2$ for the non-sticky dendrimers for $\chi = 0.3$. The sticky dendrimers with $\epsilon_d = 4$ have exactly the same subdiffusion exponents as that of non-sticky dendrimers. With increasing ϵ_d, they become subdiffusive much earlier with the minimum diffusion exponent leveling off at higher concentrations. In Figure 7.9(b), the processed α_{min} values for phages and the simulation results for dendrimers are plotted as functions of mucin concentration (upper x-axis) and c/c^* (bottom x-axis) respectively. It is remarkable that the minimum diffusion exponents of dendrimers with $\epsilon_d = 6$ and the T4 phage follow a similar trend with increasing concentration and are in agreement within error bars. Additionally, the non-sticky dendrimers and T4Δ*hoc* become subdiffusive at similar concentrations. Note that χ is a free parameter chosen such that the non-sticky dendrimer becomes subdiffusive at about $2c^*$. Therefore, using our model of sticky dendrimers in an associative polymer network, we have validated the BAM model which attributes the subdiffusion of phages at lower mucin concentrations to its adherence to the mucin network.

7.3 Conclusions

The transport of various types of probe particles through polymer solutions and networks holds significant interest for biomedical (Siepmann and Siepmann, 2012; Peppas *et al.*, 2000), industrial (Hermans, 1968) and biological applications (Chatterjee and Cherayil, 2011; Tabei *et al.*, 2013; Goodrich *et al.*, 2018). Some of these particles interact with their surroundings while others undergo simple Brownian motion. This study used Brownian Dynamics simulations to examine dendrimers as probe particles within networks of associative polymers, focusing on how both non-sticky and sticky interactions affect network structure and dendrimer behaviour. This is achieved by having various types of stickers (type A for network formation, type B and C for network-dendrimer interactions present on the respective polymer architectures) in the system having specific functions. Essential interactions like excluded volume and hydrodynamic interactions are included. Moreover, we compared our results with experimental observations of bacteriophage diffusion within mucus.

The mean squared displacement of non-sticky dendrimers exhibits all the characteristic features of dendrimers in a semidilute polymer solution: dendrimers with a size smaller than network correlation length remain diffusive at all times while at higher concentrations when its size is greater than ξ, a subdiffusive behaviour is observed at intermediate times sandwiched between short time and terminal diffusive behaviour. The strength and spacing between the network-

forming stickers seem to not affect the dynamics of non-sticky dendrimers. For sticky dendrimers, however, the MSD reveals subdiffusive motion even when their size is smaller than ξ, with the MSD decreasing with increasing dendrimer-linear chain interaction strength and spacing between stickers of type B on linear chains. This is due to the higher residence time of sticky dendrimers within the network owing to its attractive interaction with the network. In this study, we also observed a non-Gaussian probability distribution of displacement of sticky dendrimers at times when they exhibited subdiffusion which is consistent with that observed in the case of nanoparticles and flexible viruses. The deviation from Gaussian behaviour increased with increasing ϵ_{d} and concentration.

Our results show that non-sticky dendrimers and dendrimers with low ϵ_{d} have similar diffusion exponents. There is a transition from $\alpha = 1$ at low concentrations to $\alpha < 1$ in the semidilute regime. The concentration at which this transition happens depends on the size ratio between the dendrimer and the linear chain. However, at higher interaction strengths, due to the longer binding time of the dendrimer to the network, they become more subdiffusive, which is reflected in the values of the minimum diffusion exponent. Similarly, with the availability of more stickers to the dendrimer, it tends to be more subdiffusive. It is also interesting to note that the minimum diffusion exponents level off at higher concentrations regardless of their strength of sticking to the network.

As a final study, we have compared the dynamics of dendrimers in our simulations with that of bacteriophages within mucus. The experimental data was revisited to extract the minimum value of the diffusion exponent from each trajectory. The instantaneous derivative of the MSD obtained from both simulations as well as experiments was calculated to show agreement with the value obtained from the line of best fit. We suspect that the diffusion exponent of adherent phages in experiments by Barr *et al.* (2015) is fluctuating about a mean value at higher concentrations. We could establish an agreement between the diffusion exponents of the adherent and non-adherent phages and the sticky and non-sticky dendrimers in our model. Sticky dendrimers with an interaction strength of $6k_BT$ have subdiffusion exponents similar to that of T4 phage in the mucus network, while the non-sticky dendrimer remains diffusive until its size becomes larger than the correlation length of the polymer network.

Chapter 8

Conclusions and Future Work

8.1 Conclusions

In this thesis, we have investigated the diffusion of the dendrimers in polymer solutions and networks using Brownian dynamics simulations, by comparing our observations with that of bacteriophages and nanoparticles in similar environments. We use coarse-grained models of bead-spring chains for phages and mucus networks. The phage is modelled as a dendrimer (branched polymer) and the mucus layer is modelled as a network of linear chains, both containing beads connected by FENE springs. The formation of the network and the interaction between the dendrimer and the network are due to associative groups or stickers on them. The well-depth of the SDK potential controls the strength of interaction between stickers. The advantages of our model are as follows: (a) polymers of any architecture and any number can be simulated. (b) It is possible to include any number of stickers with specific rules of association. (c) We have included hydrodynamic interactions due to which the dynamics of the polymers can be studied.
The conclusions of our study are listed below:

1. Non-sticky dendrimers in semidilute polymer solution: We simulated a system of dendrimers in a semidilute polymer solution of linear chains to compare its properties with that of linear polymers and nanoparticles.

   (a) The radius of gyration was observed to follow the scaling law for linear chains irrespective of their architecture (Figure 5.4).

   (b) Dendrimers with size smaller than correlation length are diffusive at all times, while that which is larger than correlation length becomes subdiffusive at intermediate times, followed by a terminal diffusive regime.

(c) The terminal diffusivity of functionality three dendrimers had a similar behaviour to the self diffusivity of linear polymers, whereas the functionality four dendrimers showed deviations (Figure 5.10). The latter is also shown to have a more compact structure by calculating their shape functions.

(d) The diffusivity of the simulated dendrimers does not follow the scaling predictions for nanoparticles, instead, we propose a new scaling law for low-generation dendrimers in a semidilute solution (shown in Figure 5.11). The high-functionality dendrimer was found to have a scaling exponent between that of a floppy linear chain and a hard sphere.

From our analysis, it is evident that dendrimers, like linear polymers, show signatures of screening of excluded volume interactions in semidilute concentrations which results in a decrease in their size. The viscosity of the solution increases leading to a decrease in the diffusivity of dendrimers. Also, we have demonstrated that functionality is a key parameter that controls the behaviour of dendrimers. This can be used to tune their structure to map to different microbial systems like filamentous viruses to bacteriophages.

2. Static properties of dendrimers in a polymer network: We computed the radius of gyration and internal bead density of sticky and non-sticky dendrimers in a network of linear chains.

   (a) The non-sticky dendrimers in the network had the same static properties as that in the solution, implying that the state of the background polymers is unimportant.

   (b) The adherence to the network caused the sticky dendrimers to stretch beyond their size in a dilute solution. This resulted in a higher probability of finding beads away from its core. However, with increasing concentration, the normalised radius decreases (Figures 6.3 and 6.4).

   (c) The mesh size distribution of the network is bimodal in the presence of non-sticky dendrimers due to its repulsive interaction with the network (Figure 6.7). In the presence of sticky dendrimers, the bimodality is absent, but the distribution is broader due to the stretching and squeezing of the network caused by the sticking of dendrimers (Figure 6.8).

3. Dynamics of dendrimers in a polymer network: The dynamic properties of non-sticky and sticky dendrimers in network was computed:

   (a) Similar to the static properties, the dynamic properties of non-sticky dendrimers in the network did not differ from those in a solution.

(b) The probability distribution function of displacement for sticky dendrimers showed slight deviation from the Gaussian distribution (Figure 7.4).

(c) The sticky dendrimers exhibited subdiffusion even when their size is smaller than correlation length, with the subdiffusion exponent decreasing with increasing ϵ_d. This is true at all concentrations (Figure 7.6).

(d) The terminal diffusivity of both sticky and non-sticky dendrimers was observed to follow the analytical predictions of Dell and Schweizer (2014) for nanoparticles in the polymer network (Figure 7.7).

4. Finally, using an associative linear polymer network to model mucus network and sticky dendrimers for bacteriophages, we have obtained a quantitative match with the experimentally observed diffusion exponents (Figure 7.9), with the following caveats:

   (a) No direct match between mucin concentrations reported in experiments by Barr *et al.* (2015) and c/c^* in our simulations was made.

   (b) The dendrimer architecture and size ratio between dendrimer and linear chain χ are free parameters, chosen such that the transition of non-sticky dendrimers to subdiffusive regime happens at around $c/c^* = 2$.

   Within this choice, we find that sticky dendrimers in associative polymer networks effectively capture the dynamics of phages in mucus.

Phages have been used in a range of applications in biotechnology. With the advance of phage therapy, the need to understand how phages interact with their environment and host is also increasing. Apart from this, phages have been used vastly as drug delivery agents. The outcome of this research is expected to be helpful in understanding many complex behaviours observed in this field.

8.2 Future Work

This work represents a significant advance in understanding the dynamics of dendrimers in polymer solutions and networks. However, several directions for further exploration remain, each offering the potential to expand the impact of this research. Below, we outline some ideas for extending the current model and its applications, emphasizing their relevance to the broader field of soft matter physics:

1. While this study has successfully analysed critical properties of dendrimer diffusion in polymer solutions and networks, a few important aspects remain unexplored due to time

constraints. These include investigating further how sticky dendrimers influence the mesh size distribution of the polymer network, quantifying the non-Gaussian parameter of the probability distribution of displacement for sticky dendrimers, and exploring how the number of stickers on dendrimers affects their dynamics and interactions with the network. Addressing these factors will provide a more comprehensive understanding of dendrimer behaviour and guide the design of functionalised dendrimers for targeted applications.

2. Even though our model captures the subdiffusive behaviour of bacteriophages in mucus, there are several differences between the simulated and biological systems.

   (a) Bacteriophages such as T4 are rigid, hard-sphere structures, which lack the ability to stretch, unlike the flexible dendrimers in our model. Incorporating a bending potential between dendrimer arms and using FENE-Fraenkal springs to mimic rod-like rigidity (Pincus *et al.*, 2020) could bridge this gap and align the model more closely with biological realities.

   (b) Mucus networks exhibit a broad range of binding energies due to diverse glycan compositions (Wu *et al.*, 2024; Chin *et al.*, 2022), whereas the current model assumes uniform interaction strengths for dendrimer-linear chain stickers. Introducing a distribution of binding energies (ϵ_d) will enable the model to capture this biochemical heterogeneity, enhancing its applicability to mucus-embedded systems.

3. Beyond T4 phage and mucus, the developed model and algorithm can be extended to study other systems of growing interest in the field of soft matter:

   (a) Semiflexible particles and networks: Biological systems often feature semiflexible structures, such as cytoskeletal networks and filamentous viruses. By incorporating bending potentials into the current model, we can simulate the transport of semiflexible particles through semiflexible networks under biologically relevant conditions.

   (b) Interpenetrating polymer networks (IPN): These systems consist of two or more interwoven polymer networks without covalent bonds (Banerjee *et al.*, 2010), offering tunable properties for applications such as artificial scaffolds and drug delivery (Dragan, 2014). Our model can simulate IPNs by treating both polymer species as network-forming linear chains with distinct properties. This extension would contribute to the design and optimization of IPNs for biomedical applications.

   (c) Microrheology: The use of microscopic probe particles to study the viscoelastic properties of materials like polymer solutions and gels, biological fluids and

colloidal suspensions has gained importance due to advances in experimental setups (MacKintosh and Schmidt, 1999; Squires and Mason, 2010). A recent experimental study highlights the importance of the properties of probe particles in microrheological measurements (Zhu *et al.*, 2023). This system can be simulated using the multi-species BD algorithm we have developed, using the mean squared displacement measurements of the probe particles to obtain the complex modulus of the polymer network.

The directions outlined above provide a robust framework for future research, with the potential to address critical open questions and extend the applicability of this work to diverse systems.

Appendix A

A.1 Radius of gyration versus number of beads for various topologies

In order to determine the dendrimer parameters and length of linear chains in the solution, we used their respective radius of gyration versus number of beads per molecule plots. In Fig A.1 (a),(b) and (c), the functionality (f) and generation number (g) of the dendrimer is fixed and number of beads is varied by changing the spacer length (s). Linear chains and dendrimers follow the scaling law given below:

$$R_{g0}^{lc} = a^{lc} \left(N_b^{lc}\right)^{\nu} \tag{A.1}$$

$$R_{g0}^{d} = a^{d} \left(N_b^{d}\right)^{\nu} \tag{A.2}$$

Here ν is the Flory exponent, $\nu = 0.588$. This information is used to construct Table 1 in the main text, for the various systems we have studied.

A.2 Distribution of radius of gyration

Dendrimers are soft colloids and can have shape and size fluctuations based on the forces experienced by each of its constituent beads. This is evident from the distribution of its radius of gyration, $\psi(R_g^d)$. It is calculated by obtaining R_g^d from many trajectories at different instances in time and binning them. The variance of the distribution of R_g^d gives a measure of the size fluctuations. It is clear from Fig. A.2(a) that increasing functionality reduces the softness of dendrimers resulting in lesser fluctuations. The $f = 4$ dendrimer has a significant decrease in variance compared to the $f = 3$ dendrimers, especially the $(f, s, g) = (3, 1, 1)$ that has a similar number of beads per molecule to that of the $f = 4$ dendrimer. The fluctuations decrease at higher concentrations, but the distribution is similar at all concentrations irrespective of the architecture (shown in Fig. A.2(b)).

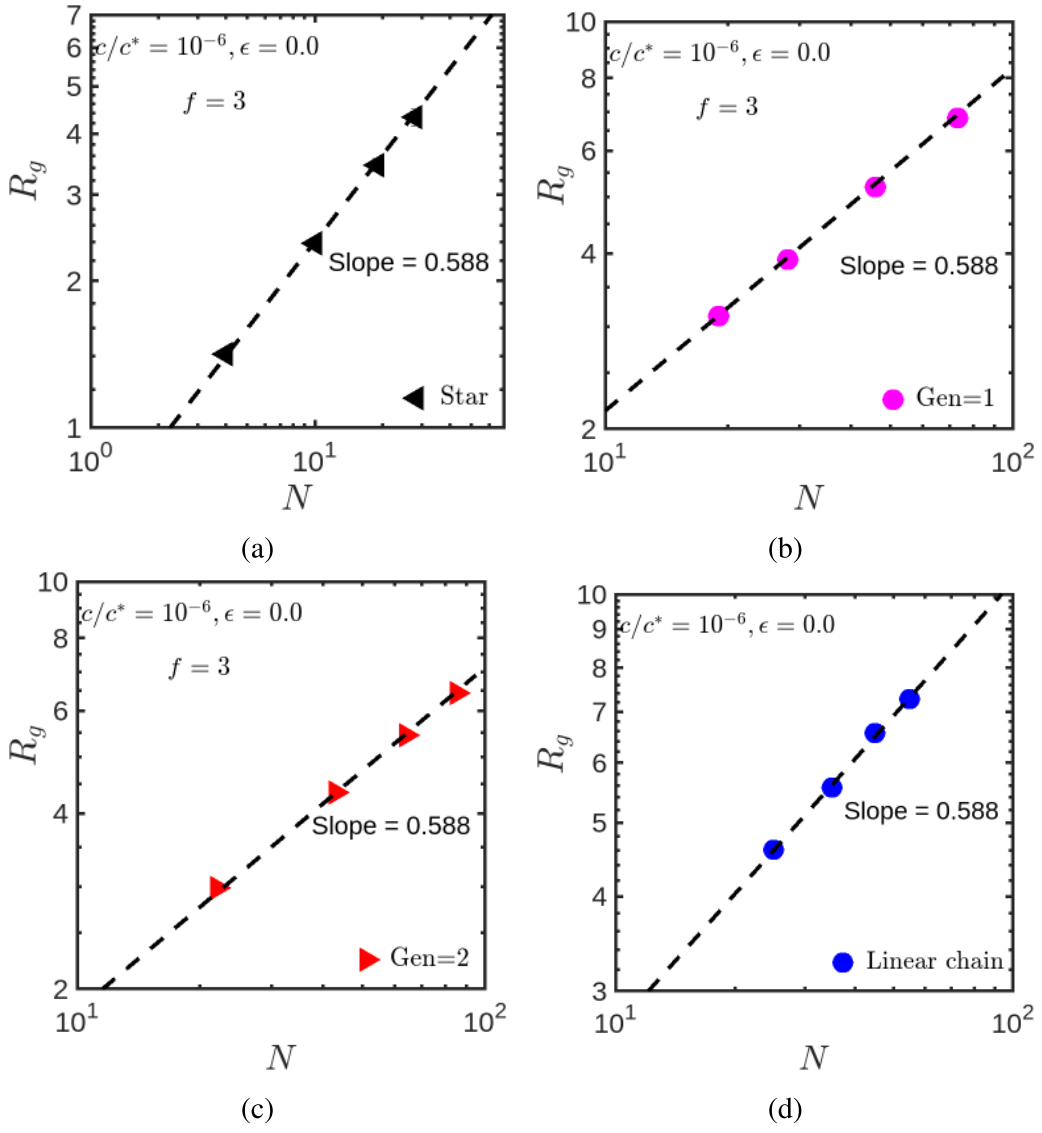

Figure A.1: Radius of gyration versus number of beads per molecule (a) Star polymers with functionality 3. (b) Generation 1 dendrimer with functionality 3. (c) Generation 2 dendrimer with functionality 3. (d) Linear chains. The dashed lines are the scaling law given by eqns (A.1) and (A.2)

.

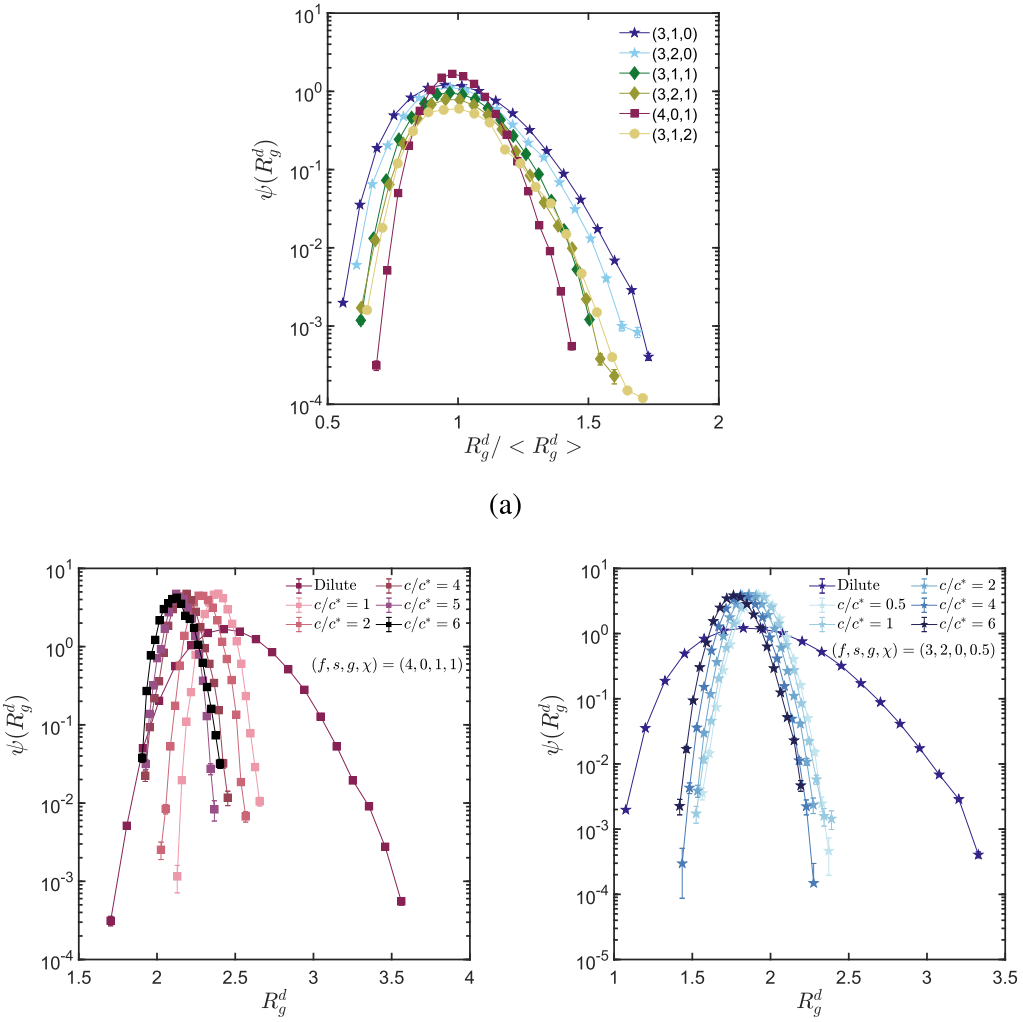

Figure A.2: Distribution function of the radius of gyration of dendrimers (a) Dendrimers of different architectures in dilute solution. The dendrimer architecture is included in the order (f, s, g). Note that the x-axis is the normalised radius of gyration. (b) Effect of concentration on the size fluctuation of $(f, s, g, \chi) = (4, 0, 1, 1)$ dendrimers. (c) Effect of concentration on the size fluctuation of $(f, s, g, \chi) = (3, 1, 0, 0.5)$ dendrimers.

A.3 Asphericity

The asphericity B of a molecule is defined as Theodorou and Suter (1985); Bishop and Michels (1986); Kumari *et al.* (2020):

$$B = \langle \lambda_3^2 \rangle - \frac{1}{2}\left[\langle \lambda_1^2 \rangle + \langle \lambda_2^2 \rangle\right] \tag{A.3}$$

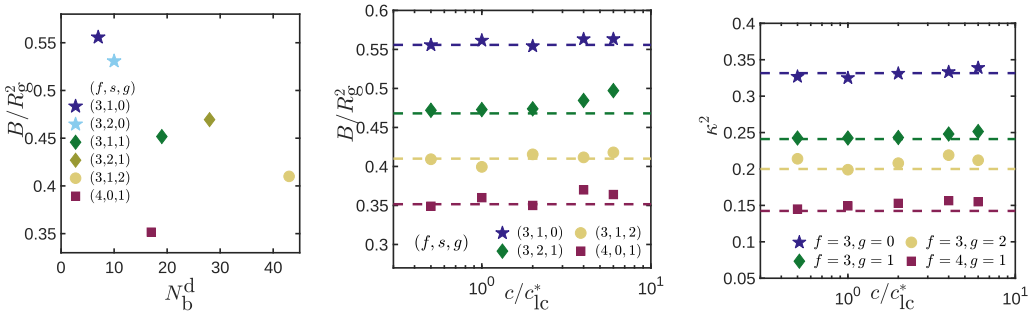

(a) (b) (c)

Figure A.3: Effect of architecture and solution concentration on the shape of dendrimers. (a) Asphericity of dendrimers of different architectures in dilute solution as a function of the number of beads in a dendrimer molecule. The symbols represent dendrimer topology given by the combination f, s, g. (b) Effect of concentration of the solution on asphericity of dendrimers. All $f = 3$ architectures considered have one spacer bead ($s = 1$). The dashed lines are the asphericity in the dilute solution given in (a). (c) Effect of concentration of the solution on relative shape anisotropy of dendrimers. The dashed lines are the κ^2 in the dilute solution given in Fig.6(a) of the main text.

Molecules with tetrahedral or greater symmetry have $B = 0$, otherwise $B > 0$. In Fig. A.3(a), the asphericity of dendrimers of different architectures in dilute solution, calculated using eqn (A.3), is plotted as a function of the number of beads per molecule. In a dilute solution, an increase in generation number decreases B, implying a more spherically symmetric arrangement of beads within the molecule. The functionality four dendrimer has the lowest B value. A similar trend is observed in the case of the relative shape anisotropy. The concentration of the solution seems to not affect the asphericity and shape anisotropy of dendrimer molecules as seen in Fig. A.3(b) and (c).

A.4 Bead density distribution

The linear bead density distribution along the 3 axes of the gyration tensor of $(f, s, g) = (3, 1, 1)$ dendrimer in dilute solution is shown in Fig. A.4(a). The characteristic features of the distribution are observed along the major axis while it is Gaussian-like along the minor axes.

An alternative estimate of the internal density can also be obtained by counting the number of beads within concentric shells of constant thickness Δr starting from the centre of mass of the

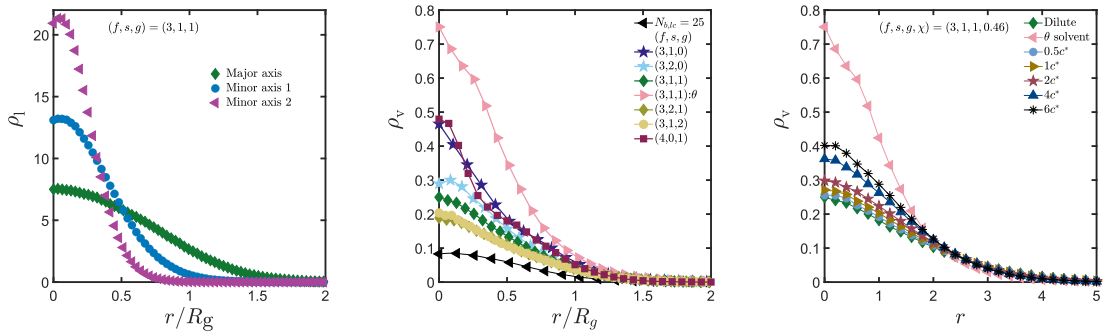

(a) (b)

Figure A.4: (a) Linear bead density distribution along the 3 axes for a $f = 3, s = 1, g = 1$ dendrimer in athermal solvent condition. (b) Effect of architecture on the volumetric bead densities of dendrimers in dilute solution. Black triangles represent linear chain with 25 beads and dendrimers are represented using the combination f, s, g. (c) Effect of concentration on the volumetric bead density distribution of $f = 3, s = 1, g = 1$ dendrimer in a semidilute solution of linear chains with $\chi = 0.46$. Pink triangles in both figures represent $f = 3, s = 1, g = 1$ dendrimer in theta solvent conditions.

molecule. The volumetric bead density is given by:

$$\rho_{\mathrm{V}}(r) = \frac{n_{\mathrm{b}}(r + \Delta r) - n_{\mathrm{b}}(r)}{\Delta \mathrm{V}} \tag{A.4}$$

where $n_{\mathrm{b}}(r)$ is the number of beads of a molecule in a sphere of radius r, ΔV is the volume of a spherical shell of thickness Δr given by $\frac{4}{3}\pi(r + \Delta r)^3 - \frac{4}{3}\pi r^3$. In Fig. A.4(b), the volumetric bead densities in concentric shells starting from the centre of the molecule have been plotted for dendrimers in dilute solution. The density is maximum at the centre for all dendrimer architectures, which drops monotonically towards the periphery of the molecule. It is important to note that the dendrimers with a higher number of beads have lower core volumetric density. This might be because of the higher effective repulsion the individual beads near the centre feel, causing them to occupy regions towards the periphery. The $f = 3, s = 1, g = 1$ molecule in theta solvent has a significantly higher density at the core due to its collapsed state. In semidilute solution, the dendrimer volumetric bead density transitions from that in dilute solution to theta solvent conditions as solution concentration increases (shown in Fig. A.4(c)). This is consistent with the observations of linear bead density along the major axis and can be attributed to the onset of screening of EV at higher concentrations.

A.5 Mean squared displacement

The effect of solution concentration on the mean squared displacement of dendrimers is shown in Fig. A.5(a). Subdiffusion is completely absent at low concentrations because the dendrimer

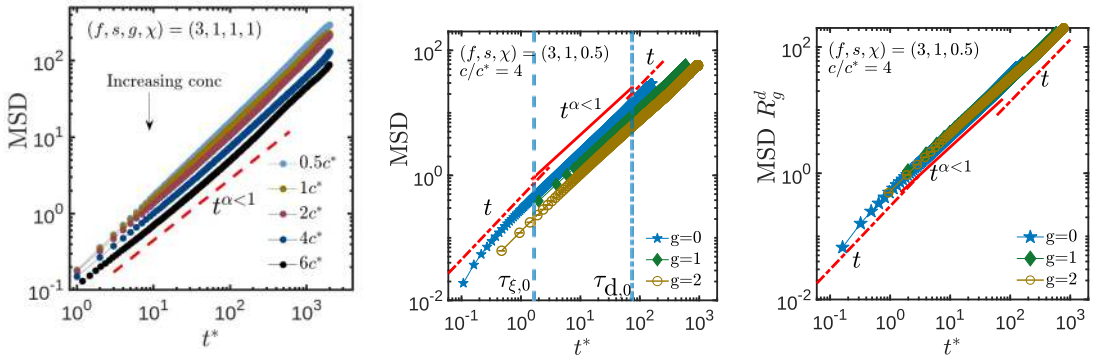

(a) (b) (c)

Figure A.5: Mean squared displacement of dendrimers as a function of time (a) Effect of solution concentration on the mean squared displacement of generation one ($g = 1$) dendrimers with functionality $f = 3$ and one spacer bead ($s = 1$) in a solution of linear chains with 43 beads ($N_b^{lc} = 43$). The size ratio between the dendrimers and linear chains is 0.46 ($\chi = 0.46$). (b) Effect of generation number of dendrimers on its mean squared displacement. The concentration is $4c^*$ and dendrimer parameters are $f = 3, s = 1, \chi = 0.5$. The vertical dashed and dashed-dotted lines are τ_ξ and τ_d for the generation zero dendrimer respectively. (c) Collapse of mean squared displacement of dendrimers of different architectures considered in (b).

size is much smaller than the solution correlation length. As concentration increases, due to the interaction between dendrimer molecules and the increased number of linear chains, a subdiffusive period exists ($\tau_\xi < t < \tau_d$) and the mean squared displacement of dendrimers decreases. Thus, with increased concentration, the dendrimers become less diffusive due to hindered motion. The values of τ_ξ and τ_ξ changes with concentration as reported in Tables A.1, A.2 and A.3. Table A.1 contains the values of τ_ξ and Table A.2 contains the values of τ_d for all $f = 3$ dendrimers at all concentrations. Table A.3 contains τ_ξ and τ_d for the $f = 4, g = 1$ dendrimer. When the size of the dendrimer is smaller than the correlation length (ξ) of the solution, it exhibits normal diffusion at all time scales and the concept of the time scales τ_ξ and τ_d does not exist.

The size of dendrimers varies with their generation number. Therefore, at a constant concentration, f and s, a generation 2 dendrimer will experience more hindrance to its motion compared to a simple star polymer ($g = 0$), causing the former to diffuse slower than the latter as shown in Fig. A.5(b). The mean squared displacement of dendrimers is given by MSD $= 6\,D\,t$, where D is the diffusivity. The Stokes-Einstein relation for a particle of radius R is $D = k_BT/6\pi\eta R$. Therefore, MSD $\approx k_BTt/\eta R$, and MSD $R \approx k_BTt/\eta$. Using this simple scaling argument, we have collapsed MSD data for dendrimers of different generations as shown in Fig. A.5(c).

An examination of the position of the centre of mass of a dendrimer molecule in our simulations as a function of time shows that it does not have long waiting times or hopping motion

Table A.1: The time scale τ_ξ (given by eqn 17 in the main text) for the various architectures at different concentrations.

(χ, f, s, g)	c/c^*				
	0.5	1	2	4	6
$(0.5, 3, 1, 0)$	–	–	8.4	1.68	1.1
$(0.5, 3, 2, 0)$	–	–	14.6	2.9	1.9
$(0.46, 3, 1, 1)$	–	–	33.5	7.02	4.7
$(0.46, 3, 2, 1)$	–	–	65.1	13.62	9.1
$(0.5, 3, 1, 2)$	–	–	82.5	17.34	6.96
$(1.0, 3, 1, 1)$	–	18.3	3.96	0.96	0.6

Table A.2: The time scale τ_d (defined by eqn 18 in the main text) for the various architectures at different concentrations.

(χ, f, s, g)	c/c^*				
	0.5	1	2	4	6
$(0.5, 3, 1, 0)$	–	–	48.9	72.9	93.1
$(0.5, 3, 2, 0)$	–	–	92.1	136.3	175.6
$(0.46, 3, 1, 1)$	–	–	168	248.6	302.4
$(0.46, 3, 2, 1)$	–	–	304.3	480.3	543.3
$(0.5, 3, 1, 2)$	–	–	556.8	864	1017.6
$(1.0, 3, 1, 1)$	–	245.7	369.6	517.4	676.8

Table A.3: The time scales τ_ξ and τ_d (defined by eqns 17 and 18 in the main text) for the $(\chi, f, s, g) = (1, 4, 0, 1)$ dendrimer.

c/c^*	τ_ξ	τ_d
0.5	–	–
1.0	9.2	124.8
2.0	1.9	181.4
4.0	0.6	247.6
5.0	0.4	273.6
6.0	0.3	305.2
6.5	0.2	313.9

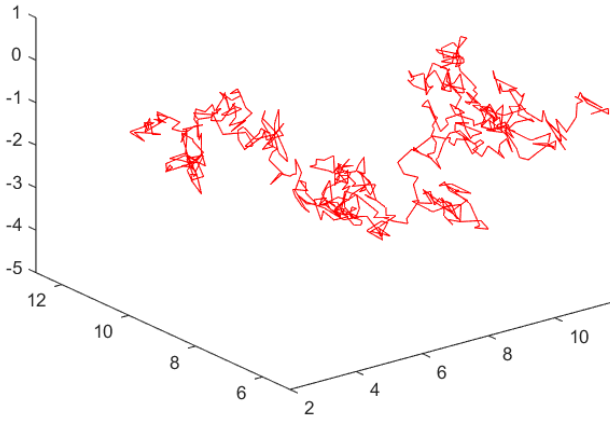

Figure A.6: 3D plot of the movement of the centre of mass of the dendrimer. It is a $(f, s, g, \chi) = (3, 1, 1, 1)$ dendrimer molecule at $c/c^* = 6$ in the presence of hydrodynamic interactions.

(Fig. A.6). Rather the molecule moves in space via smooth random movements even at high concentrations.

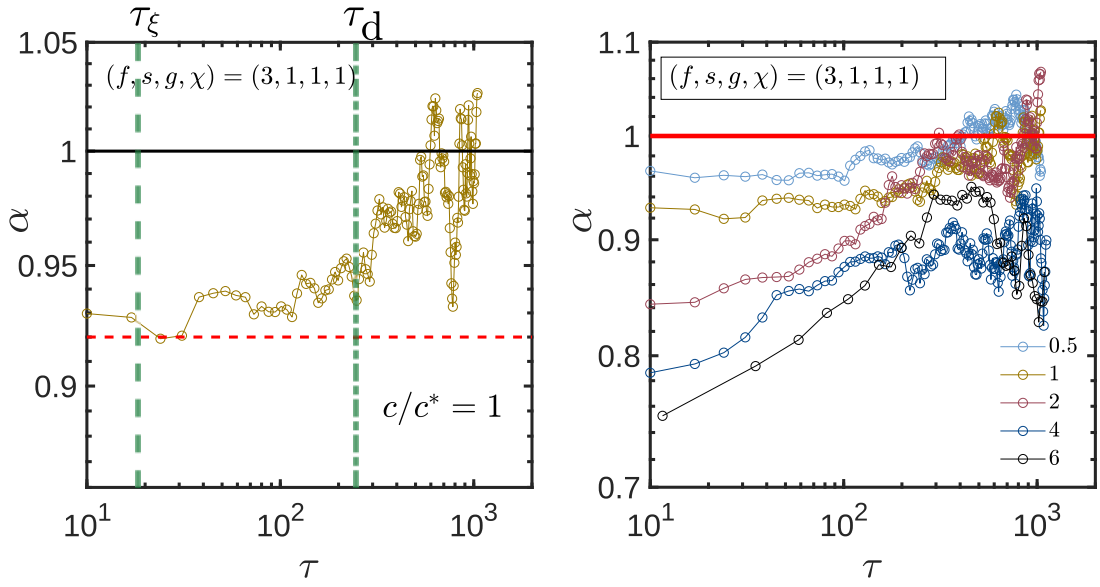

Figure A.7: Diffusion exponent of $(f, s, g, \chi) = (3, 1, 1, 1)$ dendrimer as a function of time (a) The concentration considered is $c/c^* = 1$. Vertical lines represent τ_ξ (dashed) and τ_d (dashed-dotted) for $c/c^* = 1$. The horizontal dashed line is the value obtained from mean squared displacement versus time plots and the solid line is unity. (b) Diffusion exponent for different concentrations.

A.6 Diffusion exponent as a function of time

The subdiffusion exponent can also be obtained by taking instantaneous derivatives in the mean squared displacement as given below:

$$\alpha = \frac{d \log(\mathrm{MSD}(\tau))}{d \log \tau} \tag{A.5}$$

Fig. A.7(a) shows the diffusion exponents of $(f, s, g, \chi) = (3, 1, 1, 1)$ dendrimer as a function of time at $c/c^* = 1$. It is clear that the dendrimer becomes subdiffusive when $\tau_\xi < \tau < \tau_d$ with the value of α in the subdiffusive regime similar to that obtained from the time exponent in the mean squared displacement plots. It transitions to a diffusive regime beyond τ_d. Similar behaviour is observed for all concentrations as shown in Fig. A.7(b).

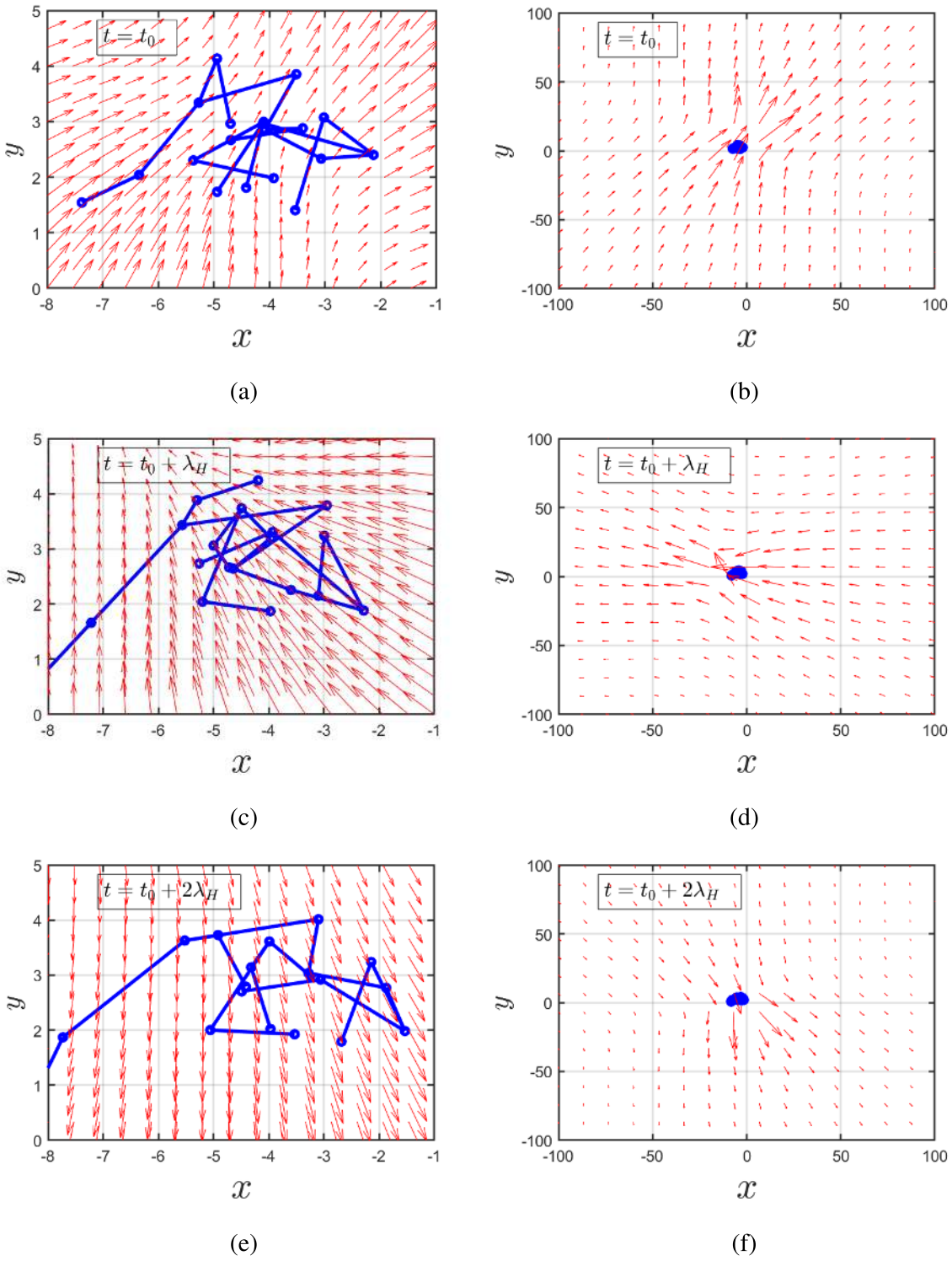

Figure A.8: The flow field about a $(f, s, g, \chi) = (3, 1, 1, 1)$ dendrimer molecule at $c/c^* = 6$ in the presence of hydrodynamic interactions. The rows in the panel represent different instances in time. The first column (Fig (a), (c) and (e)) shows the velocity field about a dendrimer at a length scale of the order of the size of the dendrimer. The grid size is equal to the correlation length of the solution. The second column (Fig (b), (d) and (f)) shows the velocity field at a length scale much larger than the dendrimer size. The grid size is $\approx 50\xi$.

A.7 Velocity field due to hydrodynamic interactions

As pointed out in the manuscript, the subdiffusive motion of dendrimers is observed at intermediate times ($\tau_\xi < t < \tau_d$) which corresponds to the mean squared displacement of the dendrimer in the range $\xi < \text{MSD} < 2R_g^d$. This suggests that on such time scales, the distance covered by a dendrimer is of the order of the cage size formed by polymer strands in the solution. To examine this closely, we have now computed the velocity fields within the solution due to hydrodynamic interactions as shown in Fig. A.8. This velocity perturbation is obtained by calculating the product of the RPY tensor and the force exerted by each monomer at a point. Fig. A.8 (a), (c) and (e) show the velocity field at lengthscales comparable to dendrimer size at different instances in time while Fig. A.8 (b), (d) and (f) show the fields at large length scales corresponding to them. This enables us to see the effect of HI which we have observed in MSD plots. As is clear in the zoomed-in figures, each monomer on the dendrimer feels forces of different magnitudes and directions due to its location relative to the backflow. The net effect would be to randomize the direction of motion on small length and time scales, leading to slower diffusion. At longer times, ($t > \tau_d$), the mean squared displacement of the dendrimer is much larger than its size. When observed from such large lengthscales, the entire molecule is like a single particle placed at its centre of mass with the orientation of individual beads being unimportant. The flow field set up due to HI seems to be in a particular direction and we would expect it to enhance diffusion. This explains the effect of HI at intermediate and long timescales.

A.8 Probability distribution functions

The distribution of a $f = 3, s = 1, g = 1$ at different concentrations (Fig. A.9(a)) and dendrimers of different architectures (Fig. A.9(c)) in the subdiffusive regime were also found to be Gaussian. Even the special case of a dendrimer with functionality $f = 4$, which is a denser molecule, does not exhibit a non-Gaussian behaviour at any of the concentrations in the subdiffusive regime (shown in Fig. A.9(b)).

A.9 Comparison with diffusivity of other soft colloids

We compared the dynamics of polymer grafted nanoparticles (PGNP), also called hairy colloids, in a solution of free polymer from work done by Poling-Skutvik *et al.* (2019) with our simulations. According to them, the normalised diffusivity for various PGNP-free polymer systems can be collapsed if the normalised concentration (c/c^*) of free polymers is scaled with the ratio $\left(M_{w,f}/M_{w,g}\right)^{-1/8}$. In our system, the radius of gyration of dendrimers and linear chains in dilute solution are related by the following equation:

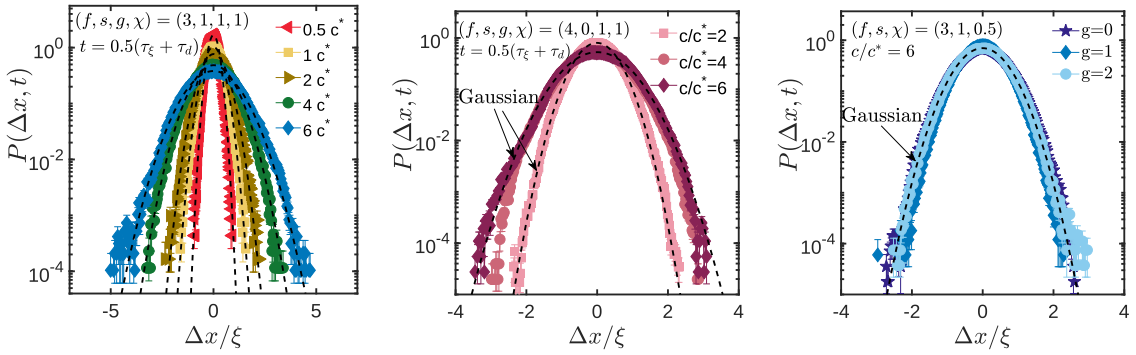

(a) (b) (c)

Figure A.9: Probability distribution function of displacement for dendrimers. (a) Generation one dendrimer ($f = 3, s = 1, \chi = 1$) in a semidilute solution of different concentrations in the subdiffusive regime $\tau_\xi > t > \tau_d$ (at $t = 0.5(\tau_\xi + \tau_d)$). (b) PDD for $f = 4$ dendrimer ($s = 0, g = 1, \chi = 1$) in the subdiffusive regime at different concentrations (at $t = 0.5(\tau_\xi + \tau_d)$). (c) Functionality three dendrimers of different generations in a semidilute solution of concentration $6c^*$ in the subdiffusive regime. The dashed lines in all figures are Gaussian fits to the data.

$$\chi = \frac{R^{\mathrm{d}}_{\mathrm{g0}}}{R^{\mathrm{lc}}_{\mathrm{g0}}} \tag{A.6}$$

If $\beta = N^{\mathrm{d}}_b / N^{\mathrm{lc}}_b$, then using eqns (A.1) and (A.2),

$$\chi = \frac{a^{\mathrm{d}}}{a^{\mathrm{lc}}} \beta^{\nu} \tag{A.7}$$

The overlap concentration of dendrimers is

$$c^*_{\mathrm{d}} = \frac{N^{\mathrm{d}}_{\mathrm{b}}}{(4/3)\,\pi (R^{\mathrm{d}}_{\mathrm{g0}})^3} \tag{A.8}$$

Substituting eqns (A.6) and (A.7) in A.8 gives

$$c^*_{\mathrm{d}} = c^*_{\mathrm{lc}} \left(\frac{N^{\mathrm{d}}_b}{N^{\mathrm{lc}}_b} \right)^{1-3\nu} \left(\frac{a^{lc}}{a^d} \right)^3 \tag{A.9}$$

Using eqn (A.9), we have shown that dendrimer diffusivity for all architectures can be collapsed if we use c/c^*_{lc} scaled by $\left(N^{\mathrm{lc}}_{\mathrm{b}}/N^{\mathrm{d}}_{\mathrm{b}}\right)^{-0.76}$ instead of c/c^*_{d} (Fig.A.10(a)). Fig . A.10(b) shows the normalised diffusivity as a function of the size of the dendrimer or PGNP ($M_{w,f} = 15000$kDa, $M_{w,g} = 355$ kDa)(Poling-Skutvik *et al.*, 2019) relative to the system correlation length. Clearly, PGNP does not follow the same scaling behaviour as our simulated dendrimers. Rather they follow the nanoparticle scaling at intermediate values of $2R/\xi$. PGNP can reduce its size with

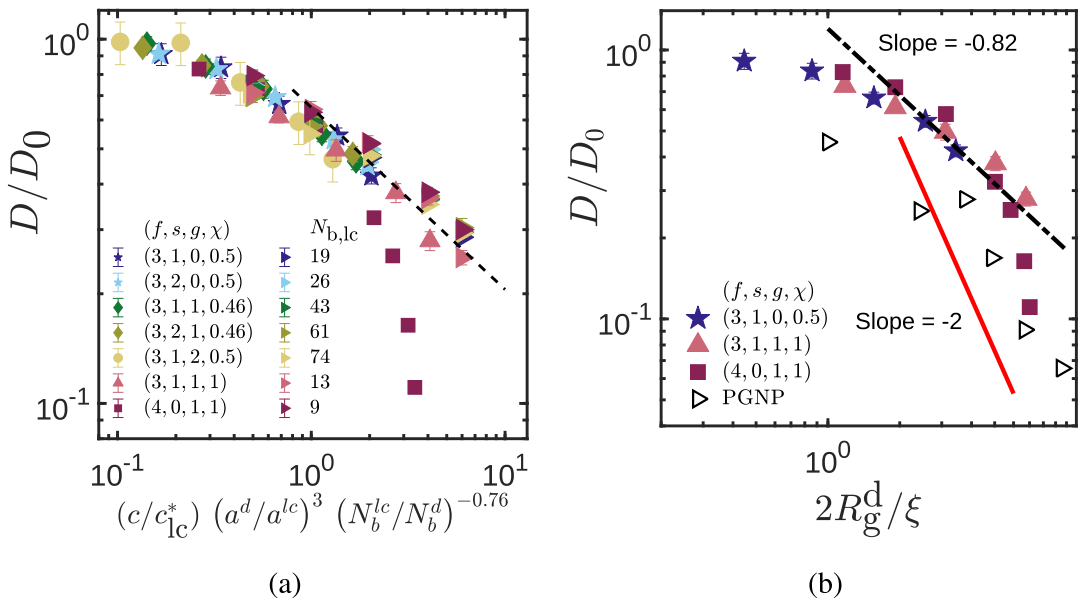

Figure A.10: Effect of solution concentration and size of tracer on its diffusivity. (a)Normalised diffusivity of dendrimers as a function scaled c/c^*_{lc}. For comparison, data for linear chains is also included with c/c^*_{lc} in the x-axis. (b) Normalised diffusivity for dendrimers and PGNPs as a function of its size relative to the solution correlation length. The dashed line is the proposed scaling law for dendrimers and the solid line is the predictions of scaling theory.

increasing concentration similar to dendrimers. However, due to the presence of the nanoparticle which occupies almost 25% of the internal space, there is a limit beyond which it cannot shrink. Therefore, PGNP becomes nanoparticle-like at higher concentrations. Dendrimers reduce size with concentration and even start showing screening of excluded volume interactions as seen in the internal bead distribution plots.

A.10 Scaling law for dendrimer diffusivity

Also, the correlation length (ξ) of the solution, radius of gyration of dendrimers ($R_{\mathrm{g}}^{\mathrm{d}}$) and linear chains ($R_{\mathrm{g}}^{\mathrm{lc}}$) in semidilute solutions depends on concentration as follows:

$$\xi = R_{\mathrm{g0}}^{\mathrm{lc}} \left(\frac{c}{c^*_{\mathrm{lc}}} \right)^{\mu} \tag{A.10}$$

where $\mu = (-\nu) / (3\nu - 1)$.

$$R_{\mathrm{g}}^{\mathrm{d}} = R_{\mathrm{g0}}^{\mathrm{d}} \left(\frac{c}{c^*_{\mathrm{d}}} \right)^{\delta} \tag{A.11}$$

where $\delta = (1 - 2\nu) / (2\,(3\nu - 1))$.

$$D^{\mathrm{d}} = D_0^{\mathrm{d}} \left(\frac{c}{c^*_{\mathrm{d}}} \right)^{\omega} \tag{A.12}$$

where $\omega = (\nu - 1) / (3\nu - 1)$. Dividing eqn (A.11) by eqn (A.10),

$$\frac{2R_g^d}{\xi} = \frac{2R_{g0}^d}{R_{g0}^{lc}} \left(\frac{c}{c_d^*}\right)^{\delta} \left(\frac{c}{c_{lc}^*}\right)^{-\mu} \tag{A.13}$$

We also have the overlap concentration of linear chains given by:

$$c_{lc}^* = \frac{N_b^{lc}}{(4/3)\,\pi (R_{g0}^{lc})^3} \tag{A.14}$$

Taking the ratio of equations (3.8) and (A.14) and substituting the values of χ and β give:

$$c_{lc}^* = \left(\chi^3/\beta\right) c_d^* \tag{A.15}$$

Therefore,

$$\frac{2R_g^d}{\xi} = \frac{2\chi^{(1+3\mu)}}{\beta^{\mu}} \left(\frac{c}{c_d^*}\right)^{\delta-\mu} \tag{A.16}$$

$$\frac{c}{c_d^*} = \left[\left(\frac{2R_g^d}{\xi}\right)\left(\frac{\beta^{\mu}}{2\chi^{(1+3\mu)}}\right)\right]^{1/(\delta-\mu)} \tag{A.17}$$

From equation A.12,

$$\frac{c}{c_d^*} = \left[\frac{D^d}{D_0^d}\right]^{(1/\omega)} \tag{A.18}$$

Equating equation A.17 and A.18, we get

$$\frac{D^d}{D_0^d} = \gamma \left(\frac{2R_g^d}{\xi}\right)^{\omega/(\delta-\mu)} \tag{A.19}$$

where $\gamma = \left(\frac{\beta^{\mu}}{2\chi^{(1+3\mu)}}\right)^{\omega/(\delta-\mu)}$ and $\frac{\omega}{\delta-\mu} = 2(\nu - 1)$.

A.11 The Mittag-Leffler function

The in-built MATLAB routine for evaluating the Mittag-Leffler function with two parameters was used for the fitting the modified Mittag-leffler function through the simulation data. The code can be found at: `https://www.mathworks.com/matlabcentral/fileexchange/8738-mittag-leffler-function`.

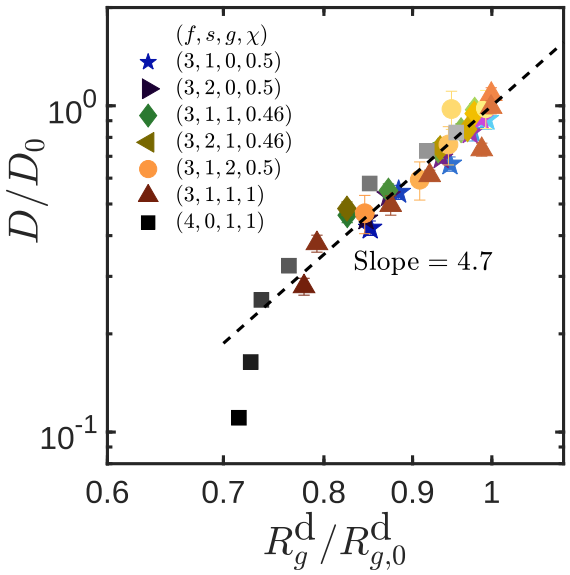

Figure A.11: Normalised diffusivity as a function of the normalised radius of gyration for different dendrimer architectures. The dashed line has a slope equal to 4.7.

A.12 Diffusivity as a function of radius of gyration

According to the predictions of the scaling theory Cai *et al.* (2011), the long-time diffusivity of a nanoparticle in semidilute polymer solution is given by

$$D_{\mathrm{t}} \approx \frac{k_B T}{\eta_{\mathrm{eff}}(\tau_d) d} \tag{A.20}$$

where $\eta_{\mathrm{eff}}(\tau_d) = \eta_s (d/\xi)^2$ is the effective viscosity experienced by a nanoparticle of size d in a solution with solvent viscosity η_s and correlation length ξ. On substituting this in eqn (A.20), the result $D_{\mathrm{t}} \propto 1/d^3$ is obtained as pointed out by the reviewer. The size of a nanoparticle remains constant at all polymer concentrations. However, this is not true in the case of dendrimers. The radius of dendrimers decreases with concentration as follows:

$$R_{\mathrm{g}}^{\mathrm{d}} = R_{\mathrm{g0}}^{\mathrm{d}} \left(\frac{c}{c_{\mathrm{d}}^*} \right)^{\delta} \tag{A.21}$$

where $\delta = (1 - 2\nu)/(2\,(3\nu - 1))$. Therefore,

$$\frac{c}{c_{\mathrm{d}}^*} = \left(\frac{R_{\mathrm{g}}^{\mathrm{d}}}{R_{\mathrm{g0}}^{\mathrm{d}}} \right)^{(1/\delta)} \tag{A.22}$$

The diffusivity of most of the dendrimer architectures follows the scaling law for linear chains as given below:

$$D^{\mathrm{d}} = D_0^{\mathrm{d}} \left(\frac{c}{c_{\mathrm{d}}^*} \right)^{\omega} \tag{A.23}$$

where $\omega = (\nu - 1)/(3\nu - 1)$. Substituting eqn (A.22) in eqn (A.23), we have

$$\frac{D^{\mathrm{d}}}{D_0^{\mathrm{d}}} = \left(\frac{R_{\mathrm{g}}^{\mathrm{d}}}{R_{\mathrm{g0}}^{\mathrm{d}}} \right)^{(\omega/\delta)} \tag{A.24}$$

Substituting for $\nu = 0.588$ in athermal conditions, $\omega/\delta = 4.7$. Fig A.11 shows the variation of normalised diffusivity as a function of normalised dendrimer size. All the dendrimer architectures, except the $f = 4$ dendrimer collapse to a universal curve. This shows that the diffusivity scales as $(R_g^d)^{4.7}$ instead of the -3 scaling of nanoparticles.

Appendix B

B.1 Parameters related to dendrimers and linear chains

Two dendrimer architectures and χ ratios were simulated in this study achieved by varying the dendrimer parameters and length of linear chains. A list of all these are given in table 5.1 and the dendrimer architectures are shown in figure B.1.

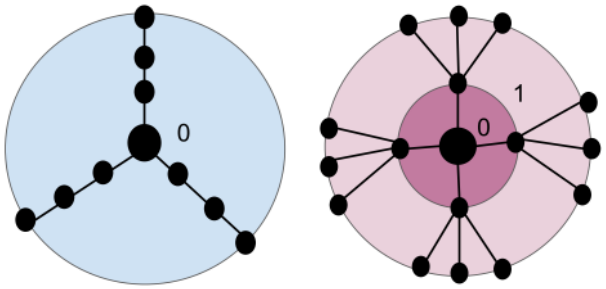

(a) (b)

Figure B.1: Dendrimer architectures used in this study (a) A functionality three star polymer with two spacer beads $(f, s, g) = (3, 2, 0)$.(b) A generation one dendrimer with functionality four and no spacer beads $(f, s, g) = (4, 0, 1)$.

B.2 Procedure for choice of sticker positions

As mentioned in the main text, there are two types of stickers on the linear chains: Type A which is responsible for the network formation, and Type B which interacts with the stickers on the dendrimer. The spacing between these stickers is determined based on the ratio l_N/ξ^* and l_d/ξ^*. The stepwise procedure for fixing the bead tags is given below:

1. Find the end-to-end distance (R^{lc}_{e0}) and radius of gyration (R^{lc}_{g0}) of the linear chain from dilute simulations.

2. Calculate the correlation length at $c/c^* = 1$, named ξ^*.

Table B.1: List of dendrimer parameters and linear chain lengths used in each system. g is the generation number, f is the functionality, s is the number of spacer beads, N_b^d is the number of beads in a dendrimer molecule, R_{g0}^d is the radius of gyration of the dendrimer in the solvent, χ is the ratio between the radius of gyration of dendrimers and linear chains in dilute limit, N_b^{lc} is the number of beads in the background linear chain, R_{g0}^{lc} is the radius of gyration of the linear chain.

	f	s	g	N_b^d	R_{g0}^d	χ	R_{g0}^{lc}	N_b^{lc}
a	3	2	0	10	2.40	0.50	4.80	26
b	3	2	0	10	2.40	0.30	7.2	65
c	4	0	1	17	2.49	0.5	4.98	29

3. Find the ratio $x = R_{e0}^{lc}/\xi^*$.

4. The number of stickers in the chain is then given by $n_{st} = x + 1$.

In general, the first bead of the linear chain is taken to be a sticker of type A and the subsequent sticker beads are assigned using the procedure mentioned above. Stickers of type B are then placed at equal intervals between the type A stickers.
Even though the ratios l_N/ξ^* and l_d/ξ^* are chosen in the beginning, these are only approximate values since the beads are discrete quantities. The actual values are reported in table B.2.

B.3 Algorithm for the calculation of mesh size

The algorithm for mesh size calculation is given below:

1. Obtain the association array of stickers from the simulation: It contains the indices of stickers that are stuck along with the indices of stickers to which it is stuck. The default entry for any unstuck sticker is -1.

2. Eliminate all the unstuck stickers from the array.

3. Identify the chain to which each sticker belongs.

4. Remove all the stickers that form intra-chain associations (loops).

5. Calculate the distance between all the adjacent stickers on the same chain.

Table B.2: Actual and approximate values of l_N/ξ^* and l_d/ξ^*.

	f, s, g, χ	approx l_N/ξ^*	actual l_N/ξ^*	approx l_d/ξ^*	actual l_d/ξ^*
a	3, 2, 0, 0.5	1	1.3	1	1.3
b	3, 2, 0, 0.5	0.5	0.8	0.5	0.8
c	3, 2, 0, 0.5	0.25	0.4	0.25	0.4
d	3, 2, 0, 0.5	0.1	0.3	–	–
e	3, 2, 0, 0.3	2	2.4	0.5	0.6
f	3, 2, 0, 0.3	1	1.6	0.5	0.6
g	4, 0, 1, 0.5	1	1.5	1	0.5
h	4, 0, 1, 0.5	0.5	0.8	0.5	0.8
i	4, 0, 1, 0.5	1	1.5	0.25	0.4

B.4 Mesh size distribution in the presence of non-sticky dendrimers

The mesh size distribution of non-sticky dendrimers at intermediate concentrations ($c/c^* = 1, 2, 4$) for $\epsilon_N = 8$ and $l_N/\xi^* = (0.5, 1)$ is shown in figure B.2. The bimodality which is present at lower concentrations disappears gradually with increasing concentration.

To further understand the role of dendrimers that have repulsive interaction with the network in determining the latter's mesh size distribution, we chose $c/c^* = 0.3$ in which case the bimodality is maximum. It has almost the same number of dendrimers and linear chains. We varied the number of dendrimers keeping the number of linear chains fixed in the simulation box shown in figure B.3(a). On plotting the mesh size distribution, it has been observed that the distribution lacks bimodality at lower concentrations of dendrimers. It is most prominent when there are almost the same number of dendrimers and linear chains. As the number of dendrimers increases, the bimodality drops again. When there are fewer dendrimers, they hardly affect the linear chains. However, when there are enough of them to occupy a significant amount of 'cages' in the network, they expand the cages they occupy while squeezing adjacent empty cages. As their number is further increased, they fill up all the polymer 'cages' due to which repulsion from adjacent cages cancel each other. It is also important to note that the mean mesh size remains

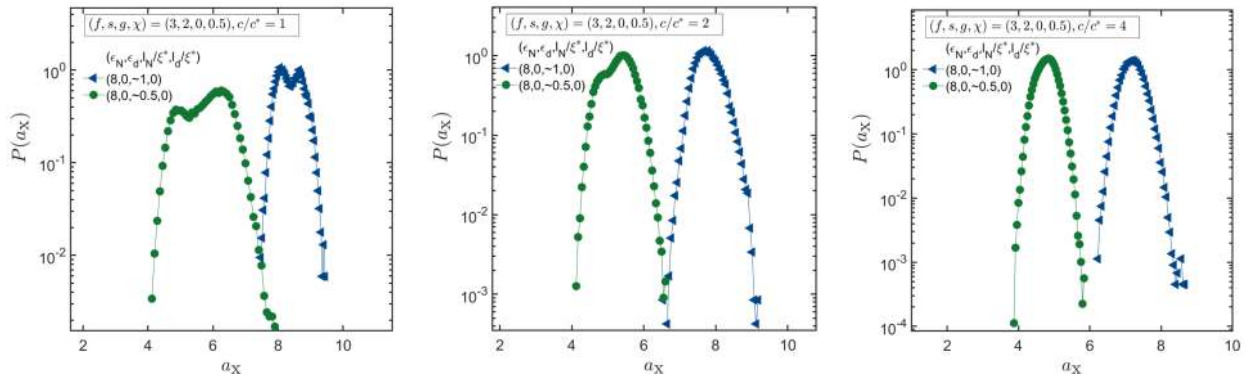

(a) (b) (c)

Figure B.2: Mesh size distribution of non-sticky dendrimers

The mesh size distribution of non-sticky dendrimer with $\epsilon_N = 8$ and $l_N/\xi^* = (0.5, 1)$ at concentrations (a) $c/c^* = 1$ (b) $c/c^* = 2$ and (c) $c/c^* = 4$.

constant. This is because the sticker parameters and the number of linear chains remain constant. Figure B.3(b) shows the mean squared displacement of the dendrimers in the same set of systems. It is clear that the behaviour of the distribution of mesh sizes of the network does not affect the diffusivity of dendrimers.

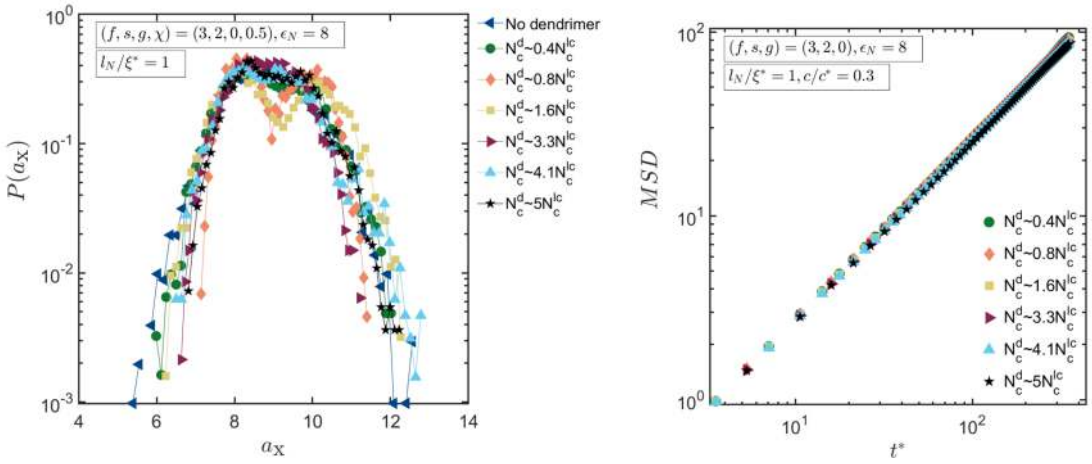

(a) (b)

Figure B.3: Effect of varying the number of dendrimers (a) Mesh size distribution of the network with increasing number of dendrimers while keeping the number of linear chains fixed. (b) The mean squared displacement od the dendrimers in the systems considered in (a).

We have also observed similar trends of the disappearance of bimodality with increasing concentration with different values of l_N as shown in figure B.4.

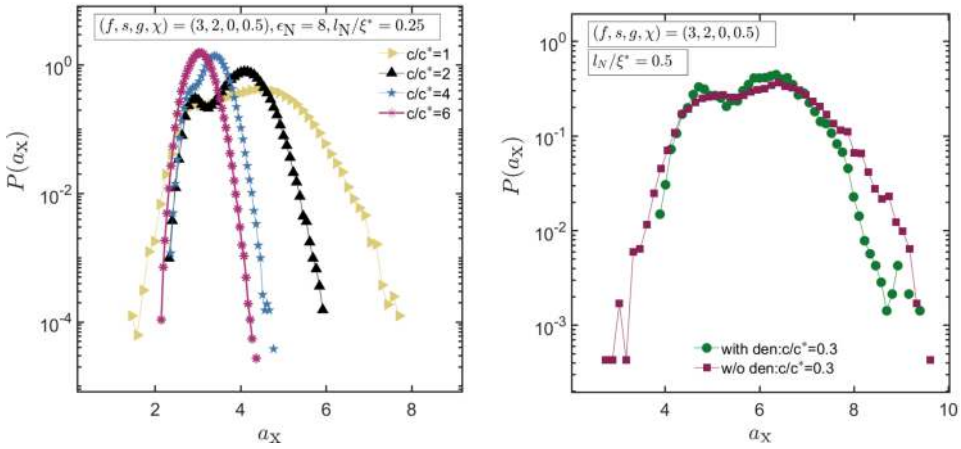

(a) (b)

Figure B.4: Effect of concentration and presence of dendrimers on the mesh size distribution (a) The sticker strength is $\epsilon_N = 8$ and spacing between stickers is $l_N/\xi^* = 0.25$. The concentration of linear chains in the system is increased systematically. (b) In this system, $\epsilon_N = 8$ and $l_N/\xi^* = 0.5$.

B.5 Size of dendrimer relative to characteristic lengthscales

The key factor that determines the nature of diffusion of nanoparticles in a polymer network, which has been identified by all theories is their size relative to the mesh size of the network. However, in our simulations, this mesh size could be the correlation length or the distance between stickers. To analyse this ratio, we have chosen the system of a sticky and non-sticky star polymer with $\epsilon_N = 8$ and $l_N/\xi^* = 1$. The sticker strength of dendrimer interaction, $\epsilon_d = 8$ and $l_d/\xi^* = 1$. This is the system in which the radius of gyration of dendrimer had the highest value at intermediate concentration. In Figure B.5, we have plotted the ratio between the $2R_g^d$ of the dendrimer to ξ, a_x and l_N.

B.6 Effect of network forming stickers on sticky dendrimers

In Section 7.1.1 in the main text, we have shown that the properties of non-sticky dendrimers are unaffected by the network-forming sticker related parameters, ϵ_N and l_N. In this section, we show that the same holds for a sticky dendrimer as well. Figure B.6 shows that the radius of gyration and mean squared displacement of dendrimers with $\epsilon_d = 4$ is not affected by the decrease in the distance between the network forming stickers l_d.

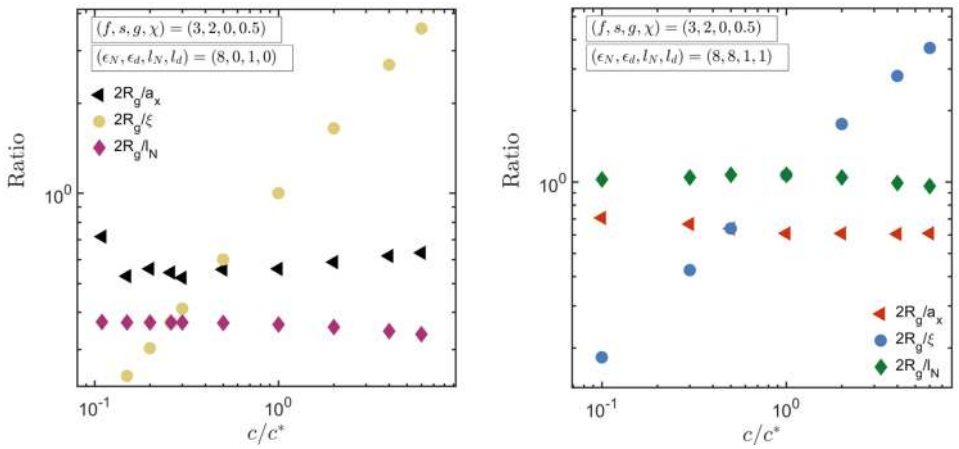

(a) (b)

Figure B.5: Relative size of dendrimer to characteristic lengthscales of the system (a) Non-sticky dendrimer (b) Sticky dendrimer.

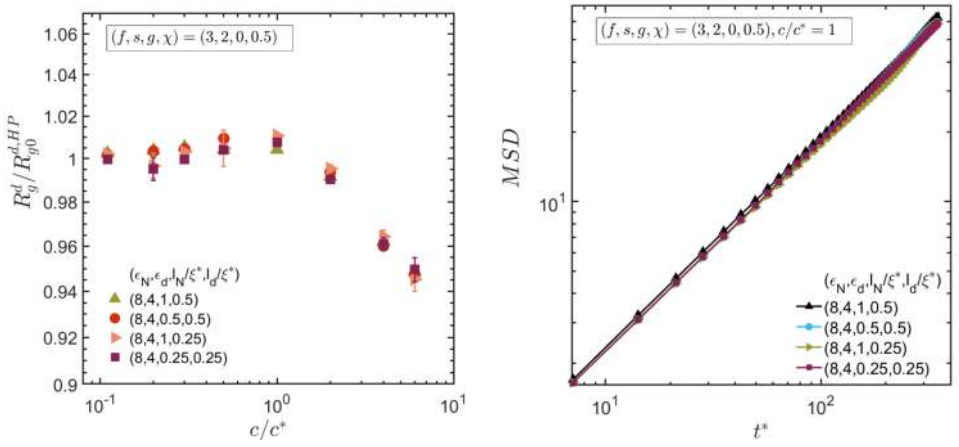

(a) (b)

Figure B.6: Effect of network forming stickers on the properties of sticky dendrimers (a) Radius of gyration of sticky dendrimers for different l_N (b) Mean squared displacement of the same system of dendrimers considered in (a).

B.7 Probability distribution function of sticky dendrimers

As an extension to our analysis of the probability distribution function of displacement of sticky dendrimers reported in the main text, we also analysed systems at varying l_{d} which is shown in Figure B.7. We have considered the system with the highest sticker energies $(\epsilon_{\mathrm{N}}, \epsilon_{\mathrm{d}}) = (8, 8)$. It is observed that its displacement is not affected by l_{d} and the dendrimer has the same probability distribution function of displacement in all cases.

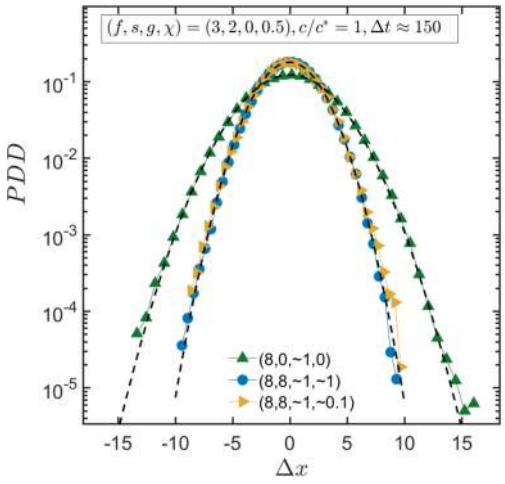

Figure B.7: Effect of varying the number of dendrimers on the mesh size distribution

B.8 Important timescales related to sticky dendrimers in network

There are four important timescales that affect the dynamics of sticky dendrimers in polymer networks, namely $\tau_{l_{\mathrm{N}}}$, $\tau_{l_{\mathrm{d}}}$, $\tau_{a_{\mathrm{x}}}$ and τ_{M}. The first three are the relaxation times of chains of length l_{N}, l_{d} and a_{x} given by

$$\tau_{l_{\mathrm{N}}} \equiv \frac{\eta_s l_{\mathrm{N}}^3}{k_B T} \tag{B.1}$$

$$\tau_{l_{\mathrm{d}}} \equiv \frac{\eta_s l_{\mathrm{d}}^3}{k_B T} \tag{B.2}$$

$$\tau_{a_{\mathrm{x}}} \equiv \frac{\eta_s a_{\mathrm{x}}^3}{k_B T} \tag{B.3}$$

The fourth important timescale, τ_M is the renormalised bond lifetime Robe *et al.* (2024). It is obtained by calculating an autocorrelation function ($C_M(\Delta t)$) from the association matrix (M_2). The M_2 matrix gives information about all the interchain associations of type A stickers. The autocorrelation function is calculated as

$$C_M(\Delta t) = \langle M_2(t) \cdot M_2(t + \Delta t) \rangle \tag{B.4}$$

This autocorrelation function is fitted with an single exponential function to obtain the renormalised bond lifetime, τ_M. This algorithm is similar to that used by Robe *et al.* (2024).

B.9 Dynamics of functionality 4 dendrimer

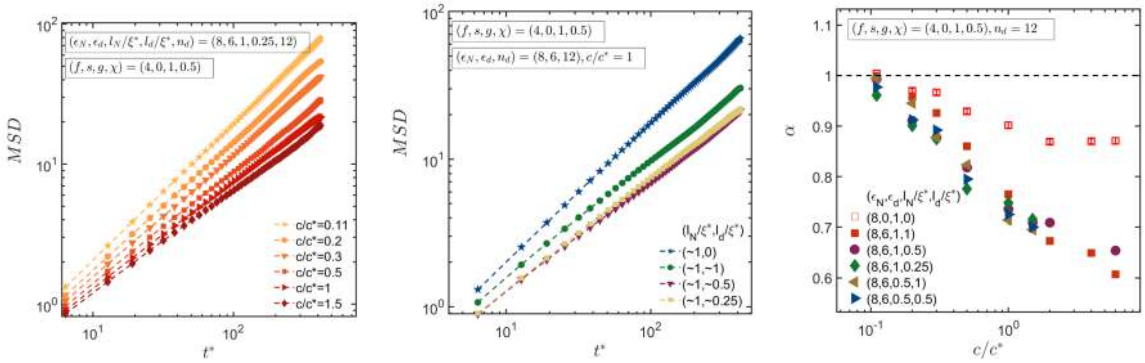

(a) (b) (c)

Figure B.8: Dynamics of functionality four dendrimers. $\epsilon_N = 8$ and $\epsilon_d = 6$ for systems considered in all the figures. (a) Effect of linear chain concentration on the mean squared displacement (b) Effect of l_d on the mean squared displacement. The blue symbols represent a non-sticky dendrimer in a similar environment. (c) Effect of l_d and l_N on diffusion exponent. A non-sticky dendrimer with the same architecture is also included for comparison.

All the results mentioned in the main text are for a functionality three star polymer with two spacer beads. In order to investigate the effect of dendrimer architecture on its mobility through a polymer network, we simulated a generation one, functionality four dendrimer without any spacers. This architecture showed a different behaviour from other lower-generation dendrimers with a similar number of beads Mariya *et al.* (2024). All the end beads of dendrimers are stickers, therefore, there are 12 stickers on each dendrimer. The background linear chains have sticker strength $\epsilon_N = 8$ and the dendrimer interacts with the network with a strength $\epsilon_d = 6$. It was concluded from the results obtained for star polymer that its stickiness affects the properties only if ϵ_d is high enough, based on which these values were chosen. Similar to the star polymers, the mean squared displacement of higher generation dendrimer decreases with increasing

concentration (Figure B.8(a)) and decreasing the spacing between dendrimer interaction stickers on the network (Figure B.8(b)). The diffusion exponents in the intermediate regime were extracted from the mean squared displacement for a range of systems. Figure B.8(c) shows that sticky dendrimers are more subdiffusive compared to its non-sticky counterparts, with the diffusion exponent dropping with increasing concentration. At high concentrations, α_{min} seems to level off. This is true for all systems considered and consistent with that observed in the case of star polymers.

B.10 Analysis of experimental data for phages

A re-analysis of the experimental data reported by Barr *et al.* (2015) for T4 and T4Δ*hoc* phages in varying mucin concentration was performed to extract the minimum diffusion exponent in the intermediate time regime. For this, the best-fit line for the intermediate time MSD data was plotted for T4 and T4Δ*hoc* phages as shown in figures B.9(a) and B.9(b).

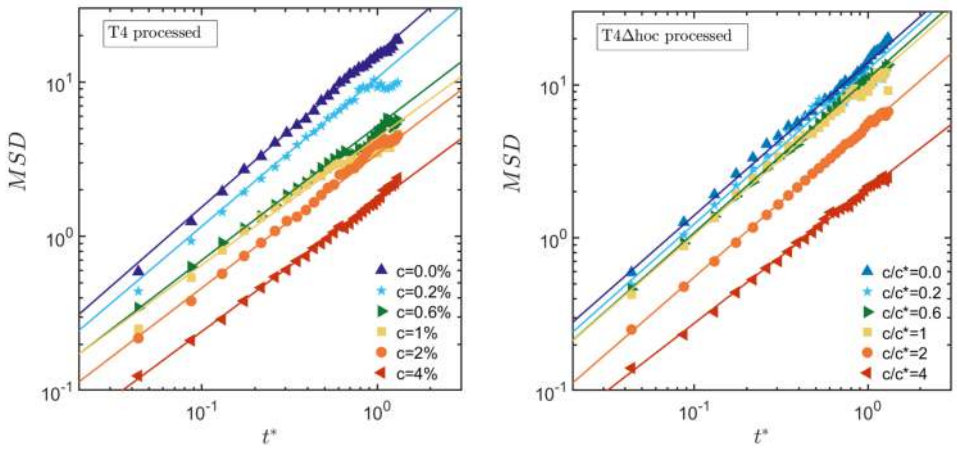

(a) (b)

Figure B.9: Mean squared displacement of experimental data (a) MSD versus time of T4 phage for varying mucin concentrations. (b) MSD of T4Δ*hoc* phages. The lines in both plots are lines of best fit to the intermediate time data.

The slope of these lines gives the subdiffusion exponent. Alternatively, the instantaneous derivative of the MSD data can be calculated, the mean of which in intermediate times can be compared with the values obtained from the line of best fit. Figures B.10 and B.11 give a comparison of these quantities with that reported by Barr *et al.* (2015), along with the instantaneous α as a function of time. At almost all concentrations for both T4 and T4Δ*hoc*, the mean of instantaneous α and that obtained from our analysis agree, however, it differs slightly from that reported in the original work. This is because the authors used a line of best fit for the entire

trajectory which at times is noisy too. These processed values of diffusion exponent is used in figure 17(b) in the main text.

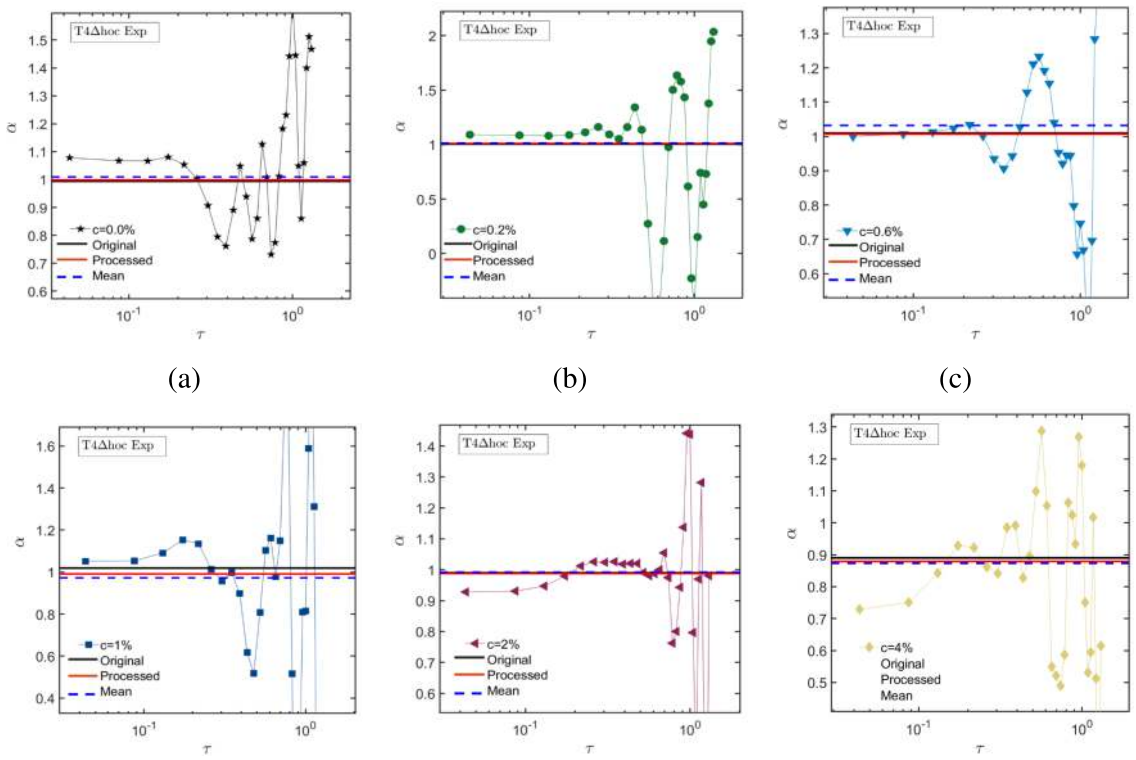

Figure B.10: Diffusion exponent of T4Δ*hoc* phage as a function of time for mucin varying concentrations: $c = 0\%, 0.2\%, 0.6\%, 1\%, 2\%, 4\%$, in (a)-(f) respectively. The black horizontal line the value reported by Barr *et al.* (2015), the red horizontal line is the slope of the best-fit line through intermediate time data and the dashed blue line is the mean of instantaneous α at intermediate times.

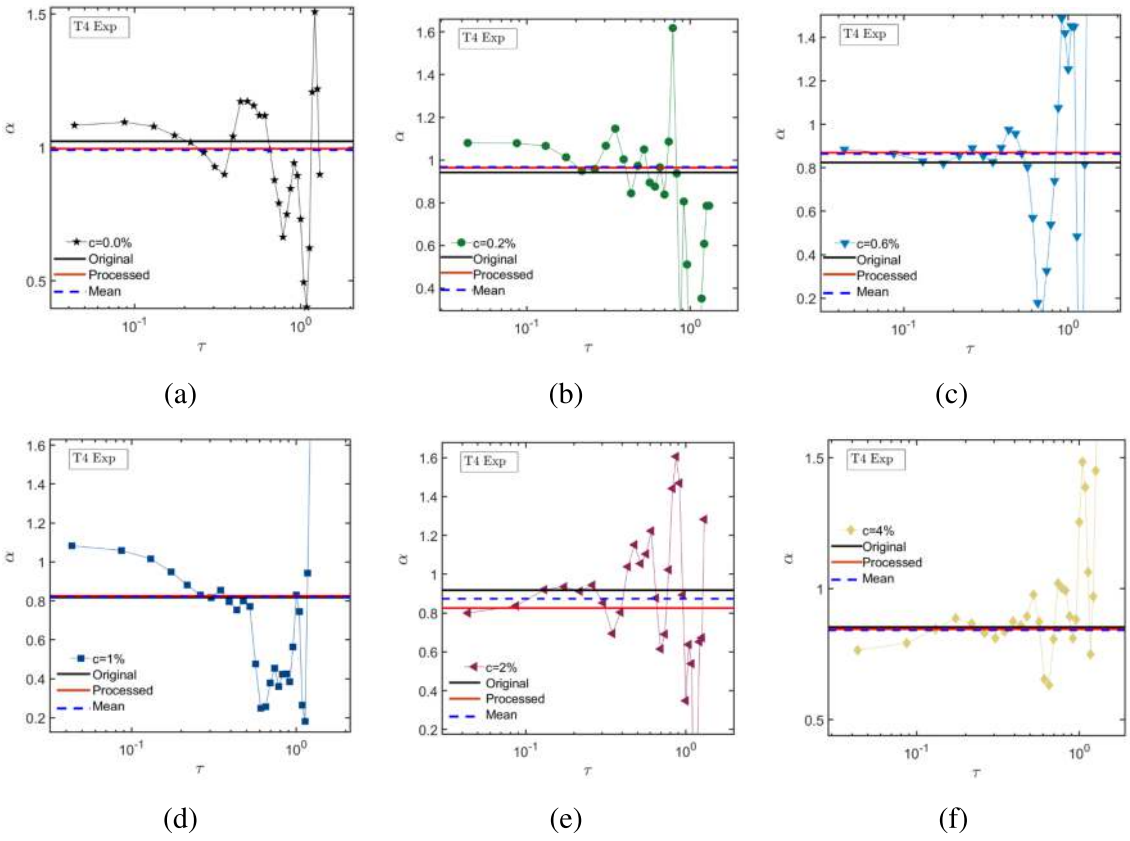

Figure B.11: Diffusion exponent of T4 phage as a function of time for mucin varying concentrations: $c = 0\%, 0.2\%, 0.6\%, 1\%, 2\%, 4\%$, in (a)-(f) respectively. The black horizontal line the value reported by Barr *et al.* (2015), the red horizontal line is the slope of the best-fit line through intermediate time data and the dashed blue line is the mean of instantaneous α at intermediate times.

References

Aghebati-Maleki, A., Dolati, S., Ahmadi, M., Baghbanzhadeh, A., Asadi, M., Fotouhi, A., Yousefi, M., and Aghebati-Maleki, L., 2020, "Nanoparticles and cancer therapy: Perspectives for application of nanoparticles in the treatment of cancers," *Journal of Cellular Physiology* **235**, 1962–1972.

Alai, M. S., Lin, W. J., and Pingale, S. S., 2015, "Application of polymeric nanoparticles and micelles in insulin oral delivery," *Journal of Food and Drug Analysis* **23**, 351–358.

Altenberger, A. R., and Tirrell, M., 1984, "On the theory of self-diffusion in a polymer gel," *The Journal of Chemical Physics* **80**, 2208–2213.

Altveş, S., Yildiz, H. K., and Vural, H. C., 2020, "Interaction of the microbiota with the human body in health and diseases," *Bioscience of Microbiota, Food and Health* **39**, 23–32.

Amblard, F., Maggs, A. C., Yurke, B., Pargellis, A. N., and Leibler, S., 1996, "Subdiffusion and anomalous local viscoelasticity in actin networks," *Physical Review Letters* **77**, 4470.

Amsden, B., 1998, "Solute diffusion within hydrogels. mechanisms and models," *Macromolecules* **31**, 8382–8395.

Anderson, J. A., Glaser, J., and Glotzer, S. C., 2020, "Hoomd-blue: A python package for high-performance molecular dynamics and hard particle monte carlo simulations," *Computational Materials Science* **173**, 109363.

Ando, D., and Gopinathan, A., 2017, "Cooperative interactions between different classes of disordered proteins play a functional role in the nuclear pore complex of baker's yeast," *PLOS One* **12**, e0169455.

Axpe, E., Chan, D., Offeddu, G. S., Chang, Y., Merida, D., Hernandez, H. L., and Appel, E. A., 2019, "A multiscale model for solute diffusion in hydrogels," *Macromolecules* **52**, 6889–6897.

Babayekhorasani, F., Dunstan, D. E., Krishnamoorti, R., and Conrad, J. C., 2016, "Nanoparticle diffusion in crowded and confined media," *Soft Matter* **12**, 8407–8416.

Baghbanbashi, M., and Kakkar, A., 2022, "Polymersomes: Soft nanoparticles from miktoarm stars for applications in drug delivery," *Molecular Pharmaceutics* **19**, 1687–1703.

Bailey, E. J., Griffin, P. J., Composto, R. J., and Winey, K. I., 2019, "Multiscale dynamics of small, attractive nanoparticles and entangled polymers in polymer nanocomposites," *Macromolecules* **52**, 2181–2188.

Baille, W., Malveau, C., Zhu, X., Kim, Y., and Ford, W., 2003, "Self-diffusion of hydrophilic poly (propyleneimine) dendrimers in poly (vinyl alcohol) solutions and gels by pulsed field gradient nmr spectroscopy," *Macromolecules* **36**, 839–847.

Banerjee, S., Ray, S., Maiti, S., Sen, K. K., Bhattacharyya, U., Kaity, S., and Ghosh, A., 2010, "Interpenetrating polymer network (ipn): a novel biomaterial," *International Journal of Applied Pharmaceutics* **2**, 28–34.

Barr, J. J., 2017, "A bacteriophage's journey through the human body," *Immunological Reviews* **279**, 106–122.

Barr, J. J., Auro, R., Furlan, M., Whiteson, K. L., Erb, M. L., Pogliano, J., Stotland, A., Wolkowicz, R., Cutting, A. S., Doran, K. S., *et al.*, 2013a, "Bacteriophage adhering to mucus provide a non–host-derived immunity," *Proceedings of the National Academy of Sciences* **110**, 10771–10776.

Barr, J. J., Auro, R., Sam-Soon, N., Kassegne, S., Peters, G., Bonilla, N., Hatay, M., Mourtada, S., Bailey, B., Youle, M., *et al.*, 2015, "Subdiffusive motion of bacteriophage in mucosal surfaces increases the frequency of bacterial encounters," *Proceedings of the National Academy of Sciences* **112**, 13675–13680.

Barr, J. J., Youle, M., and Rohwer, F., 2013b, "Innate and acquired bacteriophage-mediated immunity," *Bacteriophage* **3**, 10771–6.

Batoulis, J., and Kremer, K., 1988, "Residual 3-body interactions of a θ-polymer: star polymers," *Europhysics Letters* **7**, 683.

Bik, E. M., 2009, "Composition and function of the human-associated microbiota," *Nutrition Reviews* **67**, S164–S171.

Bird, R. B., Curtiss, C. F., Armstrong, R. C., and Hassager, O., 1987a, *Dynamics of Polymeric Liquids*, Vol. 2 (John Wiley and Sons, New York).

Bird, R. B., Curtiss, C. F., Armstrong, R. C., and Hassager, O., 1987b, *Dynamics of Polymeric Liquids, Volume 2: Kinetic Theory* (Wiley).

Bishop, M., and Michels, J., 1986, "Polymer shapes in three dimensions," *The Journal of Chemical Physics* **85**, 5961–5962.

Bober, Z., Bartusik-Aebisher, D., and Aebisher, D., 2022, "Application of dendrimers in anticancer diagnostics and therapy," *Molecules* **27**, 3237.

Boris, D., and Rubinstein, M., 1996, "A self-consistent mean field model of a starburst dendrimer: dense core vs dense shell," *Macromolecules* **29**, 7251–7260.

Bosko, J. T., and Prakash, J. R., 2008, "Effect of molecular topology on the transport properties of dendrimers in dilute solution at θ temperature: A brownian dynamics study," *The Journal of Chemical Physics* **128**, 034902.

Bosko, J. T., and Prakash, J. R., 2011, "Universal behavior of dendrimer solutions," *Macromolecules* **44**, 660–670.

Bustos, N. A., Ribbeck, K., and Wagner, C. E., 2023, "The role of mucosal barriers in disease progression and transmission," *Advanced Drug Delivery Reviews* **200**, 115008.

Cadix, A., Wilson, J., Carouhy, T., Harrisson, S., and Guichon, H., 2015, "A new class of associative polymer for hydraulic fracturing applications," in *SPE European Formation Damage Conference and Exhibition* (SPE). pp. SPE–174210.

Cai, C., and Chen, Z. Y., 1997, "Rouse dynamics of a dendrimer model in the ϑ condition," *Macromolecules* **30**, 5104–5117.

Cai, L.-H., Panyukov, S., and Rubinstein, M., 2011, "Mobility of nonsticky nanoparticles in polymer liquids," *Macromolecules* **44**, 7853–7863.

Cai, L.-H., Panyukov, S., and Rubinstein, M., 2015, "Hopping diffusion of nanoparticles in polymer matrices," *Macromolecules* **48**, 847–862.

Cannon, J. W., Aronovitz, J. A., and Goldbart, P., 1991, "Equilibrium distribution of shapes for linear and star macromolecules," *Journal de Physique I* **1**, 629–645.

Carroll, B., Bocharova, V., Carrillo, J.-M. Y., Kisliuk, A., Cheng, S., Yamamoto, U., Schweizer, K. S., Sumpter, B. G., and Sokolov, A. P., 2018, "Diffusion of sticky nanoparticles in a polymer melt: Crossover from suppressed to enhanced transport," *Macromolecules* **51**, 2268–2275.

Castillo-Tejas, J., Carro, S., and Manero, O., 2017, "Shear banding in telechelic associative polymers by molecular dynamics," *ACS Macro Letters* **6**, 190–193.

Castillo-Tejas, J., Castrejón-González, O., Carro, S., González-Coronel, V., Alvarado, J., and Manero, O., 2016, "Associative polymers. part iii: Shear rheology from molecular dynamics," *Colloids and Surfaces A: Physicochemical and Engineering Aspects* **491**, 37–49.

Chatterjee, D., and Cherayil, B. J., 2011, "Subdiffusion as a model of transport through the nuclear pore complex," *The Journal of Chemical Physics* **135**

Chen, A., Zhao, N., and Hou, Z., 2017, "The effect of hydrodynamic interactions on nanoparticle diffusion in polymer solutions: a multiparticle collision dynamics study," *Soft Matter* **13**, 8625–8635.

Chen, R., Kotkar, S. B., Poling-Skutvik, R., Howard, M. P., Nikoubashman, A., Conrad, J. C., and Palmer, J. C., 2021, "Nanoparticle dynamics in semidilute polymer solutions: Rings versus linear chains," *Journal of Rheology* **65**, 745–755.

Chen, R., Poling-Skutvik, R., Howard, M. P., Nikoubashman, A., Egorov, S. A., Conrad, J. C., and Palmer, J. C., 2019, "Influence of polymer flexibility on nanoparticle dynamics in semidilute solutions," *Soft Matter* **15**, 1260–1268.

Chen, R., Poling-Skutvik, R., Nikoubashman, A., Howard, M. P., Conrad, J. C., and Palmer, J. C., 2018, "Coupling of nanoparticle dynamics to polymer center-of-mass motion in semidilute polymer solutions," *Macromolecules* **51**, 1865–1872.

Chen, Y., Xu, H., Ma, Y., Liu, J., and Zhang, L., 2022, "Diffusion of polymer-grafted nanoparticles with dynamical fluctuations in unentangled polymer melts," *Physical Chemistry Chemical Physics* **24**, 11322–11335.

Chen, Z. Y., and Cai, C., 1999, "Dynamics of starburst dendrimers," *Macromolecules* **32**, 5423–5434.

Cheng, Y., Prud'Homme, R. K., and Thomas, J. L., 2002, "Diffusion of mesoscopic probes in aqueous polymer solutions measured by fluorescence recovery after photobleaching," *Macromolecules* **35**, 8111–8121.

Chin, W. H., Kett, C., Cooper, O., Müseler, D., Zhang, Y., Bamert, R. S., Patwa, R., Woods, L. C., Devendran, C., Korneev, D., *et al.*, 2022, "Bacteriophages evolve enhanced persistence to a mucosal surface," *Proceedings of the National Academy of Sciences* **119**, e2116197119.

Cho, H. W., Kim, H., Sung, B. J., and Kim, J. S., 2020, "Tracer diffusion in tightly-meshed homogeneous polymer networks: A brownian dynamics simulation study," *Polymers* **12**, 2067.

Choi, J., Cargnello, M., Murray, C. B., Clarke, N., Winey, K. I., and Composto, R. J., 2015, "Fast nanorod diffusion through entangled polymer melts," *ACS Macro Letters* **4**, 952–956.

Colby, R. H., and Rubinstein, M., 2003, "Polymer physics," *New-York: Oxford University* **100**, 274.

Cukier, R., 1984, "Diffusion of brownian spheres in semidilute polymer solutions," *Macromolecules* **17**, 252–255.

Daoud, M., Cotton, J., Farnoux, B., Jannink, G., Sarma, G., Benoit, H., Duplessix, C., Picot, C., and de Gennes, P., 1975, "Solutions of flexible polymers. neutron experiments and interpretation," *Macromolecules* **8**, 804–818.

De, M., Ghosh, P. S., and Rotello, V. M., 2008, "Applications of nanoparticles in biology," *Advanced Materials* **20**, 4225–4241.

Dell, Z. E., and Schweizer, K. S., 2014, "Theory of localization and activated hopping of nanoparticles in cross-linked networks and entangled polymer melts," *Macromolecules* **47**, 405–414.

Doi, M., Edwards, S. F., and Edwards, S. F., 1988, *The theory of polymer dynamics*, Vol. 73 (Oxford University Press).

Dragan, E. S., 2014, "Design and applications of interpenetrating polymer network hydrogels. a review," *Chemical Engineering Journal* **243**, 572–590.

Edwards, R. A., and Rohwer, F., 2005, "Viral metagenomics," *Nature Reviews Microbiology* **3**, 504–510.

Fiore, A. M., Balboa Usabiaga, F., Donev, A., and Swan, J. W., 2017, "Rapid sampling of stochastic displacements in brownian dynamics simulations," *The Journal of Chemical Physics* **146**, 124116.

Fraser, J. S., Maxwell, K. L., and Davidson, A. R., 2007, "Immunoglobulin-like domains on bacteriophage: weapons of modest damage?." *Current Opinion in Microbiology* **10**, 382–387.

Ganazzoli, F., La Ferla, R., and Terragni, G., 2000, "Conformational properties and intrinsic viscosity of dendrimers under excluded-volume conditions," *Macromolecules* **33**, 6611–6620.

Ge, T., 2023, "Scaling perspective on dynamics of nanoparticles in polymers: Length-and time-scale dependent nanoparticle-polymer coupling," *Macromolecules* **56**, 3809–3837.

Ge, T., 2024, "Theoretical and computational perspective on hopping diffusion of nanoparticles in cross-linked polymer networks," *Dynamics and Transport in Macromolecular Networks: Theory, Modeling, and Experiments*, 175–197.

Ge, T., Kalathi, J. T., Halverson, J. D., Grest, G. S., and Rubinstein, M., 2017, "Nanoparticle motion in entangled melts of linear and nonconcatenated ring polymers," *Macromolecules* **50**, 1749–1754.

Ge, T., and Rubinstein, M., 2019, "Mobility of polymer-tethered nanoparticles in unentangled polymer melts," *Macromolecules* **52**, 1536–1545.

Ge, T., Rubinstein, M., and Grest, G. S., 2020, "Effects of tethered polymers on dynamics of nanoparticles in unentangled polymer melts," *Macromolecules* **53**, 6898–6906.

de Gennes, P.-G., 1979, *Scaling Concepts in Polymer Physics* (Cornell University Press).

de Gennes, P.-G., and Hervet, H., 1983, "Statistics of «starburst» polymers," *Journal de Physique Lettres* **44**, 351–360.

Gillies, E. R., and Frechet, J. M., 2005, "Dendrimers and dendritic polymers in drug delivery," *Drug Discovery Today* **10**, 35–43.

Giupponi, G., and Buzza, D., 2004, "Monte carlo simulation of dendrimers in variable solvent quality," *The Journal of Chemical Physics* **120**, 10290–10298.

Glass, J. E., Schulz, D. N., and Zukoski, C., 1991, "Polymers as rheology modifiers: an overview,"

Godec, A., Bauer, M., and Metzler, R., 2014, "Collective dynamics effect transient subdiffusion of inert tracers in flexible gel networks," *New Journal of Physics* **16**, 092002.

Gomez-Solano, J. R., Blokhuis, A., and Bechinger, C., 2016, "Dynamics of self-propelled janus particles in viscoelastic fluids," *Physical Review Letters* **116**, 138301.

Goodrich, C. P., Brenner, M. P., and Ribbeck, K., 2018, "Enhanced diffusion by binding to the crosslinks of a polymer gel," *Nature communications* **9**, 4348.

Grabowski, C. A., and Mukhopadhyay, A., 2014, "Size effect of nanoparticle diffusion in a polymer melt," *Macromolecules* **47**, 7238–7242.

Gratz, M., and Tschope, A., 2019, "Size effects in the oscillatory rotation dynamics of ni nanorods in poly (ethylene oxide) solutions," *Macromolecules* **52**, 6600–6612.

Guan, J., Wang, B., and Granick, S., 2014, "Even hard-sphere colloidal suspensions display fickian yet non-gaussian diffusion," *ACS Nano* **8**, 3331–3336.

Guinier, A., Fournet, G., Walker, C. B., and Yudowitch, K. L., 1955, *Small-angle Scattering of X-rays* (Wiley New York).

Guo, H., Bourret, G., Lennox, R. B., Sutton, M., Harden, J. L., and Leheny, R. L., 2012, "Entanglement-controlled subdiffusion of nanoparticles within concentrated polymer solutions," *Physical Review Letters* **109**, 055901.

Hall, L. M., and Schweizer, K. S., 2008, "Many body effects on the phase separation and structure of dense polymer-particle melts," *The Journal of Chemical Physics* **128**

Harreis, H., Likos, C., and Ballauff, M., 2003, "Can dendrimers be viewed as compact colloids? a simulation study of the fluctuations in a dendrimer of fourth generation," *The Journal of Chemical Physics* **118**, 1979–1988.

He, W., Song, H., Su, Y., Geng, L., Ackerson, B. J., Peng, H., and Tong, P., 2016, "Dynamic heterogeneity and non-gaussian statistics for acetylcholine receptors on live cell membrane," *Nature Communications* **7**, 11701.

Hermans, J., 1968, "Role of diffusion in gel permeation chromatography," *Journal of Polymer Science Part A-2: Polymer Physics* **6**, 1217–1226.

Holyst, R., Bielejewska, A., Szymański, J., Wilk, A., Patkowski, A., Gapiński, J., Żywociński, A., Kalwarczyk, T., Kalwarczyk, E., Tabaka, M., *et al.*, 2009, "Scaling form of viscosity at all length-scales in poly (ethylene glycol) solutions studied by fluorescence correlation spectroscopy and capillary electrophoresis," *Physical Chemistry Chemical Physics* **11**, 9025–9032.

Huang, C.-C., Winkler, R. G., Sutmann, G., and Gompper, G., 2010, "Semidilute polymer solutions at equilibrium and under shear flow," *Macromolecules* **43**, 10107–10116.

Jabrane, T., Laloi, M., Dubé, M., and Mangin, P., 2010, "Printing and coating of t4 phage based bioactive paper," *Advances in Printing and Media Technology* **37**, 351–358.

Jain, A., Sasmal, C., Hartkamp, R., Todd, B. D., and Prakash, J. R., 2015, "Brownian dynamics simulations of planar mixed flows of polymer solutions at finite concentrations," *Chemical Engineering Science* **121**, 245–257.

Jain, A., Sunthar, P., Dünweg, B., and Prakash, J. R., 2012, "Optimization of a brownian-dynamics algorithm for semidilute polymer solutions," *Physical Review E* **85**, 066703–1–066703–15.

Jaishankar, A., and McKinley, G. H., 2013, "Power-law rheology in the bulk and at the interface: quasi-properties and fractional constitutive equations," *Proceedings of the Royal Society A* **469**, 20120284.

Jaisingh, A., and Nebhani, L., 2024, "Dendrimers and hyperbranched polymers as promising and versatile additives in polyolefins," *ACS Applied Engineering Materials* **2**, 236–261.

Jee, A.-Y., Curtis-Fisk, J. L., and Granick, S., 2014, "Nanoparticle diffusion in methycellulose thermoreversible association polymer," *Macromolecules* **47**, 5793–5797.

Jiang, N., Zhang, H., Yang, Y., and Tang, P., 2021, "Molecular dynamics simulation of associative polymers: Understanding linear viscoelasticity from the sticky rouse model," *Journal of Rheology* **65**, 527–547.

Kalwarczyk, T., Sozanski, K., Ochab-Marcinek, A., Szymanski, J., Tabaka, M., Hou, S., and Holyst, R., 2015, "Motion of nanoprobes in complex liquids within the framework of the length-scale dependent viscosity model," *Advances in Colloid and Interface Science* **223**, 55–63.

Kalwarczyk, T., Ziebacz, N., Bielejewska, A., Zaboklicka, E., Koynov, K., Szymanski, J., Wilk, A., Patkowski, A., Gapinski, J., Butt, H.-J., and Hołyst, R., 2011, "Comparative analysis of viscosity of complex liquids and cytoplasm of mammalian cells at the nanoscale," *Nano Letters* **11**, 2157–2163.

Kamerlin, N., and Elvingson, C., 2016, "Tracer diffusion in a polymer gel: simulations of static and dynamic 3d networks using spherical boundary conditions," *Journal of Physics: Condensed Matter* **28**, 475101.

Karim, M., Indei, T., Schieber, J. D., and Khare, R., 2016, "Determination of linear viscoelastic properties of an entangled polymer melt by probe rheology simulations," *Physical Review E* **93**, 012501.

Kesharwani, P., Gorain, B., Low, S. Y., Tan, S. A., Ling, E. C. S., Lim, Y. K., Chin, C. M., Lee, P. Y., Lee, C. M., Ooi, C. H., Choudhury, H., and Pandey, M., 2018, "Nanotechnology based approaches for anti-diabetic drugs delivery," *Diabetes Research and Clinical Practice* **136**, 52–77.

Kłos, J. S., and Sommer, J.-U., 2009, "Properties of dendrimers with flexible spacer-chains: A monte carlo study," *Macromolecules* **42**, 4878–4886.

Kłos, J., and Sommer, J.-U., 2013, "Simulations of neutral and charged dendrimers in solvents of varying quality," *Macromolecules* **46**, 3107–3117.

Kohli, I., Alam, S., Patel, B., and Mukhopadhyay, A., 2013, "Interaction and diffusion of gold nanoparticles in bovine serum albumin solutions," *Applied Physics Letters* **102**

Kohli, I., and Mukhopadhyay, A., 2012, "Diffusion of nanoparticles in semidilute polymer solutions: Effect of different length scales," *Macromolecules* **45**, 6143–6149.

de Kort, D. W., Rombouts, W. H., Hoeben, F. J., Janssen, H. M., Van As, H., and van Duynhoven, J. P., 2015, "Scaling behavior of dendritic nanoparticle mobility in semidilute polymer solutions," *Macromolecules* **48**, 7585–7591.

Kostansek, E., 2006, "Associative polymer/particle dispersion phase diagrams iii: Pigments," *Journal of Coatings Technology and Research* **3**, 165–171.

Kozer, N., Kuttner, Y. Y., Haran, G., and Schreiber, G., 2007, "Protein-protein association in polymer solutions: from dilute to semidilute to concentrated," *Biophysical Journal* **92**, 2139–2149.

Kröger, M., Alba-Pérez, A., Laso, M., and Öttinger, H. C., 2000, "Variance reduced brownian simulation of a bead-spring chain under steady shear flow considering hydrodynamic interaction effects," *The Journal of Chemical Physics* **113**, 4767–4773.

Kroger, M., Peleg, O., and Halperin, A., 2010, "From dendrimers to dendronized polymers and forests: Scaling theory and its limitations," *Macromolecules* **43**, 6213–6224.

Kumar, P., Theeyancheri, L., Chaki, S., and Chakrabarti, R., 2019, "Transport of probe particles in a polymer network: Effects of probe size, network rigidity and probe–polymer interaction," *Soft Matter* **15**, 8992–9002.

Kumari, K., Duenweg, B., Padinhateeri, R., and Prakash, J. R., 2020, "Computing 3d chromatin configurations from contact probability maps by inverse brownian dynamics," *Biophysical Journal* **118**, 2193–2208.

La Ferla, R., 1997, "Conformations and dynamics of dendrimers and cascade macromolecules," *The Journal of Chemical Physics* **106**, 688–700.

Lampo, T. J., Stylianidou, S., Backlund, M. P., Wiggins, P. A., and Spakowitz, A. J., 2017, "Cytoplasmic rna-protein particles exhibit non-gaussian subdiffusive behavior," *Biophysical Journal* **112**, 532–542.

Langevin, D., and Rondelez, F., 1978, "Sedimentation of large colloidal particles through semidilute polymer solutions," *Polymer* **19**, 875–882.

Layre, A.-M., Volet, G., Wintgens, V., and Amiel, C., 2009, "Associative network based on cyclodextrin polymer: a model system for drug delivery," *Biomacromolecules* **10**, 3283–3289.

Lee, C. C., MacKay, J. A., Fréchet, J. M., and Szoka, F. C., 2005, "Designing dendrimers for biological applications," *Nature Biotechnology* **23**, 1517–1526.

Leiman, P., Kanamaru, S., Mesyanzhinov, V., Arisaka, F., and Rossmann, M., 2003, "Structure and morphogenesis of bacteriophage t4," *Cellular and Molecular Life Sciences* **60**, 2356–2370.

Likos, C., Löwen, H., Watzlawek, M., Abbas, B., Jucknischke, O., Allgaier, J., and Richter, D., 1998, "Star polymers viewed as ultrasoft colloidal particles," *Physical Review Letters* **80**, 4450.

Liu, M., and Fréchet, J. M., 1999, "Designing dendrimers for drug delivery," *Pharmaceutical Science & Technology Today* **2**, 393–401.

Lu, Y., and Hu, G.-H., 2021, "A potential barrier in the diffusion of nanoparticles in ordered polymer networks," *Soft Matter* **17**, 6374–6382.

Lyulin, S. V., Darinskii, A. A., Lyulin, A. V., and Michels, M., 2004a, "Computer simulation of the dynamics of neutral and charged dendrimers," *Macromolecules* **37**, 4676–4685.

Lyulin, S. V., Evers, L., van der Schoot, P., Darinskii, A. A., Lyulin, A. V., and Michels, M., 2004b, "Effect of solvent quality and electrostatic interactions on size and structure of dendrimers. brownian dynamics simulation and mean-field theory," *Macromolecules* **37**, 3049–3063.

Mackay, M. E., Dao, T. T., Tuteja, A., Ho, D. L., Van Horn, B., Kim, H.-C., and Hawker, C. J., 2003, "Nanoscale effects leading to non-einstein-like decrease in viscosity," *Nature Materials* **2**, 762–766.

MacKintosh, F., and Schmidt, C., 1999, "Microrheology," *Current Opinion in Colloid & Interface Science* **4**, 300–307.

Mainardi, F., 2020, "Why the mittag-leffler function can be considered the queen function of the fractional calculus?." *Entropy* **22**, 1359.

Maldonado-Camargo, L., and Rinaldi, C., 2016, "Breakdown of the stokes–einstein relation for the rotational diffusivity of polymer grafted nanoparticles in polymer melts," *Nano Letters* **16**, 6767–6773.

Mandelbrot, B. B., and Van Ness, J. W., 1968, "Fractional brownian motions, fractional noises and applications," *SIAM Review* **10**, 422–437.

Mariya, S., Barr, J. J., Sunthar, P., and Prakash, J. R., 2024, "Universal scaling of the diffusivity of dendrimers in a semidilute solution of linear polymers," *Soft Matter* **20**, 993–1008.

Masaro, L., and Zhu, X., 1999, "Physical models of diffusion for polymer solutions, gels and solids," *Progress in Polymer Science* **24**, 731–775.

Mason, T. G., and Weitz, D. A., 1995, "Optical measurements of frequency-dependent linear viscoelastic moduli of complex fluids," *Physical Review Letters* **74**, 1250.

McShane, A., Bath, J., Jaramillo, A. M., Ridley, C., Walsh, A. A., Evans, C. M., Thornton, D. J., and Ribbeck, K., 2021, "Mucus," *Current Biology* **31**, R938–R945.

Metzler, R., and Klafter, J., 2000, "The random walk's guide to anomalous diffusion: a fractional dynamics approach," *Physics reports* **339**, 1–77.

Mitchell, M. J., Billingsley, M. M., Haley, R. M., Wechsler, M. E., Peppas, N. A., and Langer, R., 2021, "Engineering precision nanoparticles for drug delivery," *Nature Reviews Drug Discovery* **20**, 101–124.

Molaei, M., Atefi, E., and Crocker, J. C., 2018, "Nanoscale rheology and anisotropic diffusion using single gold nanorod probes," *Physical Review Letters* **120**, 118002.

Moncure, P. J., Simon, Z. C., Millstone, J. E., and Laaser, J. E., 2022, "Relationship between gel mesh and particle size in determining nanoparticle diffusion in hydrogel nanocomposites," *The Journal of Physical Chemistry B* **126**, 4132–4142.

Montroll, E. W., and Weiss, G. H., 1965, "Random walks on lattices. ii," *Journal of Mathematical Physics* **6**, 167–181.

Murat, M., and Grest, G. S., 1996, "Molecular dynamics study of dendrimer molecules in solvents of varying quality," *Macromolecules* **29**, 1278–1285.

Nahali, N., and Rosa, A., 2018, "Nanoprobe diffusion in entangled polymer solutions: Linear vs. unconcatenated ring chains," *The Journal of Chemical Physics* **148**

Najafi, F., Salami-Kalajahi, M., and Roghani-Mamaqani, H., 2021, "A review on synthesis and applications of dendrimers," *Journal of the Iranian Chemical Society* **18**, 503–517.

Netz, P. A., and Dorfmüller, T., 1997, "Computer simulation studies of diffusion in gels: Model structures," *The Journal of Chemical Physics* **107**, 9221–9233.

Nikzamir, M., Hanifehpour, Y., Akbarzadeh, A., and Panahi, Y., 2021, "Applications of dendrimers in nanomedicine and drug delivery: A review," *Journal of Inorganic and Organometallic Polymers and Materials* **31**, 2246–2261.

Norregaard, K., Metzler, R., Ritter, C. M., Berg-Sørensen, K., and Oddershede, L. B., 2017, "Manipulation and motion of organelles and single molecules in living cells," *Chemical reviews* **117**, 4342–4375.

Okumoto, M., Tasaka, Y., Nakamura, Y., and Norisuye, T., 1999, "Excluded-volume effects in star polymer solutions: Six-arm star polystyrene in cyclohexane near the ϑ temperature," *Macromolecules* **32**, 7430–7436.

Okumoto, M., Terao, K., Nakamura, Y., Norisuye, T., and Teramoto, A., 1997, "Excluded-volume effects in star polymer solutions: Four-arm star polystyrene in cyclohexane near the ϑ temperature," *Macromolecules* **30**, 7493–7499.

Omari, R. A., Aneese, A. M., Grabowski, C. A., and Mukhopadhyay, A., 2009, "Diffusion of nanoparticles in semidilute and entangled polymer solutions," *The Journal of Physical Chemistry B* **113**, 8449–8452.

Pan, S., Ahirwal, D., Nguyen, D. A., Sridhar, T., Sunthar, P., and Prakash, J. R., 2014, "Viscosity radius of polymers in dilute solutions: Universal behavior from dna rheology and brownian dynamics simulations," *Macromolecules* **47**, 7548–7560.

Pancharoen, M., 2009, "Physical properties of associative polymer solutions," *Master of Science Thesis, Stanford: Department Of Energy Resources Engineering of Stanford University*

Patteson, A., Gopinath, A., Goulian, M., and Arratia, P., 2015, "Running and tumbling with e. coli in polymeric solutions," *Scientific Reports* **5**, 15761.

Peppas, N. A., Bures, P., Leobandung, W., and Ichikawa, H., 2000, "Hydrogels in pharmaceutical formulations," *European journal of pharmaceutics and biopharmaceutics* **50**, 27–46.

Phillies, G. D. J., 2015, "In complex fluids the gaussian diffusion approximation is generally invalid," *Soft Matter* **11**, 580–586.

Phillies, G. D., Gong, J., Li, L., Rau, A., Zhang, K., Yu, L. P., and Rollings, J., 1989, "Macroparticle diffusion in dextran solutions," *The Journal of Physical Chemistry A* **93**, 6219–6223.

Pincus, I., Rodger, A., and Prakash, J. R., 2020, "Viscometric functions and rheo-optical properties of dilute polymer solutions: Comparison of fene-fraenkel dumbbells with rodlike models," *Journal of Non-Newtonian Fluid Mechanics* **285**, 104395.

Poling-Skutvik, R., Krishnamoorti, R., and Conrad, J. C., 2015, "Size-dependent dynamics of nanoparticles in unentangled polyelectrolyte solutions," *ACS Macro Letters* **4**, 1169–1173.

Poling-Skutvik, R., Lee, J., Narayanan, S., Krishnamoorti, R., and Conrad, J. C., 2018, "Tunable assembly of gold nanorods in polymer solutions to generate controlled nanostructured materials," *ACS Applied Nano Materials* **1**, 877–885.

Poling-Skutvik, R., Slim, A. H., Narayanan, S., Conrad, J. C., and Krishnamoorti, R., 2019, "Soft interactions modify the diffusive dynamics of polymer-grafted nanoparticles in solutions of free polymer," *ACS Macro Letters* **8**, 917–922.

Quesada-Pérez, M., Maroto-Centeno, J. A., del Mar Ramos-Tejada, M., and Martín-Molina, A., 2021, "Universal description of steric hindrance in flexible polymer gels," *Physical Chemistry Chemical Physics* **23**, 14997–15002.

Quesada-Pérez, M., Maroto-Centeno, J.-A., Ramos-Tejada, M. d. M., and Martín-Molina, A., 2022, "Coarse-grained simulations of solute diffusion in crosslinked flexible hydrogels," *Macromolecules* **55**, 1495–1504.

Rao, V. B., and Black, L. W., 2010, "Structure and assembly of bacteriophage t4 head," *Virology journal* **7**, 1–14.

Rietveld, I. B., and Bedeaux, D., 2000, "Self-diffusion of poly (propylene imine) dendrimers in methanol," *Macromolecules* **33**, 7912–7917.

Robe, D., Santra, A., McKinley, G. H., and Prakash, J. R., 2024, "Evanescent gels: Competition between sticker dynamics and single-chain relaxation," *Macromolecules* **57**, 4220–4235.

Rodríguez-Suárez, J. M., Butler, C. S., Gershenson, A., and Lau, B. L., 2020, "Heterogeneous diffusion of polystyrene nanoparticles through an alginate matrix: the role of cross-linking and particle size," *Environmental Science & Technology* **54**, 5159–5166.

Rossow, T., and Seiffert, S., 2015, "Supramolecular polymer networks: Preparation, properties, and potential," *Supramolecular Polymer Networks and Gels*, 1–46.

Rubinstein, M., and Colby, R. H., 2003, *Polymer Physics* (Oxford university press).

Rubinstein, M., and Dobrynin, A. V., 1997, "Solutions of associative polymers," *Trends in Polymer Science* **5**, 181–186.

Rubinstein, M., and Semenov, A. N., 2001, "Dynamics of entangled solutions of associating polymers," *Macromolecules* **34**, 1058–1068.

Safi Samghabadi, F., Slim, A. H., Smith, M. W., Chabi, M., and Conrad, J. C., 2022, "Dynamics of filamentous viruses in polyelectrolyte solutions," *Macromolecules* **55**, 10694–10702.

Salata, O. V., 2004, "Applications of nanoparticles in biology and medicine," *Journal of Nanobiotechnology* **2**, 1–6.

Santra, A., Dünweg, B., and Ravi Prakash, J., 2021, "Universal scaling and characterization of gelation in associative polymer solutions," *Journal of Rheology* **65**, 549–581.

Santra, A., Kumari, K., Padinhateeri, R., Dünweg, B., and Prakash, J. R., 2019, "Universality of the collapse transition of sticky polymers," *Soft Matter* **15**, 7876–7887.

Sanz-Gaitero, M., Seoane-Blanco, M., and van Raaij, M. J., 2021, "Structure and function of bacteriophages," *Bacteriophages: Biology, Technology, Therapy*, 19–91.

Sathaliyawala, T., Islam, M. Z., Li, Q., Fokine, A., Rossmann, M. G., and Rao, V. B., 2010, "Functional analysis of the highly antigenic outer capsid protein, hoc, a virus decoration protein from t4-like bacteriophages," *Molecular Microbiology* **77**, 444–455.

Savage, D. C., 1977, "Microbial ecology of the gastrointestinal tract," *Annual Review of Microbiology* **31**, 107–133.

Schuster, B. S., Suk, J. S., Woodworth, G. F., and Hanes, J., 2013, "Nanoparticle diffusion in respiratory mucus from humans without lung disease," *Biomaterials* **34**, 3439–3446.

Schweizer, K. S., and Curro, J. G., 1997, "Integral equation theories of the structure, thermodynamics, and phase transitions of polymer fluids," *Advances in Chemical Physics* **98**, 1–142.

Schwiertz, A., 2016, "Microbiota of the human body," *Advances in Experimental Medicine and Biology* **902**, v.

Sheng, Y.-J., Jiang, S., and Tsao, H.-K., 2002, "Radial size of a starburst dendrimer in solvents of varying quality," *Macromolecules* **35**, 7865–7868.

Siepmann, J., and Siepmann, F., 2012, "Modeling of diffusion controlled drug delivery," *Journal of controlled release* **161**, 351–362.

Slim, A. H., Poling-Skutvik, R., and Conrad, J. C., 2020, "Local confinement controls diffusive nanoparticle dynamics in semidilute polyelectrolyte solutions," *Langmuir* **36**, 9153–9159.

Smith, M., Poling-Skutvik, R., Slim, A. H., Willson, R. C., and Conrad, J. C., 2021, "Dynamics of flexible viruses in polymer solutions," *Macromolecules* **54**, 4557–4563.

Soddemann, T., Dünweg, B., and Kremer, K., 2001, "A generic computer model for amphiphilic systems," *European Physical Journal E* **6**, 409–419.

Sorichetti, V., Hugouvieux, V., and Kob, W., 2021, "Dynamics of nanoparticles in polydisperse polymer networks: From free diffusion to hopping," *Macromolecules* **54**, 8575–8589.

Sozański, K., Wiśniewska, A., Kalwarczyk, T., and Hołyst, R., 2013, "Activation energy for mobility of dyes and proteins in polymer solutions: from diffusion of single particles to macroscale flow," *Physical Review Letters* **111**, 228301.

Squires, T. M., and Mason, T. G., 2010, "Fluid mechanics of microrheology," *Annual Review of Fluid Mechanics* **42**, 413–438.

Stark, W. J., Stoessel, P. R., Wohlleben, W., and Hafner, A., 2015, "Industrial applications of nanoparticles," *Chemical Society Reviews* **44**, 5793–5805.

Sunthar, P., and Prakash, J. R., 2006, "Dynamic scaling in dilute polymer solutions: The importance of dynamic correlations," *Europhysics Letters* **75**, 77.

Tabei, S. A., Burov, S., Kim, H. Y., Kuznetsov, A., Huynh, T., Jureller, J., Philipson, L. H., Dinner, A. R., and Scherer, N. F., 2013, "Intracellular transport of insulin granules is a subordinated random walk," *Proceedings of the National Academy of Sciences* **110**, 4911–4916.

Tande, B. M., Wagner, N. J., Mackay, M. E., Hawker, C. J., and Jeong, M., 2001, "Viscosimetric, hydrodynamic, and conformational properties of dendrimers and dendrons," *Macromolecules* **34**, 8580–8585.

Theodorou, D. N., and Suter, U. W., 1985, "Shape of unperturbed linear polymers: polypropylene," *Macromolecules* **18**, 1206–1214.

Timoshenko, E. G., Kuznetsov, Y. A., and Connolly, R., 2002, "Conformations of dendrimers in dilute solution," *The Journal of Chemical Physics* **117**, 9050–9062.

Tong, P., Ye, X., Ackerson, B. J., and Fetters, L., 1997, "Sedimentation of colloidal particles through a polymer solution," *Physical Review Letters* **79**, 2363.

Tuteja, A., Mackay, M. E., Narayanan, S., Asokan, S., and Wong, M. S., 2007, "Breakdown of the continuum stokes- einstein relation for nanoparticle diffusion," *Nano Letters* **7**, 1276–1281.

Vlassopoulos, D., 2004, "Colloidal star polymers: Models for studying dynamically arrested states in soft matter," *Journal of Polymer Science Part B: Polymer Physics* **42**, 2931–2941.

Wagner, C., Wheeler, K., and Ribbeck, K., 2018, "Mucins and their role in shaping the functions of mucus barriers," *Annual Review of Cell and Developmental Biology* **34**, 189–215.

Wang, B., Anthony, S. M., Bae, S. C., and Granick, S., 2009, "Anomalous yet brownian," *Proceedings of the National Academy of Sciences of the United States of America* **106**, 15160–15164.

Wang, B., Kuo, J., Bae, S. C., and Granick, S., 2012, "When brownian diffusion is not gaussian," *Nature Materials* **11**, 481–485.

Wang, J., O'Connor, T. C., Grest, G. S., Zheng, Y., Rubinstein, M., and Ge, T., 2021, "Diffusion of thin nanorods in polymer melts," *Macromolecules* **54**, 7051–7059.

Winnik, M. A., and Yekta, A., 1997, "Associative polymers in aqueous solution," *Current Opinion in Colloid & Interface science* **2**, 424–436.

Wu, J., Fu, K., Hou, C., Wang, Y., Ji, C., Xue, F., Ren, J., Dai, J., Barr, J. J., and Tang, F., 2024, "Bacteriophage defends murine gut from escherichia coli invasion via mucosal adherence," *Nature Communications* **15**, 4764.

Xia, J., and Olvera de la Cruz, M., 2024, "Dynamics and structure of unentangled associative polymers," *Macromolecules*

Xu, Z., Dai, X., Bu, X., Yang, Y., Zhang, X., Man, X., Zhang, X., Doi, M., and Yan, L.-T., 2021, "Enhanced heterogeneous diffusion of nanoparticles in semiflexible networks," *ACS nano* **15**, 4608–4616.

Xue, C., Zheng, X., Chen, K., Tian, Y., and Hu, G., 2016, "Probing non-gaussianity in confined diffusion of nanoparticles," *The Journal of Physical Chemistry Letters* **7**, 514–519.

Yamamoto, U., Carrillo, J.-M. Y., Bocharova, V., Sokolov, A. P., Sumpter, B. G., and Schweizer, K. S., 2018, "Theory and simulation of attractive nanoparticle transport in polymer melts," *Macromolecules* **51**, 2258–2267.

Yang, S.-G., Xie, H.-J., Saba, H., Cseh, L., and Ungar, G., 2020, "Fluorescence microscopy tracking of dyes, nanoparticles and quantum dots during growth of polymer spherulites," *Polymer* **191**, 122246.

Yang, X., Forier, K., Steukers, L., Van Vlierberghe, S., Dubruel, P., Braeckmans, K., Glorieux, S., and Nauwynck, H. J., 2012, "Immobilization of pseudorabies virus in porcine tracheal respiratory mucus revealed by single particle tracking," *PLOS One* **7**, e51054.

Ye, X., Tong, P., and Fetters, L., 1998, "Transport of probe particles in semidilute polymer solutions," *Macromolecules* **31**, 5785–5793.

You, W., and Yu, W., 2019, "Slow linear viscoelastic relaxation of polymer nanocomposites: contribution from confined diffusion of nanoparticles," *Macromolecules* **52**, 9094–9104.

Zhang, X., Dai, X., Habib, M. A., Gao, L., Chen, W., Wei, W., Tang, Z., Qi, X., Gong, X., Jiang, L., *et al.*, 2024, "Unconventionally fast transport through sliding dynamics of rodlike particles in macromolecular networks," *Nature Communications* **15**, 525.

Zhou, H., and Chen, S. B., 2009, "Brownian dynamics simulation of tracer diffusion in a cross-linked network," *Physical Review E* **79**, 021801.

Zhu, H., Quah-Ivarson, S. P., Zhang, Y., Fluerasu, A., Yu, X., Zheng, B., Yin, X., Liu, W., and Bhatia, S. R., 2023, "Microscale dynamics in thermoreversible hydrogels: Impact of probe size and concentration," *European Polymer Journal* **199**, 112434.

List of Publications

First author publications

The following is a list of research outputs that were produced as a result of the principal projects undertaken during the PhD candidature.

Journal papers (Published)

J1 Mariya, S., Barr, J. J., Sunthar, P., Prakash, J. R. (2024), "Universal scaling of the diffusivity of dendrimers in a semidilute solution of linear polymers". *Soft Matter*, 20(5), 993-1008. Link

Manuscript under preparation

M1 Mariya, S., Barr, J. J., Sunthar, P., Prakash, J. R. (2024), “Subdiffusion of sticky dendrimers in an associative polymer network”. (Submitted)

M2 Mariya, S., Barr, J. J., Sunthar, P., Prakash, J. R. (2024), “Modelling the subdiffusive motion of bacteriophages within mucus”. (Manuscript with authors)

Conferences attended

C1 Mariya, S., Barr, J. J., Sunthar, P., Prakash, J. R., "The subdiffusive motion of sticky dendrimers in an associative polymer network". International Soft Matter Conference organised by the Soft Matter Association of the Americas in Raleigh, North Carolina, from 29th July to 2nd August 2024 (Talk).

C2 Mariya, S., Barr, J. J., Sunthar, P., Prakash, J. R., "Universal scaling of the diffusivity of dendrimers in a semidilute solution of linear polymers". Perspectives in Hydrodynamics conference organised by Chemical engineering department at IIT Bombay, from 26th to 29th February 2024 (Poster).

C3 Mariya, S., Barr, J. J., Sunthar, P., Prakash, J. R., "Modelling the subdiffusive motion of bacteriophages within mucus". Fluid Mechanics Colloquium organised by fluid mechanics community at IIT Bombay, on 19th October 2023 (Talk).

C4 Mariya, S., Barr, J. J., Sunthar, P., Prakash, J. R., "Universal diffusion of dendrimers in a semidilute solution of linear polymers". Poster competition organised by IITB-Monash Research Academy on 17th August 2023 (Best poster runner-up award).

C5 Mariya, S., Barr, J. J., Sunthar, P., Prakash, J. R., "Universal scaling of the diffusivity of dendrimers in a semidilute solution of linear polymers". 8th Pacific Rim Conference on Rheology organised by the Canadian Society of Rheology in Vancouver, Canada, from 15th to 19th May 2023 (Talk).

C6 Mariya, S., Barr, J. J., Sunthar, P., Prakash, J. R., "Modelling the subdiffusive motion of bacteriophages within mucus". Faculty of Engineering Post Graduate Student Conference organised by Faculty of Engineering at Monash University on 1st December 2022 (Talk: Best speaker runner-up award).

C7 Mariya, S., Barr, J. J., Sunthar, P., Prakash, J. R., "Dendrimer diffusion in semidilute solution of linear chains". First Monash Scientific High Performance Computing Showcase and User Meeting organised by Monash University on 29th September 2022 (Poster).

C8 Mariya, S., Barr, J. J., Sunthar, P., Prakash, J. R., "Are soft dendrimers dynamically equivalent to hard spheres?". Eighth Statistical Mechanics of Soft Matter Conference held at Monash University from 12-15th July 2022 (Talk).

Acknowledgements

Embarking on a journey as challenging and rewarding as a PhD is never a solitary endeavour, and this work would not have been possible without the support and encouragement of many individuals and institutions. This section is a humble acknowledgment of their invaluable roles in my academic and personal growth throughout this journey.

I would like to express my heartfelt gratitude to my supervisors, Prof. J. Ravi Prakash (Department of Chemical and Biological Engineering, Monash University), Prof. P. Sunthar (Department of Chemical Engineering, IIT Bombay), and Prof. Jeremy Barr (School of Biological Sciences, Monash University), for their unwavering support, insightful guidance, and inspiration throughout this journey. Their expertise and encouragement have not only shaped the direction of my research but also profoundly influenced my growth as a researcher. Their ability to challenge and motivate me instilled in me a spirit of critical and independent thinking that I will carry forward in my career.

I am deeply thankful to the members of my Research Progress Committee (RPC) - Prof. Rajarshi Chakrabarti, Prof. Ranjith Padinhateeri, and Prof. Mark Flegg - for their valuable feedback and constructive suggestions during my Annual Progress Seminars (APS) and pre-synopsis seminar. I am equally grateful to all the professors who attended and provided feedback on my presentations over the past five years, especially Prof. Gareth McKinley, Prof. Ron Larson, and Prof. Jason Picardo. Each interaction was an enriching experience that encouraged me to think more deeply about my work.

I extend my gratitude to the computational resources that made this research possible, including Monash University (MASSIVE and MonArch), National Computational Infrastructure (NCI) Australia (Gadi and Topaz), and additional resources obtained through the Adapter Scheme (2022) and DUG-HPCaaS. I also acknowledge the funding support from the Department of Biotechnology (DBT) India and the IITB-Monash Research Academy.

It has been a privilege to be part of the Molecular Rheology Group at Monash University. I sincerely thank my group members, Dr. Nick Robe, Dr. Aritra Santra, Dr. Kiran Kumari, Dr. Ramalingam Kailasham, Dr. Isaac Pincus, Mr. Avishek Kumar, and Mr. Amit Varakhedkar, for the stimulating discussions and invaluable feedback during mock presentations. I am also

grateful to the staff at the IITB-Monash Research Academy, the Department of Chemical and Biological Engineering at Monash University, and the Department of Chemical Engineering at IIT Bombay for their assistance and support.

This journey would not have been possible without the individuals who inspired me to pursue this challenging path. I am deeply indebted to Br. Tomy Varghese (Principal, St. Patrick's Academy) for encouraging me to explore paths less taken, to Prof. Ajith Kumar (IUAC, New Delhi) for introducing me to the joy of scientific discovery and Dr. Radhika (IITB hospital) for helping me manage stressful situations. I am also profoundly grateful to all my teachers from St. Patrick's Academy (Kerala), St. Stephen's College (Delhi), and the National Institute of Technology (Rourkela) for shaping my academic foundation.

I thank my friends for making my time in Bombay and Melbourne unforgettable. Finally, my deepest gratitude goes to my family and loved ones for their unwavering belief in me and this journey. Their trust, encouragement, and sacrifices have been my greatest source of strength, and I dedicate this achievement to them.

Silpa Mariya
IIT Bombay
12 May 2025